Université libre de Bruxelles

École Polytechnique de Bruxelles
OPERA - Wireless Communications Group

Université catholique de Louvain

École Polytechnique de Louvain
ICTEAM - Electrical Engineering

Multi-Polarized Sensing for Cognitive-Radio

Dissertation originale présentée en vue de l'obtention du Grade de

Docteur en Sciences de l'Ingénieur

et préparée sous la direction des Professeurs
Philippe De Doncker, François Horlin et Claude Oestges

par
Ali Panahandeh

Défense privée: 4 sep 2012
Soutenance publique: 9 oct 2012

Composition du Jury:

Prof. Philippe Emplit (Président)
Prof. Philippe De Doncker (Promoteur)
Prof. Claude Oestges (Promoteur)
Prof. François Horlin (co-Promoteur)
Prof. Danielle Vanhoenacker-Janvier
Prof. Luc Vandendorpe
Prof. Aziz Benlarbi-Delaï
Prof. Jean-Michel Dricot

To my parents.

Remerciements

Je tiens tout d'abord à remercier mon promoteur de thèse à l'ULB, Philippe De Doncker. C'est lui qui m'a proposé d'effectuer une thèse de doctorat lorsque j'étais en quatrième année d'études et qui m'a initié au monde passionnant de la recherche. Je le remercie profondément pour la confiance qu'il m'a accordée tout au long de ces quatre années de thèse. Son soutien, son suivi attentif, sa présence, son exigence et ses qualités scientifiques et humaines m'ont permis de mener à bien ce travail. Je remercie également mon promoteur de thèse à l'UCL, Claude Oestges, de m'avoir donné l'opportunité d'accéder à ses connaissances et expériences dans la recherche. Je le remercie pour son suivi, sa présence, sa bonne humeur et son soutien tout au long de ce doctorat. Je remercie également mon co-promoteur de thèse François Horlin. Cette thèse de doctorat, je la dois également à lui, qui m'a motivé à entamer une thèse il y a cinq ans. Je le remercie pour ses conseils, son aide et sa bonne humeur.

J'exprime ma gratitude envers l'ensemble des membres de mon jury de thèse pour leur participation dans ce jury ainsi que pour leurs remarques constructives qui ont permis d'améliorer la qualité de ce travail.

Je remercie également l'ensemble des anciens ou actuels membres de l'équipe OPERA Wireless pour avoir contribué à faire régner, durant ces années, une ambiance chaleureuse et productive. Je remercie tout d'abord les plus vieux. Un grand merci à JIM de qui j'ai beaucoup appris autant d'un point de vue technique qu'humain. Ses conseils, son ouverture et sa culture générale, digne d'une encyclopédie, m'ont beaucoup apporté durant ces années. Je remercie Olivier Delangre pour tout ce qu'il m'a appris et pour son professionnalisme qui, dans un environnement académique, m'a beaucoup inspiré. Je remercie Stéphane pour les échanges que nous avons eu et pour le savoir qu'il a partagé avec moi. Un grand merci à Kiki de qui j'ai beaucoup appris et avec qui j'ai eu l'opportunité de réaliser de nombreuses collaborations. Je remercie Bellou pour les divers coups de main et pour les activités qu'il a organisées. Je remercie Xavier pour son accueil chaleureux au début de ma thèse.

Je tiens également à remercier les plus jeunes du service. L'ambiance dynamique et amicale qu'ils ont créée au sein du service nous a permis à chacun de mieux avancer dans sa recherche. Je les remercie pour tout-ce qu'on a accompli ensemble durant ces années. Un grand merci à Julien pour ses coups de main et son humour. Merci à Mathieu pour ses initiatives, ses coups de main et sa sympathie. Je remercie Ourouk pour les discussions très enrichissantes et agréables que nous avons eues et pour ses encouragements aux moments les plus difficiles. Je remercie Jessica pour son entraide et les discussions et les échanges intéressants que nous avons eus. Un grand merci à "Monsieur Thibault" pour avoir boosté l'ambiance du service avec sa venue et pour toutes les activités que nous avons faites ensemble. Je le remercie également pour les coups de main qu'il m'a donnés. Je remercie Théo pour sa bonne humeur, ses coups de main et sa chaine de News. Enfin, je tiens à remercier mes deux chers amis et collègues de bureau Oli et Jon. Nous avons commencé ensemble ce parcours et j'ai eu l'opportunité de partager des moments inoubliables en leur présence. Leur soutien, leurs encouragements et leurs conseils ont été d'une valeur inestimable tout au long de cette thèse. Un grand merci à Jon pour ses initiatives, sa bonne volonté, ses coups de main et sa bonne humeur. Merci à Olivier de qui j'ai beaucoup appris sur tous les plans. Je le remercie pour ses conseils, son écoute et son aide durant ces quatre années.

Je me dois également d'exprimer mes remerciements envers les chercheurs du service ECTEAM à l'UCL pour le travail que nous avons partagé, entre collaborations et entraides.

Il est bien sûr difficile de mentionner tous ceux qui directement ou indirectement ont contribué à la réussite de cette thèse. Je pense à tous mes amis qui ont certainement eu leur part de mérite dans cet accomplissement.

Je remercie infiniment ma chère sœur qui a été à mes côtés pendant ces quatre années et qui m'a toujours apporté son soutien moral. Son aide, sa patience, son écoute et sa gentillesse font partie des points clés de cette réussite. Un grand merci à mon frère pour son soutien et ses encouragements. Je tiens également à remercier ma chère grand-mère qui nous a quittés récemment et qui m'a toujours soutenu avec ses prières.

Mes plus chaleureux remerciements sont destinés à mes chers parents à qui je dois tout ce que j'ai accompli dans ma vie. Mes remerciements ne seront jamais à la hauteur de tout ce qu'ils ont fait pour moi. Ce doctorat est sans doute le résultat de leurs sacrifices, leur soutien, leurs conseils, leur exemplarité, leurs encouragements et leurs prières.

Abstract

Abstract

In this thesis the multi-polarized Cognitive Radios (CR) are studied. CR are proposed as an interesting way to more efficiently use the frequency resources. A CR secondary user finds the frequency bands which are not utilized by primary users and communicates on them without interfering with the primary users. In order to achieve this goal the secondary user must be able to detect reliably and quickly the presence of a primary user in a frequency band. In this thesis, the impact of polarization on the spectrum sensing performances of cognitive radio systems is studied.

First the depolarization occurring in the wireless channel is studied for two cognitive radio scenarios. This is done through an extensive measurement campaign in two outdoor-to-indoor and indoor-to-indoor scenarios where the parameters characterizing the radiowaves polarization are characterized at three different spatial scales: small-scale variation, large-scale variation and distance variation.

Second, a new approach is proposed in modeling of multi-polarized channels. The polarization of received fields is characterized from an electromagnetic point of view by modeling the polarization ellipse. Theoretical formulations are proposed in order to obtain the parameters characterizing the polarization ellipse based on the signals received on three cross-polarized antennas. A system-based statistical model of the time-dynamics of polarization is proposed based on an indoor-to-indoor measurement campaign. The analytical formulations needed in order to project the polarization ellipse onto a polarized multi-antenna system are given and it is shown how the model can be generated.

Third, the impact of polarization on the spectrum sensing performances of energy detection method is presented and its importance is highlighted. The performance of spectrum sensing with multi-polarized antennas is compared with unipolar single and multi-antenna systems. This analysis is based on an analytical formulation applied to the results obtained from the multi-polarized measurement campaign. The detection probability as a function of distance between the primary transmitter and the secondary terminal and the inter-antenna correlation effect on the spectrum sensing performance are studied.

An important limitation of energy detector is its dependence on the knowledge of the noise variance. An uncertainty on the estimation of the noise variance considerably affects the performance of energy detector. This limitation is resolved by proposing new multi-polarized spectrum sensing methods which do not require any knowledge neither on the primary signal nor on the noise variance. These methods, referred to as "Blind spectrum sensing methods", are based on the use of three cross-polarized antennas at the secondary terminal. Based on an analytical formulation and the results obtained from the measurement campaign, the performances of the proposed methods are compared with each-other and with the energy detection method. The effect of antenna orientation on the spectrum sensing performance of the proposed methods and the energy detection method is studied using the proposed elliptical polarization model.

Keywords

cognitive Radio, Polarization, multi-polarized, multiple antennas, propagation channel, spectrum sensing,

Contents

List of Figures

List of Tables

Acronyms

ED	Energy Detection
BB	Base-Band
BS	Base Station
CCC	Common Control Channel
CDF	Cumulative Distribution Function
CPR	Co-Polar-Ratio
CR	Cognitive-Radio
CSI	Channel-State-Information
GBSCM	Geometry-based stochastic channel models
GLRT	Generalized-Likelihood Ratio Test
LOS	Line-Of-Sight
MIMO	Multiple-Input-Multiple-Output
MRC	Maximum-Ratio-Combining
MS	Mobile Station
NLOS	Non-Line-Of-Sight
PDF	Probability Density Function
PTx	Primary transmitter
Rx	Receiver
SC	Selection Combining
SCMSA	Statistical Channel Models with a System Approach
SLC	Square-Law-Combining
SNR	Signal-to-Noise Ratio
SPD	Sensing-Per-Difference
STE	Secondary Terminal
Tx	Transmitter
VSG	Vector-Signal Generator
WRAN	Wireless-Regional-Area-Network
XPD	Cross-Polarization-Discrimination
XPI	Cross-Polar-Isolation
XPR	Cross-Polar-Ratio

CHAPTER 1
Introduction

1.1 Introduction to Cognitive Radio systems

The Radio frequency spectrum is a unique resource and a valuable commodity shared between different types of wireless devices. Like many other natural resources, the demand for radio frequency spectrum has considerably increased during the recent years as the interest of consumers in high data rate wireless services is growing. In practice, only a limited number of wireless devices could operate on the same frequency. This limitation highlights the necessity of a careful control and management of the frequency spectrum in order to maximize its value for a maximum of users. This is the role of the national and international regulators who manage and control the spectrum ressource. The spectrum regulatory framework is currently based on static spectrum allocation and assignment. This is published in the International Telecommunication Union (ITU) Radio Regulation which contain these allocation schemes for each of the three ITU geographical regions [3]. In the European Union level, the radio spectrum is governed by the Radio Spectrum Policy Group (RSPG), Radio Spectrum Committee (RSC) and European Conference of Postal and Telecommunications Administrations (CEPT). Moreover, at the national level, the radio spectrum is governed by the national regulatory agencies who define national frequency spectrum allocation table and assign on an exclusively basis the radio spectrum to license holders or services for large geographical areas and for a long term. In United-States (US) for instance, this role is played by the Federal Communications Commission (FCC).

CHAPTER 1

Introduction

1.1 Introduction to Cognitive Radio systems

The Radio frequency spectrum is a unique resource and a valuable commodity shared between different types of wireless devices. Like many other natural resources, the demand for radio frequency spectrum has considerably increased during the recent years as the interest of consumers in high data rate wireless services is growing. In practice, only a limited number of wireless devices could operate on the same frequency. This limitation highlights the necessity of a careful control and management of the frequency spectrum in order to maximize its value for a maximum of users. This is the role of the national and international regulators who manage and control the spectrum ressource. The spectrum regulatory framework is currently based on static spectrum allocation and assignment. This is published in the International Telecommunication Union (ITU) Radio Regulation which contain these allocation schemes for each of the three ITU geographical regions [3]. In the European Union level, the radio spectrum is governed by the Radio Spectrum Policy Group (RSPG), Radio Spectrum Committee (RSC) and European Conference of Postal and Telecommunications Administrations (CEPT). Moreover, at the national level, the radio spectrum is governed by the national regulatory agencies who define national frequency spectrum allocation table and assign on an exclusively basis the radio spectrum to license holders or services for large geographical areas and for a long term. In United-States (US) for instance, this role is played by the Federal Communications Commission (FCC).

Based on the Article 5 of the ITU Radio Regulations [3], and by observing the national spectrum assignment databases, it can be concluded that the whole radio frequency spectrum has already been licensed to existing services and technologies for commercial and public interests. This is shown in figure 1.1 where the FCC frequency spectrum allocation in the frequency range 900 MHz - 5GHz is presented for the particular case of United States (US). We note that only a few frequency bands are still available and there is a real saturation of the frequency spectrum caused by the static frequency spectrum allocation policy that the national regulators are following. From a technical point of view this static frequency assignment makes the systems design and deployment easier as the system uses a dedicated frequency band instead of using many different bands in a large frequency range. This is also a good way for preventing interferences from other services and to guarantee a good quality of service. However as the demand for wireless communications services is constantly growing a considerable increase is observed for the demand of radio frequency spectrum. Given the static frequency assignment policy and the saturation of the frequency spectrum by existing technologies, it is becoming more and more difficult to release new frequency bands in order to deploy new technologies and we are facing a real shortage of the frequency spectrum ressource.

On the other hand, by analyzing the actual utilization of the already allocated radio frequencies, we note that these resources are considerably underutilized. This is shown in figure 1.2 where the frequency utilization is presented in the time domaine and for a frequency band from 0 to 2.5 GHz. We observe that a considerable portion of the allocated frequencies are not used for a large period of time. According to FCC, the temporal and geographical variations in the utilization of the allocated spectrum varies from 15% to 85% [4]. Shared Spectrum Company conducted measurements on the frequency occupation between 30 MHz

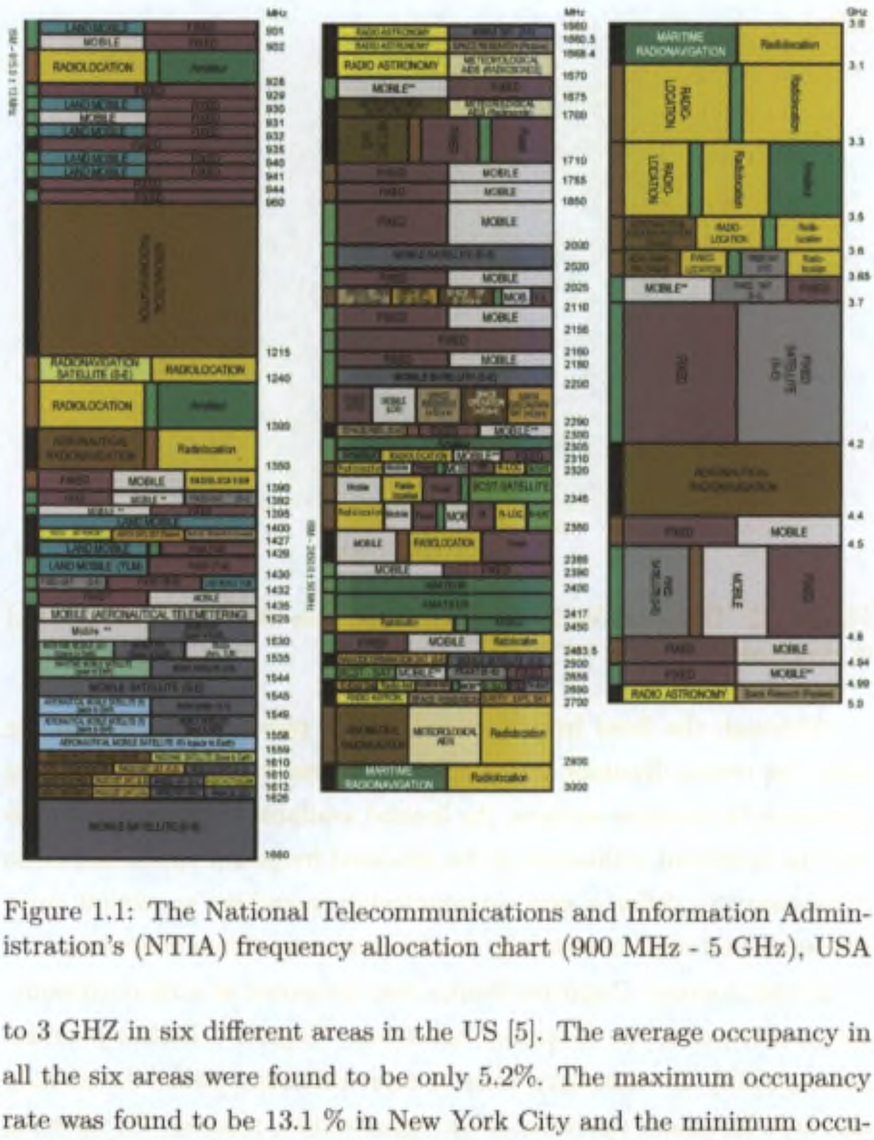

Figure 1.1: The National Telecommunications and Information Administration's (NTIA) frequency allocation chart (900 MHz - 5 GHz), USA

to 3 GHZ in six different areas in the US [5]. The average occupancy in all the six areas were found to be only 5.2%. The maximum occupancy rate was found to be 13.1 % in New York City and the minimum occupancy rate was only 1 % in a rural area. In Europe, similar occupancy measurements were conducted [6–9] (in Germany, Spain, Netherlands, Ireland, France, Czech Republic) where higher average occupancy rate values were obtained compared to US but the occupancy rate stays still low (e.g. 32 % in Aachen area in Germany and for the band 20-3000

MHz).

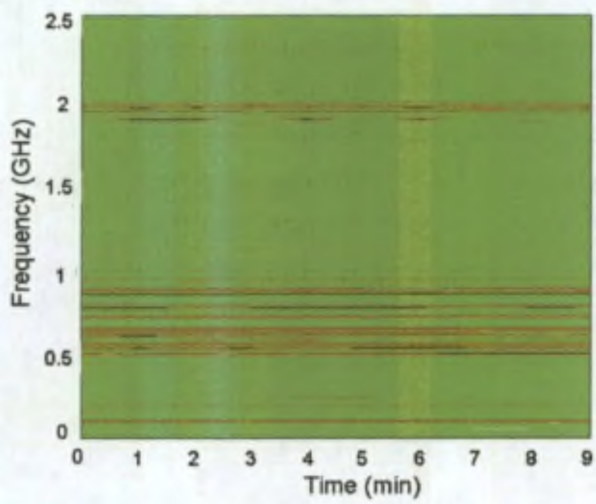

Figure 1.2: Temporal Variation of the spectrum utilization (0-2.5 GHz) in downtown Berkeley [1]

Although the fixed frequency assignment policy served well in the past, the recent dramatic increase in the access to the radio frequency spectrum for wireless services, the limited available frequency resources and the inefficient utilization of the allocated frequency spectrum, make it necessary to define a new communication paradigm to exploit more efficiently and opportunistically the frequency spectrum ressource.

In this context, Cognitive Radios were proposed as a more dynamic access method to the frequency spectrum. Cognitive Radios provides the capability for secondary users to more efficiency utilize the already allocated frequency spectrum in an opportunistic manner. By allowing a more efficient utilization of the radio spectrum, cognitive radios will facilitate the emergence of next generation of wireless services. The term Cognitive Radio could be defined as follow [4]:

"Cognitive Radios" are wireless devices which are aware of their surrounding radio environment and have the capability to adapt their be-

havior based on the environment in which they operate

The Cognitive Radio concept was first introduced by Joseph Mitola and Gerald Maguire as a new way to increase the flexibility of personal wireless services [10]. The main objective of a Cognitive Radio is to determine the best available frequency spectrum to operate in it. The basic idea of Cognitive Radios is to let a secondary network operating in the frequency resources already allocated to a primary Network without interfering with the communications of the primary licensed users. In order to achieve this goal, the secondary user (referred also to as the cognitive radio) has to sens the frequency spectrum in order to find the portions of the frequency spectrum which are not utilized by primary users at a given time and/or space. These unused portions of spectrum are referred to as *spectrum hole* ot *white space* [11]. In case a primary user starts using the spectrum hole, the cognitive radio should be able to quickly liberate the frequency hole and to transit into a new spectrum hole or to stay in the same frequency band but to adapt its transmission power level or modulation parameters in order to not interfere with the primary user (figure 1.3).

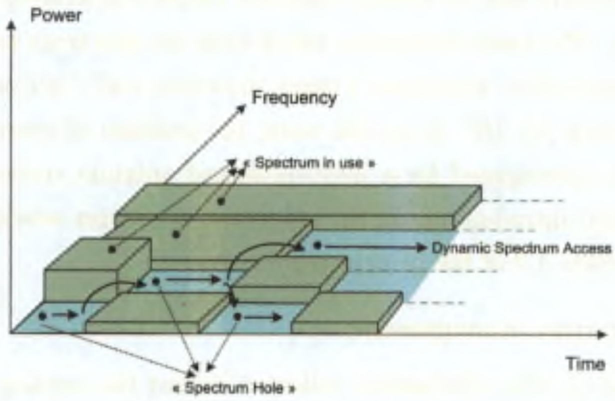

Figure 1.3: Spectrum hole concept

The cognitive capability of a cognitive radio represents its capacity to capture and sens informations on the Radio environment in which it operates in order to determine the appropriate communication parameters that it has to use [11–13]. The cognitive radio should also be reconfigurable. The reconfigurability of a cognitive radio represents its capacity to change its transmission parameters at the beginning or during a transmission based on the spectrum characteristics [14]. It allows the cognitive radio to be flexible to any changes in the radio environment and to be able to dynamically adapt itself to these changes for instance by adapting its operating frequency band or its transmission power.

The main functionalities of a cognitive radio could be summarized as 1)*Spectrum sensing* 2)*Spectrum management* 3)*Spectrum mobility* 4)*Spectrum sharing.* These functionalities are described in the following.

1. **Spectrum sensing**

   One of the most important functionalities of a cognitive radio is to be able to detect reliably and quickly the presence or not of a primary user at a given frequency band. The spectrum sensing could be done in a non cooperative way by a single cognitive radio or in a cooperative way by several cognitive radios cooperating with each other. The main techniques which exist for spectrum sensing are: *Matched filter detection*, *Energy detection* and *Cyclostationarity detection* [15–18]. As in this work, the problem of spectrum sensing is investigated for a multi-polarized antenna system, a more detailed introduction on the subject of spectrum sensing is given in section 1.2 of the present report.

2. **Spectrum management**

   Based on the information collected during the sensing step, the cognitive radio selects when to start its operation, the frequency that it has to use and the corresponding technical communication parameters. The main objective here is to transfer a maximum of information by respecting the requested QoS and without interfering with other licensed or unlicensed users. This is done through two steps: *spectrum analysis* and *spectrum decision.*

- **Spectrum analysis:**

  Different spectrum holes have different properties over time. Not only the radio channel changes over time, but the primary user activity is also changing over time. It is thus important to characterize some parameters which describe these variations. Among these parameters we can mention the following:

  - **Interference level:** Some channels are more crowded than others. From the level of interference on a channel, the cognitive radio could adapt its operating power in order not to interfere on the primary user.
  - **Path loss:** A cognitive radio could sens and operate on a large range of frequency. As the operating frequency increases, the path-loss becomes more important. For the same operating power, the operating range of a cognitive radio decreases as the operating frequency increases. Similarly, for the same operating power, a lower operating frequency increases the operating range of a cognitive radio and could then interfere with further primary users.
  - **Holding time:** It represents the average amount of time for a given frequency band that a secondary user could use that particular band before a primary user is likely to reappear.

- **Spectrum decision:**

  The spectrum bands being characterized, the best spectrum bands are chosen in order to satisfy the user QoS and to minimize the interference with licensed users.

One of the main contribution of cognitive radio systems is the ability to operate simultaneously in multiple frequency bands. In fact, by allowing multiple frequency access, a cognitive radio has access to more frequency resources [19]. Moreover, in the conventional transmission on a single frequency band, when a primary user starts using a given frequency band the communication of the secondary user is interrupted. However, the multiple-frequency band transmission is more robust in such a case as the communications on the other frequency bands are not interrupted [19]. The spectrum management framework should support this functionality in order to select the set of appropriate frequency bands with the best parameters.

A cognitive radio could also operate on heterogenous bands composed of licensed and unlicensed frequency bands. Different requirements are needed in the licensed and unlicensed bands. While in the licensed bands the cognitive radio is required not to interfere on the primary user's transmissions, on the unlicensed bands where all the users have the same access right, other spectrum sharing techniques are required. Therefore, during the spectrum decision step, the spectrum management framework should take into account the different characteristics over the heterogeneous environment.

3. **Spectrum mobility**

If a primary user starts operating on frequency band, the secondary user has to stop its operation on the corresponding frequency band and to transit its operation into a new spectrum hole. This operation is refered to as *spectrum handoff.* The transition during a spectrum handoff should be done smoothly and as quickly as possible in order to first of all minimize the interference with primary user and secondly minimize the degradation of the cognitive radio's current communication. The cognitive radio should then constantly look for alternative spectrum holes.

4. **Spectrum sharing**

   Since there is more than one cognitive radio user seeking the available frequency holes, sharing mechanisms should be implemented in order to avoid interference among cognitive radio users. The goal is to find a balance for a cognitive radio between its self-goal of transferring informations in the best way and the altruistic goal to share the available frequency resources in an equal basis between the different cognitive radio users. The sharing mechanism could be done either in a centralized or a distributed way. In the centralized case, a central entity controls the allocation of the available frequency resources to the cognitive radio users. This can be done by constructing a spectrum allocation map based on the informations on the spectrum, sensed by cognitive radio users and sent to the central entity. The distributed spectrum sharing could be considered in case where the construction of an infrastructure for the central approach is not preferred. In this case, direct cooperation between cognitive radio users determine the spectrum allocation mechanism.

   It has been shown that a cooperative approach for the spectrum sharing results in a more efficient utilization of the spectrum and a better fairness between users [20, 21]. However the cooperative approach necessitates a high amount of information exchanges among users [20–23]. As a result a trade off should be considered between the cooperative and the non-cooperative approaches in order to minimize the exchange of information between users for a fair and efficient utilization of spectrum.

Depending on the spectrum access technique, the spectrum sharing could be classified as *overlay spectrum sharing* and *underlay spectrum sharing.* In the overlay spectrum sharing case, non activity from a secondary user in a frequency band is tolerated if it is occupied by a primary user [22–24]. In the underlay spectrum sharing case, the transmission of a secondary user in a frequency band occupied by a primary user is tolerated if its transmission power does not increase the level of acceptable noise at the primary user receiver [25].

1.1.1 Architecture and Communication in Cognitive radios

Globally, two types of architectures could be considered for the deployment of a cognitive radio network:

1. **Secondary network deployed on primary network resources:**

   This is the classical approach for the architecture of a cognitive radio system. In this case the cognitive radio network is deployed in the same spectrum resources than an existing primary licensed network (figure 1.4). The primary network has an exclusively right for the access to the spectrum. Neither the primary base station nor the primary users do not have any communications with the secondary network and no modification is needed on the primary network for the deployment of the unlicensed secondary network. The secondary network has access to the spectrum resources of the primary network in an opportunistic way without interfering with the communications of the primary network.

2. **Two networks deployed on the same unlicensed bands:**

   The cognitive radio approach could also be used in the unlicensed

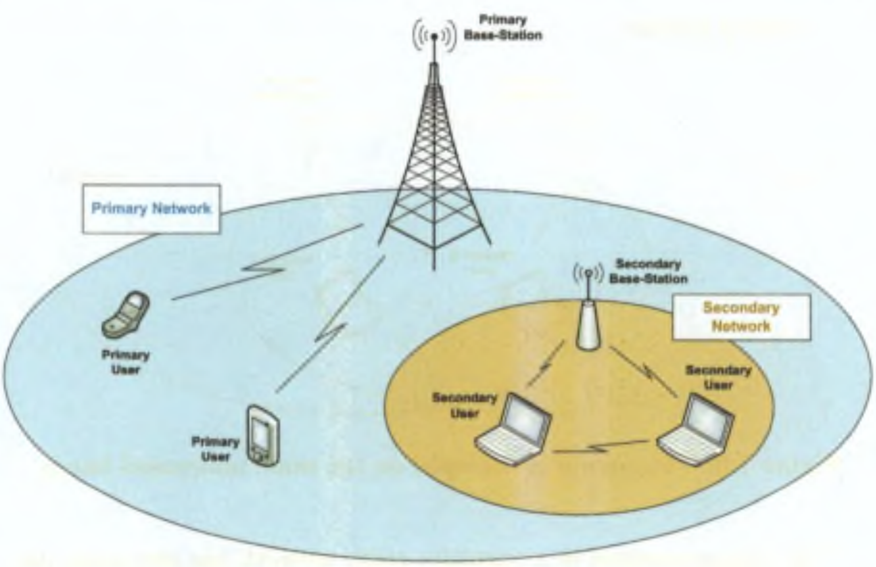

Figure 1.4: Secondary network deployed on a primary network's resources

frequency bands where no primary licensed network exists. In this case the main goal is to make possible the deployment of two or more different unlicensed networks sharing the same unlicensed spectrum resources in the best efficient way (figure 1.5). The Industrial, Scientific and Medical (ISM) band is an exemple of the unlicensed band where many different technologies exist and their mutual interference caused by their simultaneous operation in this band decreases their overall performances. A cognitive radio approach could be implemented in these technologies in order to more efficiently share the spectrum and increase the overall QoS. In this architecture, there is not any primary network and all the networks have the same spectrum access right. The cognitive radio users detect the signal received from other cognitive radio users. Fair spectrum sharing policies and techniques assure the fair and efficient co-existence of these different networks in the same frequency portion.

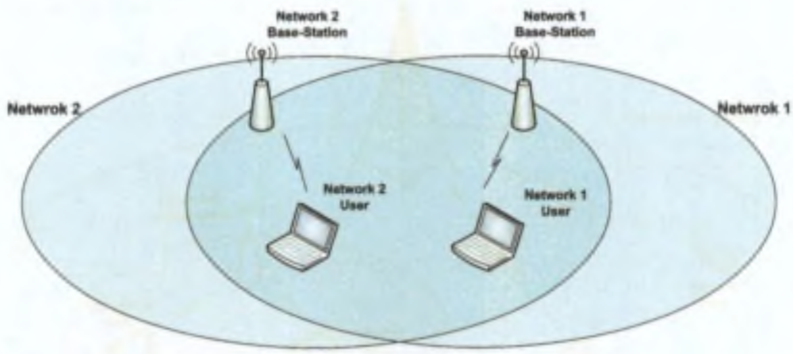

Figure 1.5: Two networks deployed on the same unlicensed bands

The communication in a cognitive radio network has also some particularities which are not present in classical communication systems. In the following, some of these particularities are listed:

- *Common Control Channel (CCC)*

  Similarly to classical communication systems, in cognitive radio systems, a CCC is needed e.g. in order to establish the communication between the transmitter and the receiver, to establish the communication with a central entity or to exchange sensing information among users.

  While in classical communication systems the CCC is implemented on a fixed frequency portion of the spectrum. In a cognitive radio approach, as all the channels are licensed to the primary network, a fixed CCC approach is not feasible anymore. As a result, other techniques should be considered in the cognitive radio case.

- *Routing*

  In cognitive radio networks, in case of a multi-hop communication, the available frequency bands may be different from one hop to another. Therefore a collaboration should be performed between the spectrum decision and the routing. The end-to-end route may consist of multiple hops implemented on different spectrum bands.

- *The coordination between the sensing and the communication steps*

  The process of spectrum sensing should be correctly synchronized with the communication process. A cognitive radio device can not permanently sens the spectrum as this operation is time and energy consuming specially in the case where a large portion of the spectrum should be sensed. Moreover, during the sensing step, the communication should be interrupted which may degrade the system performances. The sensing and the communication steps should then be carefully coordinated with each other. The performances could be improved by considering multiple radios at the cognitive radio terminal so that one of the radios exclusively performs the sensing operations [26]. This solution however, increases the cost and complexity of the system.

- *Mobility effect on the communication*

  As mentioned previously, during a spectrum handoff, the communication is stopped. The spectrum handoff results in latency which could degrade the communication performances. Moreover, a change in the operating frequency results in new channel parameters such as path-loss, interference, holding time, etc. The communication protocols should take into account these informations.

1.1.2 Cognitive Radio applications

In the following, some of the potential applications of cognitive radio networks are listed.

- *Leased network*

Some of the frequency bands allocated to the existing technologies are currently under-utilized by telecommunication operators while they have been acquired with high costs. In order to make more profits from this investment, the existing operators could lease these under-utilized resources to some secondary operators who work on a cognitive radio approach. The secondary operator makes it possible for secondary users to have opportunistically and dynamically access to the same frequency portion than the primary operator without interfering the communications inside the primary operator's network [27].

Local Area Networks (LAN) could be deployed in these underused licensed bands in order to avoid working on unlicensed bands like ISM bands which are completely congested for now.

- *Cognitive mesh network*

  In a wireless Mesh network, where the traffic is relayed by relay nodes, high capacity is required if the network density increases [28]. A cognitive network approach make it possible for relay nodes to have access to higher frequency resources and to satisfy the capacity requirements. By adding temporary or permanent spectrum to the infrastructure links used for relaying, the capacity and the coverage of wireless Mesh networks could be increased in case of high trafic load [29, 30].

- *Military network*

  The cognitive radio approach could also be used in military networks where a high degree of security is required in communications. By performing spectrum handoff, the cognitive terminals could find the best available frequency bands for their use. Moreover, in the hostile radio environment of the battlfield, the military cognitive radio could randomly adapt its communication parameters based on the variation in the radio environment.

- *Emergency network*

  The new emergency communication systems require the capacity of transferring a high volume of multimedia traffic including, voice, video and data. In order to handle these data, a significant portion of the frequency spectrum is needed. The cognitive radios, by their capacity of working on different portions of the unused licensed frequency spectrum, give access to the needed frequency resources [31]. Reliable communication with minimum latency should however be guaranteed for this kind of applications.

The emergence of wireless systems with cognitive capabilities are attested by the establishment of some standards in this field. IEEE 802.22 is considered as the first standard on cognitive radio technology [32, 33]. This standard considers the implementation of fixed-to-multipoint Wireless Regional Area Network (WRAN) on the UHF/VHF TV frequency bands between 54 and 862 MHz. Cognitive radio techniques are used in order to opportunistically communicate on geographical unused frequency bands, allocated to Television Broadcast service without interfering with this service. The main aim of this standard is to bring broadband access to populations living in hard-to-reach areas. This standard was finalized and published in July 2011 [34].

The standard IEEE 802.11k, considered as a cognitive extension of the Wi-Fi is another standard which uses cognitive capabilities [35]. In this standard, the traffic is better distributed within a Wi-Fi network by choosing the most appropriate Access-Point. Classically, a Wi-Fi user with presence of multiple Access Points (APs) will connect to the AP with the strongest signal. With the new IEEE 802.11k standard, if the AP with the strongest signal is overloaded by other Wi-Fi users, another

AP with weaker signal but less congested will be chosen.

IEEE 802.11af referred also to as White-Fi, is another standard with cognitive radio capabilities. This standard is still under study and would enable the implementation of Wi-Fi technology on the unused TV frequency bands. As the frequency bands allocated to the TV broadcasting services are at lower portions of the spectrum (under 1 GHz), the main advantage of this technology would be to increase the coverage area of current Wi-Fi networks by keeping the same transmission power or to reduce the transmission power while keeping the same coverage area. By enabling an opportunistic access to the TV spectrum, this standard would also increase the available frequency resources and would then enhance the performance of Wi-Fi systems.

1.2 Spectrum Sensing in Cognitive Radios

As exposed in the previous section, one of the most important requirement of a cognitive radio is the ability to detect reliably and quickly the presence or not of a signal from a primary user in a given frequency band. In order to avoid any interference with the primary users, a reliable detection is primordial. Different techniques exist for the detection of primary user's signal. Each technique has its own drawbacks or advantages. The principal aim of all the detectors is to distinguish between two hypothesis:

$$\begin{cases} H_1 & : \text{The presence of a signal transmitted from a primary user} \\ H_0 & : \text{The absence of a signal transmitted from a primary user} \end{cases} \tag{1.1}$$

The hypothesis H_0 represents the opportunity for a secondary user to use the available frequency band. Under H_1, the primary transmitted signal $s(t)$ is received at the cognitive radio receiver antenna over channel h and the additive zero mean white Gaussian noise $n(t)$. The received signal $r(t)$ is then given, under the two hypotheses, by:

$$\begin{cases} H_1 \ : \ r(t) \ = \ hs(t) + n(t) \\ H_0 \ : \ r(t) \ = \ n(t) \end{cases} \tag{1.2}$$

For most detectors, the detection performance is generally characterized by the following probabilities:

- *Probability of false alarm:* $P_{FA} = P(decision = H_1|H_0)$

  It represents the probability of detecting a signal from a primary transmitter while there is in fact no primary signal.

- *Probability of missed detection:* $P_{md} = P(decision = H_0|H_1)$

  It represents the probability of not detecting a signal from a primary transmitter while there is in fact a primary signal.

- *Probability of detection:* $P_d = P(decision = H_1|H_1)$

  It represents the probability of detecting a signal from a primary transmitter while there is in fact a primary signal.

A low P_d will result in missing the presence of the primary user with high probability which in turn increases the interference to the primary user. As the false alarms increase the number of missed-opportunities, a high P_{FA} results in a low spectrum utilization.

1.2.1 Spectrum sensing techniques

The different spectrum sensing techniques could be classified as *coherent* or *non coherent* detectors and *narrowband* or *wideband* detectors (Figure 1.6).

While coherent detectors requires an a priori knowledge of the primary signal, no a priori information on the primary signal is required for the non coherent detectors. The narrowband and the wideband classification is based on the bandwidth of the spectrum which is sensed.

	Coherent		Non-Coherent	
Narrowband	Matched-Filter Detection	Cyclostationary Feature detection	Energy Detection	
Wideband				Compressed Sensing

Figure 1.6: Classification of spectrum sensing techniques

Some of the most popular sensing techniques are: *Match-Filter Detection, Cyclostationary Detection, Compressed sensing* and *Energy Detection.* The classification of these techniques at each class of detector is given in figure 1.6. The description of these techniques is given in the following:

- *Matched-filter detection:*

  When the information on the primary user signal is available at the secondary terminal side, the Matched-filter detector is the optimal detector in stationary white Gaussian noise since it maximizes the received Signal-to-Noise Ratio (SNR) [36]. In this technique, the received signal samples $r(n)$ are correlated with the expected transmitted signal samples $s(n)$. The statistic of test is then given in the Base-Band representation by:

$$T = \sum_{n=0}^{N-1} r(n)s(n). \tag{1.3}$$

  This value has to be compared with a given threshold in order to decide the presence or not of a primary signal. The main advantage of the Matched-filter detector is that it requires low computational load. However as a coherent technique, the matched-filter detector requires some a priori informations about the primary user signal.

If these informations are not accurate the sensing performances are degraded. Moreover, in a cognitive radio approach where the secondary network has no access to the primary network, this detector is not feasible.

- *Energy detection:*

  Energy detector is the most popular sensing technique and has been widely applied in the past since it does not require any a priori knowledge about the transmitted signal and has a low complexity [37–39].

  This technique consists in computing the energy of the received signal. In order to measure the energy of the signal, the output signal of the bandpass filter is squared and integrated over an observation time. The output of the integrator is compared with a given threshold in order to decide the presence or not of a primary signal.

  Energy detection is used in chapter 2 of this work. In case where the secondary terminal is not aware of the primary transmitted signal and the power of the random Gaussian noise is known at the cognitive radio receiver, this technique is the optimal technique according to the *Neymen-Pearson* criterion [15]. The Neymen-Pearson criterion is a binary hypothesis testing scheme that maximizes the probability of detection P_d for a given probability of false alarm $P_{FA} = \alpha$ [37]. The decision is based on Likelihood Ratio Test (LRT). For a given variable x which follows two different statistics under H_1 and H_0, the hypothesis H_1 is decided if :

$$L(x) = \frac{f(x|H_1)}{f(x|H_0)} > \lambda \tag{1.4}$$

  where the $f(x|H_1)$ denotes the *probability density function* (pdf) of x under the H_1 hypothesis and the threshold λ is found from:

$$P_{FA} = \int_{x:L(x)>\lambda} f(x|H_0).dx = \alpha \tag{1.5}$$

Energy detection has some drawbacks. First of all, it has been shown that the number of samples required for the detection is inversely proportional to the square of the SNR [40]. Therefore, at the very low SNR regions, this technique requires a very high number of samples in order to achieve a good detection performance. It means that more time is needed for the sensing. Another drawback of Energy detection is that it requires the knowledge of the noise variance. In case of uncertainty on the noise variance, the performances of energy detection are considerably deteriorated. An uncertainty on the knowledge of the noise variance leads to the appearance of what is called an "SNR wall" [41]. It represents the limit value of SNR under which, the detector is unable to detect.

Another shortcoming is that energy detector can only determine the presence or not of a signal but cannot differentiate the types of the signal or for instance, if it is a primary or a secondary signal. Finally, Energy detector is a narrow-band detection technique and cannot be used to detect in wide range of frequencies.

- *Cyclostationary feature detection:*

  This detector uses the cyclostationary properties of the signals transmitted from the primary users [16–18]. Modulated signals are in general coupled with sine wave carrier, pulse train, hopping sequences or cyclic prefixes which results in some embeded periodicity. The mean and the autocorrelation of the modulated signals exhibit periodicity. This is not the case of the stationary noise. Since most of the signals used in wireless telecommunications are modulated, this technique differentiate the modulated signal from the stationary noise. This periodicity behavior is reflected in a particular function called spectral correlation density function.

For this detector, the hypothesis H_0 and H_1 could be expressed as:

$$\begin{cases} H_1 : & \text{The detected signal is cyclostationary} \\ H_0 : & \text{The detected signal is stationary} \end{cases} \tag{1.6}$$

This detector is thus robust to the noise variance uncertainty and compared to energy detector, achieves better performances at lower SNR regions. Moreover, this detector has the ability to distinguish different types of received signals based on their modulation and could thus also distinguish between the primary and the secondary signals provided that a priori knowledge about both signals is available at the detector [16, 17].

This detector requires however a high computational load and significantly long sensing time. Because of this complexity, cyclostationary feature detector has been less commonly implemented than the energy detector.

- *Compressed sensing:*

  The compressed sensing is a technique which facilitates wide band spectrum sensing. Energy detection and cyclostationary detection, uses a set of observation in the band of interest sampled at the Nyquist rate by an Analog to Digital Converter (ADC). Due to hardware limitations of the sampling rate, only one band at a time could be sensed by these techniques. In order to do wideband sensing, these techniques should either sens all the spectrum or to have multiple RF frontends in order to sens multiple bands. These solutions considerably increase the sensing time or the cost and complexity of the system. Compressed sensing method is proposed as a solution to relax the ADC speed requirement by enabling the sampling of wideband signals at sub-Nyquist sampling rate [42–44]. By considering sparse wideband primary signals in the spectrum, this method is based on a random sampling at a sub-Nyquist sampling rate. However such random sampling method necessitates the implementation of new ADC architectures which enable random sampling. Moreover, by using compressed sensing, because of the limited number of samples, a weak primary signal near a strong primary signal may not be properly reconstructed and detected in a wideband spectrum.

1.2.2 Some issues in spectrum sensing

Several elements could reduce the performances of spectrum sensing. In fact, the cognitive radio systems are deployed in a multi-path environment where the multi-path fading and shadowing of the primary received signals considerably attenuate the amplitude of the received signals and could highly deteriorate the sensing performance. These effects are occurring in the wireless propagation channel lying between the primary transmitter and the secondary receiver. A brief description of the wireless propagation channel and its effects on the spectrum sensing is exposed in the following.

The wireless propagation channel

In wireless communication systems, the *wireless propagation channel* refers to as the electromagnetic propagation environment that lies between a transmit and a receive antenna. By exciting a transmit antenna with a sinusoidal current, an electromagnetic wave is transmitted from the antenna. This electromagnetic wave will interact with the environment surrounding the transmitter and the receiver. When arriving at the receiver, the electromagnetic wave induces a current in the receive antenna. A baseband signal at the input of a transmitter is linked with received signal at the output of a receiver through the baseband channel *impulse response* $h(t)$:

$$y(t) = h(t) * x(t) + n(t) \tag{1.7}$$

where $x(t)$ and $y(t)$ are, respectively, the transmitted and the received signals and $n(t)$ denotes the baseband additive noise at the receiver. The operator $*$ is the convolution operator. Similarly the frequency-dependent transfert function $H(f)$is obtained by applying a Fourier transform on both sides of equation 1.7:

$$Y(f) = H(f)X(f) + N(f) \tag{1.8}$$

where Y, H, X and N denote the Fourier transform of respectively y, h, x and n.

When an antenna is excited, it transmits waves in all directions. The different waves go through different propagation paths and interact differently with the surrounding environment before arriving at the receive antenna. This results in different waves having different arriving times at the receiver. The channel impulse response is then made of different propagation paths. This is shown in figure 1.7 where an exemple of the measured impulse response is presented. The temporal resolution of the impulse response depends on the bandwidth of the system. The larger the bandwidth of the system is, the more precise the temporal resolution of the impulse response will be. A *narrow band* system refers to as a system where the different propagation paths could not be distinguished and the impulse response has only one tap. In a *wideband* system where the system has a larger bandwidth, the different propagation path are resolved at the receiver and the impulse response is made of many taps.

Different effects could be considered in a given propagation path. Beside the effect of the propagation channel on the propagation path, one

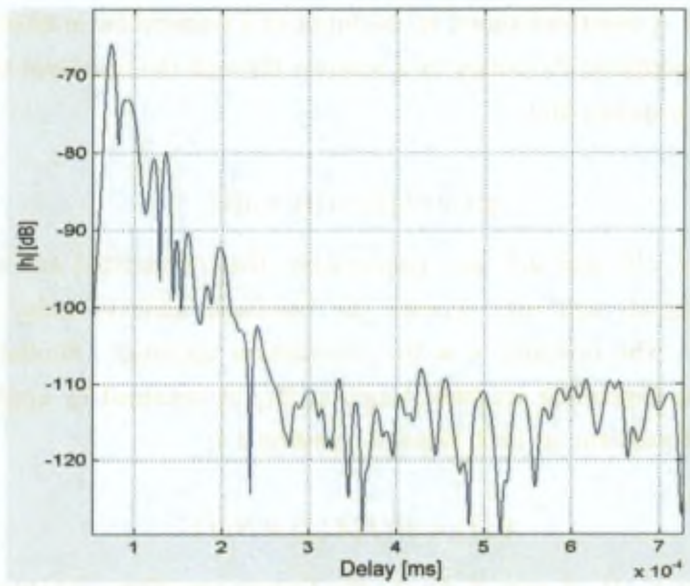

Figure 1.7: Measured channel impulse response

should note that the emission or the reception properties of an antenna depend on the direction of emission or reception of the wave and these effects should also be considered for a given propagation path.

The interaction between the transmitted wave and the propagation environment depends on many parameters and may be very complex. A deterministic characterization of the propagation channel is thus a very difficult if not impossible task. The propagation channel between two different moments will not be the same if a change is occurring in the environment e.g if someone or something has moved meanwhile. Any change in the environment will necessitate a new characterization of the propagation channel.

While a deterministic characterization of the propagation channel is infeasible, a statistical characterization of the propagation channel is a more achievable task. This requires, however, that some channel parameters have constant statistics over some space or time intervals.

In contrast to the classical Single-Input Single-Output (SISO) wireless systems where a single antenna is used at the transmitter and the receiver, *Multiple-Input Multiple-Output (MIMO) wireless systems* are referred to as the communication systems where multiple antennas are used at the transmitter and/or the receiver. The idea behind the MIMO systems is to benefit from the spatial diversity of the propagation channel in order to improve the performances of wireless communication systems.

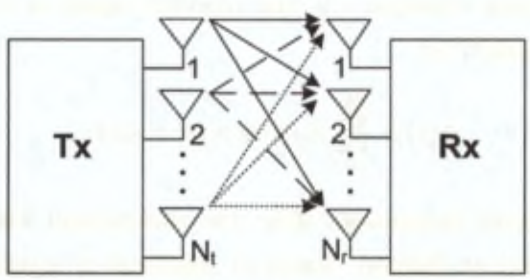

Figure 1.8: $N_t \times N_r$ MIMO sub-channels

Let us consider a MIMO systems where N_R antennas are used at the receiver and N_T antennas are used at the transmitter (figure 1.8). The MIMO channel impulse response $H(t)$ is in this case given by a matrix containing the channel impulse responses between the different antennas at the transmitter and at the receiver. The relation 1.7 becomes in this case:

$$Y(t) = H(t) * X(t) + N(t) \tag{1.9}$$

where Y is an $(N_R \times 1)$ matrix containing the received signals at the received antennas, X is an $(N_T \times 1)$ matrix containing the transmitted signals at the transmit antennas and N is an $(N_R \times 1)$ matrix containing the noise at each of the receive antennas. The matrix H links the different elements of Y with the different elements of X through the channel impulse response between these elements and is given by:

$$\begin{pmatrix} h_{11}(t) & h_{12}(t) & ... & h_{1N_T}(t) \\ h_{21}(t) & h_{22}(t) & ... & h_{2N_T}(t) \\ . & . & . & . \\ . & . & . & . \\ . & . & . & . \\ h_{N_R1}(t) & h_{N_R2}(t) & ... & h_{N_RN_T}(t) \end{pmatrix}. \tag{1.10}$$

where $h_{ij}(t)$ denotes the channel impulse response between the j^{th} transmit and the i^{th} receive antenna.

By developing equation 1.9, the received signal at the i^{th} receive antenna is obtained by:

$$y_i(t) = \sum_{j=1}^{N_T} h_{ij}(t) * x_j(t) + n_i(t). \tag{1.11}$$

Three different phenomena affect the narrowband wireless communication channel at different scales in temporal or spatial dimension. These phenomena could considerably deteriorate the performances of spectrum sensing in cognitive radio systems:

- *Small-Scale Fading*

  In narrowband systems, the different multi path components are added up at the receiver. The superposition of these multipath components could be either constructive or destructive as they have different phases. The phases mainly depend on the run-length of the multipath components and thus to the position of the transmitter, the receiver or the interacting objects in the propagation environment. For this reason, the amplitude of the total primary received signal changes over time or space if any of the primary transmitter, secondary receiver or the interacting objects are moving. The phenomenon associated with the fading of the amplitude of the received signal due to the destructive interference of the multi-path components at the receiver is called *small-scale* *fading* [45, 46]. Even a small movement could considerably effect the signal amplitude. At 2 GHz a movement of less than 10 cm can already results in a large change in the signal amplitude. By assuming that the multi-path components arrive at the receiver from all directions, and their amplitudes are distributed according to the same statistical distribution, if the channel is sampled at different spatial position in a local zone, the channel samples will have a complexe normal distribution and the amplitude of the channel samples will follow a Rayleigh distribution.

- *Large-Scale Fading, Shadowing*

  Another phenomenon which degrades the performances of spectrum sensing is the large-scale fading also called shadowing [45]. Imagine, for exemple a mobile station moving at constant distance with respect to a base station. If the mobile station goes behind a large obstacle such as a building there will be a considerable attenuation of the received signal at the mobile station. This is shown in figure 1.9 where the Line-Of-Sight (LOS) direction between the Base Station (BS) and the Mobile Station (MS) is obstructed at the position b where the power of the received signal is dropped. This is due to the fact that the MS is at the radio shadow of the obstructing object and the waves going through or around the obstruction object are highly attenuated. The MS has to move a large distance (from a few meters to some hundreds of meters) in order to get out of the radio shadow. For this reason this phenomenon is also called *large-scale fading*. Note that shadowing is not only due the obstruction of a LOS path but can occur for any multipath component. The Shadowing effects are superposed to the small-scale fading effects and can considerably deteriorate the spectrum sensing in cognitive radio systems. This is illustrated in figure 1.10, where the LOS direction between the primary transmitter and one of the cognitive radio receiver is blocked by a large object. As a result, the cognitive radio receiver will not detect the transmission of the primary transmitter in a given frequency band and may start communicating on this frequency band causing interference on its nearby primary users.

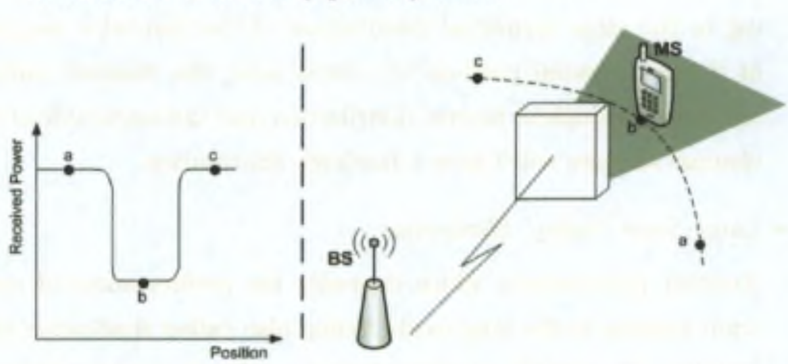

Figure 1.9: Illustration of the shadowing principle

- *Path-loss* The mean amplitude of the received signal is attenuated as the distance between the transmitter and the receiver increases. This phenomenon is called *path-loss*. For a given propagation environment, the attenuation is proportionnal to $(\frac{1}{d^n})$ where d is the distance between the transmitter and the receiver and n is the path-loss exponent. The path-loss exponent depends on the propagation environment(e.g. $n = 2$ for free-space or $1 < n < 2$ for indoor corridor or outdoor street canyon environments). As the distance between the primary transmitter and the secondary terminal increases, the secondary terminal will be less likely to detect the signals from primary transmitter since these signals are attenuated as a function of distance. This leads to the *hidden primary user problem*. The hidden primary user problem appears when a secondary transmitter is located outside the transmission range of a primary base-station while a primary receiver is located inside

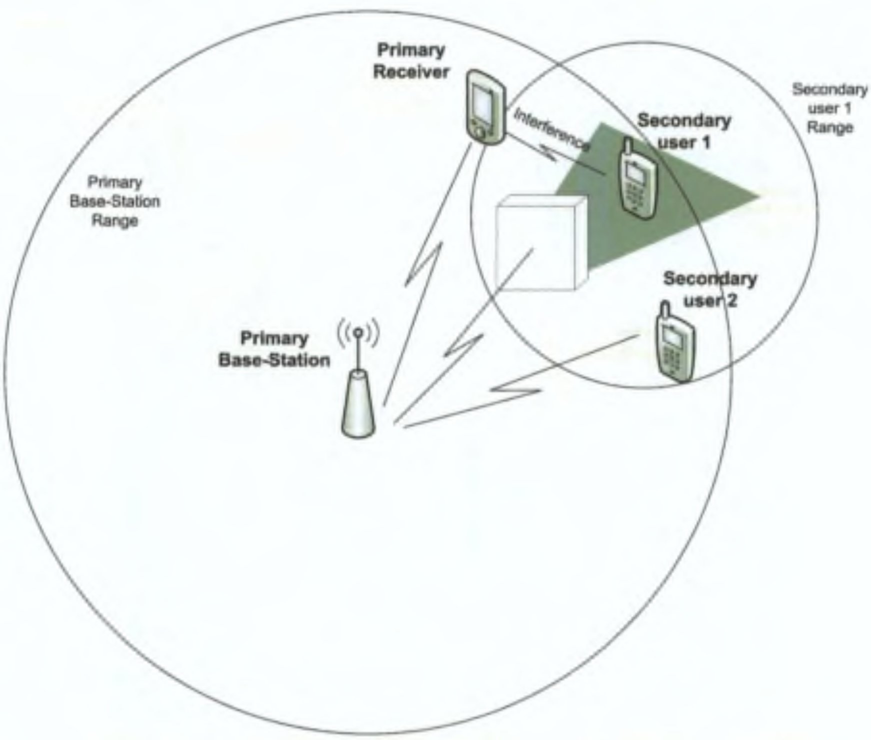

Figure 1.10: Illustration of the large-scale fading

the transmission range of the secondary transmitter [47]. This is illustrated in figure 1.11. In this case, the secondary transmitter does not detect the presence of the signal from the primary base-station in a given frequency band and will therefore transmit in this frequency band causing interference in the primary user situated in its transmission range.

The superposition of the attenuation effects described above could considerably degrade the performance of spectrum sensing in cognitive radio systems and should be taken into account in the design of these systems. Multi-user and multi-antenna concepts were proposed in order to overcome the spectrum sensing limitations due to the multipath

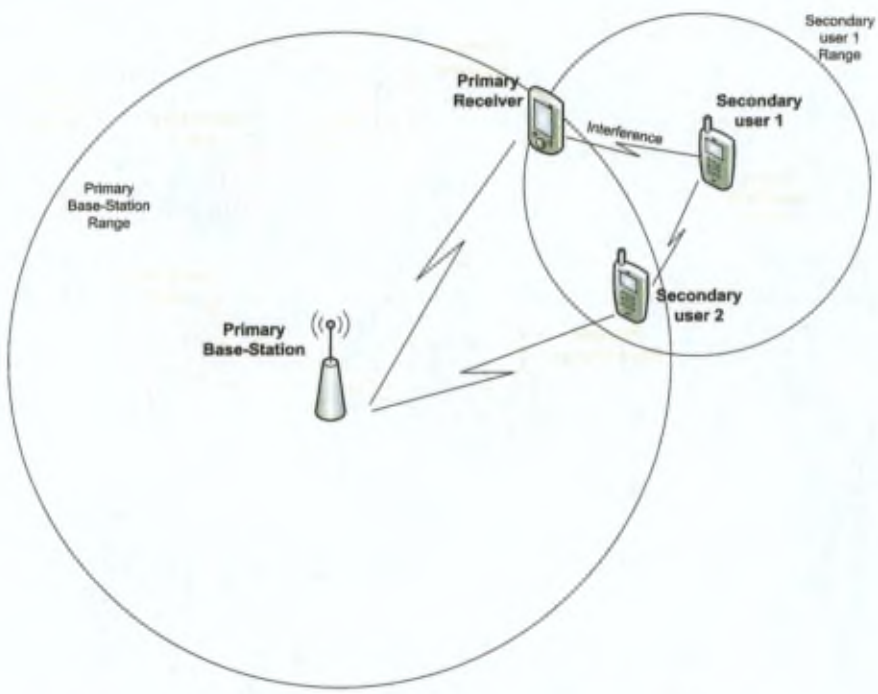

Figure 1.11: Illustration of the hidden primary user problem

aspect of the radio channel.

Multi-user spectrum sensing

The cooperation between different secondary users could improve the spectrum sensing performance [16,48,49]. In cooperative detection, cognitive radio users share with each other their observation on the primary user signals. As the different secondary users are located in different locations, they experience different fading. Due to spatial diversity, it is unlikely that all the receivers experience at the same time multipath fading or the hidden primary user problem. This is illustrated in figure 1.9 and 1.11. In figure 1.11 the secondary user 1 does not detect the primary transmitter signal in a given frequency band as it is out of the transmission range of the primary base station. However the secondary user 2 is located inside the transmission range of the primary base station and is thus able to detect the primary transmitted signals. The secondary user 2 could share its observation with the secondary user 1 so that it avoids transmitting in the given frequency band. In figure 1.9 while the secondary user 1 does not detect the signals from the primary base station in a given frequency band because of the shadowing, the secondary user 2 does not experience shadowing and detects the primary base station's signal. By sharing the spectrum observation of the secondary user 1 and 2, the interference on the primary user by the secondary user 1 is avoided.

By exploiting spatial diversity in the observations of spatially separated cognitive radio users, the overall sensing performances are considerably increased. This improvement could also be analyzed from a hardware point of view. Due to small-scale and large-scale fadings, the received SNR at the secondary user could be extremely low. The sensitivity of the cognitive radio receiver should then be very high in order to detect these extremely low signals. This will complicate the hardware implementation and will increase its cost. Moreover the sensitivity cannot be constantly increased and there is a SNR limit under which the sensitivity can not be increased anymore [50]. The sensitivity requirements and the hardware limitation issues that it causes could be considerably relaxed by using cooperation among cognitive radio users. The cumulative effects of small-scale and large-scale fading could be reduced by cooperative sensing. As a result the cooperative cognitive radio receiver should only be sensitive to the signal attenuation due to the path-loss [49] (figure 1.12). The hardware complexity and cost could thus be considerably reduced in cooperative cognitive radios.

Cooperative detection can be implemented either in a centralized or a distributed way [51, 52]. In the centralized approach, the sens-

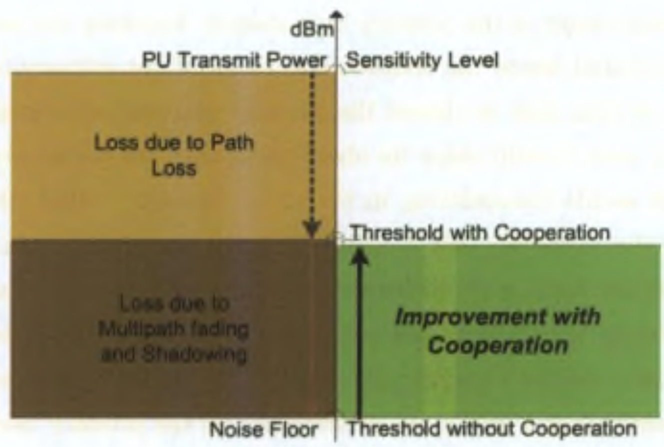

Figure 1.12: Sensitivity improvement by cooperative detection [2]

ing informations gathered by all the users are transfered to a central entity which in turn develop and transfer to the cognitive radio users, information about the available frequency resources. In the distributed approach, the sensing informations are exchanged among the cognitive radio users directly or through other cognitive radio users. However, cooperation creates some overheads such as the time and energy needed for the cooperation.

Multi-antenna spectrum sensing

Multi-antenna sensing has been proposed as an interesting way to reduce channel small-scale fading effects by introducing spatial diversity into the spectrum sensing. In the multi-antenna sensing, a set of spatially separated antennas are used at the cognitive radio receiver.

The diversity gain is maximum in a multipath environment, if the receive antennas are separated such that each antenna experiences uncorrelated fading processes. It has been shown that in a uniform scattering environment with omni-directional receive and transmit antennas, the minimum antenna separation in order to have uncorrelated fading on each antenna is approximately one half wavelength [45].

The spatial diversity in multi-antenna systems could be used in order to reduce the small-scale fading effects. In order to illustrate this statement let's consider two spatially separated antennas. If the received signals at these two antennas are uncorrelated with respect to each other, if the signal received at one of them is in a deep fade, the probability for the signal received at the other one to be in a deep fade is very low. By choosing e.g. the highest received signal, the small scale fading effects could be considerably reduced.

Two possible approaches could be used in order to make use of multi-antenna diversity:

- *Hard combination*

  The sensing technique is applied separately at the observations of each antenna. The overall decision concerning the presence or the absence of a primary signal in a given frequency band is obtained by combining the decisions obtained for each antenna.

- *Soft combination*

  The signals received at all the antennas are combined in a way to reduce the small-scale fading effects. The decision concerning the presence or not of a primary user is obtained by applying a sensing technique on the combined signal. Better performances are obtained with the soft combining technique if an appropriate combining technique is used. Different combining techniques have been proposed so far in the literature. Some of them are listed in the following:

  - *Selection Combining (SC)* In this technique the antenna with the highest SNR will be chosen at the output of the combiner. By assuming the same noise for all the antennas, the antenna which receives the signal with the highest power will be chosen at the combiner output.

- *Square-Law Combining (SLC)*

  Let $r_i(t)$ be the signal received on the i^{th} antenna (by considering a total of M antennas). By this technique, the combined signal $y(t)$ at the combiner output is given by:

$$y(t) = \sqrt{\sum_{i=1}^{M} r_i^2(t)} \tag{1.12}$$

- *Maximum Ratio Combining (MRC)*

  Let h_i be the channel between the primary transmitter and the i^{th} cognitive radio antenna. By this technique, the combined signal $y(t)$ at the combiner output is given by:

$$y(t) = \sum_{i=1}^{M} h_i^* r_i(t) \tag{1.13}$$

The fading effects are best reduced by the MRC technique since it maximizes the SNR at the output of the combiner. However MRC is a coherent combining technique which requires the channel informations at the cognitive radio receiver. In a cognitive radio scenario where there is non-interaction between the primary and the secondary networks this technique is less feasible. SLC and SC techniques are non-coherent combining techniques and do not therefore require informations on the channel between the primary transmitter and each antenna of the cognitive radio receiver. Better combining performances are obtained for the SLC technique compared to the SC technique [45].

The multi-antenna sensing could be combined with the multi-user sensing by having a multi-antenna system at each cognitive radio user.

The multi-antenna sensing will considerably reduce the small-scale fading effects and could then reduce the number of users needed in order to achieve a given performance compared to a multi-user single antenna case. Also in case where the deployment of a cooperative infrastructure is not preferred, the use of a multi-antenna system could already improve the sensing performances [53–59].

Multi-polarized spectrum sensing

Another way to profit from the channel diversity is to use polarized multi-antenna systems. In polarized multi-antenna systems, the polarization diversity is used in order to lower the inter-channel correlation. An advantage of using polarization diversity instead of spatial diversity in multi-antenna systems is that the terminal size could be considerably reduced. In a cellular 1.8 GHz GSM scenario for instance, an inter-antenna spacing of at least 8cm is required. While at the base station the compactness of the terminal may not be an issue, this large spacing between antennas will not be feasible in a mobile terminal where a compact system is needed. Moreover in order to lower the inter-antenna correlation the inter-antenna spacing should be increased in case of correlated channels. This will increase the terminal size and makes the practical implementation of the system more difficult [60–67]

This problem could be resolved by using co-located cross-polarized linear antennas which will make the system much more compact [60, 61, 63]. In fact it has been shown that low inter-antenna correlation is obtained when using perpendicularly polarized antennas [46, 60, 61, 68].

The use of cross-polarized antennas at the secondary terminal has several advantages. First of all as mentioned previously, the use of a multi-polarized antenna system at the secondary terminal let the secondary terminal to be as compact as a single antenna system while benefiting from the low inter-antenna correlation which exists in such systems.

Secondly as the polarization scheme of the multipath components arriving at the receiver may be different, by using a set of three perpendicularly polarized co-located antennas at the secondary terminal all the incident polarizations could be received. We show in chapter 3, that the polarization scheme of the received signal could completely be obtained by using a set of three perpendicularly polarized antennas.

Multi-polarized antenna systems have also some other particularities compared to classical multi-antenna systems using spatial diversity. These particularities could be used in order to improve the spectrum sensing performances. We'll see in chapter 5, how a particular property of multi-polarized antenna systems could be used in order to define a new spectrum sensing method.

In this work, the polarization of electromagnetic waves is used in order to improve the spectrum sensing of cognitive radio systems. This study requires the characterization of the multi-polarized channel and particularly the study of the polarization of electromagnetic waves in the propagation channel.

1.3 Polarization of electromagnetic waves

Let us consider a plane wave propagating through growing z axis. This wave could be represented by its two components at x and y axis:

$$\vec{E}(z,t) = E_x cos(\omega t - \beta z + \phi_x)\vec{1_x} + E_y cos(\omega t - \beta z + \phi_y)\vec{1_y} \qquad (1.14)$$

where E_x and E_y are the electric field components along the x and y axis respectively, ϕ_x and ϕ_y are the phase of the electric field along x and y axis respectively and β denotes the wave number. In case of a plane wave, there is no electric or magnetic field component in the direction of propagation. The electric and magnetic fields are perpendicular and proportional to each other. Both the electric and magnetic fields are perpendicular to the direction of propagation.

The two components of $\vec{E}$ in the plane $z = 0$, could be written as:

$$E_x(0,t) = E_x cos(\omega t + \phi_x) \tag{1.15}$$

$$E_y(0,t) = E_y cos(\omega t + \phi_y) \tag{1.16}$$

The component along the x axis oscillates between E_x and $-E_x$ over time and the component along the y axis oscillates between E_y and $-E_y$ over time. As a result the tip of the electrical field at $z = 0$ moves over time in the xy plane. The locus traced over time by the tip of the electric field in the xy plane is called the *polarization* of the wave. The system of equations in 1.15 and 1.16 represents in fact the parametric equations of an ellipse. A plane wave is elliptically polarized.

Equation 1.14 can be expressed in the phasor notation as:

$$\underline{\vec{E}}(z) = \vec{E}_0 e^{-j\beta z} \tag{1.17}$$

where

$$\vec{E}_0 = \begin{pmatrix} E_{0x} \\ E_{0y} \end{pmatrix} = \begin{pmatrix} E_x e^{j\phi_x} \\ E_{0y} e^{j\phi_y} \end{pmatrix} \tag{1.18}$$

is a complex vector.

For a wave propagating in any direction $\vec{1_\beta}$, the electric field in a spherical coordinate system (figure 1.13) can be written as:

$$\underline{\vec{E}}(\vec{r}) = \begin{pmatrix} E_\theta \\ E_\phi \end{pmatrix} e^{-j\vec{\beta}.\vec{r}} \tag{1.19}$$

where $\vec{\beta}$ denotes the wave vector and E_θ and E_ϕ are complex amplitudes.

Several particular polarization cases could be developed from the general elliptical polarization case:

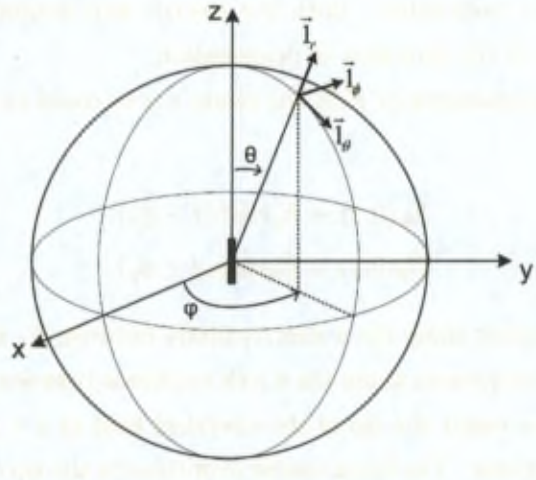

Figure 1.13: Electrical field in the spherical coordinates

1. *Linear polarization*

   In case where $E_\theta = 0$, the electrical field is directed along $\vec{1_\phi}$ axis. The polarization ellipse is in this case degenerated in a line and the polarization is called *linear polarization.* Equivalently in case where $E_\phi = 0$, the electrical field will be linearly polarized along the $\vec{1_\theta}$ axis. This is described in figure 1.14.

   Generally speaking, the wave is said to be linearly polarized if the E_θ and the E_ϕ components oscillate in phase i.e. if E_θ and E_ϕ components have the same phase ($\phi_\phi = \phi_\theta$).

2. *Circular polarization*

   If the E_θ and the E_ϕ components oscillate in quadrature ($\phi_\phi = \phi_\theta \pm \frac{\pi}{2}$) and have the same amplitude ($|E_\theta| = |E_\phi|$), the wave is circularly polarized. This is shown in figure 1.15.

3. *Elliptical polarization*

   In all other cases, the electrical field is elliptically polarized. The major and the minor axis of the polarization ellipse are not nec-

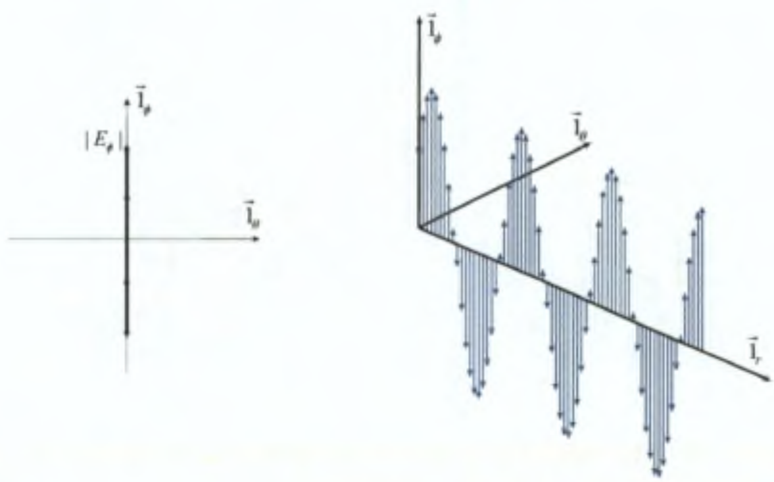

Figure 1.14: The evolution of the electrical field as a fonction of r and for a given time t for a linear polarization

essarily parallel to the $\vec{1_\theta}$ and $\vec{1_\phi}$ axis as shown in figure 1.16. When the wave is approaching to a fixed point, if the ellipse turn clockwise the wave has a left-hand elliptical polarization. The polarization is said to be right-hand elliptical in the opposite.

1.3.1 Representation of the wave polarization

The wave polarization could be represented by the **Jones' vector**. By considering the electric field representation in equation 1.19, the Jones' vector is given by:

$$\vec{E}_0 = \left(\begin{array}{c} E_\theta \\ E_\phi \end{array} \right) \tag{1.20}$$

All informations about the polarization of the wave can be obtained by the Jones' vector. The Jones' vector of a linearly polarized wave along the $\vec{1_\phi}$ is given by:

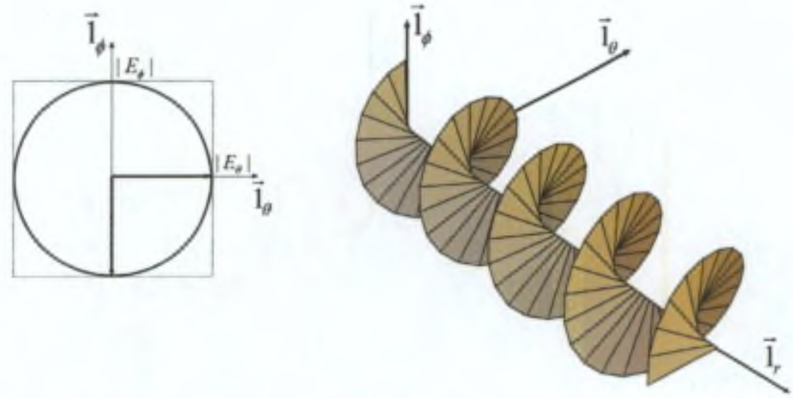

Figure 1.15: The evolution of the electrical field as a fonction of r and for a given time t for a circular polarization

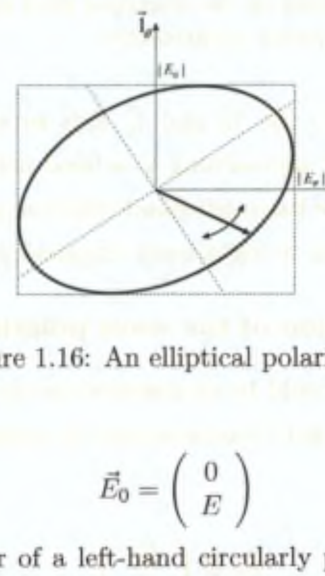

Figure 1.16: An elliptical polarization

$$\vec{E}_0 = \begin{pmatrix} 0 \\ E \end{pmatrix} \tag{1.21}$$

The Jones' vector of a left-hand circularly polarized wave is given by:

$$\vec{E}_0 = E \begin{pmatrix} 1 \\ e^{j\pi/2} \end{pmatrix} \tag{1.22}$$

The linear polarizations $\begin{pmatrix} 1 \\ 0 \end{pmatrix}$ and $\begin{pmatrix} 0 \\ 1 \end{pmatrix}$ could be used as basis functions in order to represent the Jones's vector of all the polarization states. Other polarization basis could also be defined such as the left and the right-hand circular polarizations.

Note that other methods exist in order to represent the polarization state of a plane wave. We can cite the *Stokes vector* representation and the *Poincarré sphere* representation [69]. These representations are mainly used in radar systems [70] and will not be used in the present work.

1.3.2 Antenna and propagation effects on the polarization

Different phenomena change the polarization of the electromagnetic wave transmitted from the primary base station and received at the secondary terminal. These phenomena, referred to as the *depolarization* of the electromagnetic wave, have different origins:

1. Depolarization due to the antenna

   The first change is occurring in the transmit antenna of the primary transmitter. An antenna is an electrical conductor that if excited by a time-varying current, will radiate an electromagnetic wave. The antennas are generally made in order to transmit or receive on a single polarization. For instance, a linear wire antenna which is vertically oriented should in theory transmit only on the $\vec{1_\theta}$ component. However the real-world antennas can not transmit only on one polarization and nothing on the other and there will always be some imperfection in the antennas that make them transmit also on the perpendicular polarization. For instance in the case of a vertically oriented linear wire antenna, the tiny width of the antenna creates an insignificant radiation in the $\vec{1_\phi}$ polarization.

2. Depolarization due to the orientation mis-match of the antennas:

If the transmit and receive antennas are not perfectly aligned in order to receive the same polarization, there will be a leakage between the different polarizations.

3. Depolarization due to the propagation in the channel:

   The interactions of the electromagnetic waves during their propagation in the environment surrounding the primary transmitter and the secondary receiver change the polarization scheme of the transmitted waves. This results in a leakage between the different polarizations through their propagation in the channel. As the interaction of the different multipath components with the environment is different, this results in different polarization schemes for each of the multipath components arriving at the receiver.

1.4 Channel modeling in wireless communications

The physical phenomena that change a transmitted signal through its propagation in the wireless channel are modeled by wireless channel models. Wireless channel models could be used for different reasons:

- In order to simulate the signal processing techniques, it is very important to have a precise description of the channel. It is very difficult and time-consuming to simulate the signal processing techniques in a real measurement scenario. Reproductible channel models are used in order to implement signal processing techniques without having to simulate each time in a real measurement scenario.

- Mathematical formulation of the channel could be used in order to obtain closed-form expressions of signal processing techniques which need a mathematical formulation of the channel model.

- Understanding the propagation phenomena in the wireless communication channel could be useful in order to improve the performances of wireless systems. The wireless communication systems could be optimized based on the information on what happens during the propagation in the communication channel.

The more propagation phenomena are included in a channel model the more precise that channel model will be. The channel model should be as reproductible as possible and cover different scenarios. Different channel modeling techniques have been proposed so far in the literature [71]. In the following, some of the main channel modeling techniques are explained.

1.4.1 Deterministic channel modeling

In deterministic channel models, the average values of the electric field at every location of a pre-defined environment are obtained in a deterministic manner. *Ray tracing* is one of the most popular deterministic channel modeling techniques [72–74]. In Ray tracing technique, the environment surrounding the transmitter and the receiver is first defined. Then, all the propagation paths from the transmitter to the receiver are obtained based on simple reflexion, diffraction and propagation laws. The multipath components at the receiver are then added up in order to obtain the received signal. The more interactions are considered with the environment and the more detailed the environment is defined, the more precise the model will be. The precision of the model also depends on the number of physical phenomena that need to be included in the model. The more precision is required for the model, the more computationally expensive the model will be.

Ray tracing channel modeling could be used in order to obtain for instance the average power value at each position, the path-loss coefficients, the shadowing effects, etc. Some other channel parameters such as the channel depolarization behavior are however an open issue in these models [75]. Ray tracing channel modeling is for instance used by some telecommunication operators in order to precisely obtain the average power values at each position of the space so that the spatial coverage of a wireless base station is analyzed.

Note that in practice, all the parameters describing the propagation effects cannot be defined in these models which could lead in some case in inexact values of the channel. Some statistical behavior of the channel could however be correctly defined by these models.

1.4.2 Statistical channel modeling

Statistical channel modeling techniques could be used when the channel exhibits stationary statistical behavior over the time or space dimension [76]. In these models the parameters describing the channel matrix **H** are characterized from a statistical point of view. Measurements are first realized in a typical scenario and the statistical properties of the channel are extracted from these measurements. The measurement environment should be chosen so that it represents a typical case where the channel statistical behavior remains constant for different similar environments. Some typical classification of the measurement environment is e.g. *indoor* (which may be subdivided into e.g. office, corridor, lab,... cases) or *outdoor* (which may be subdivided into e.g. urban, suburban,... cases) scenario.

The statistical channel modeling techniques could be classified in two categories:

Statistical channel models with a system approach (SCMSA)

In SCMSA, the channel is modeled based on a system approach and the physical phenomena which occur during the propagation of the multipath components in the channel are not investigated and the antenna effects are not dissociated with the channel effects. Different phenomena could be included in these statistical channel models. The more channel properties are included in the channel model, the more complete the channel model will be. A statistical channel model may for instance include only the small-scale variation of the channel. Other channel properties such as the inter-antenna correlation statistics could also be added in the model.

The major advantage of these types of channel model is their mathematical simplicity. In fact these models could be easily implemented in signal processing algorithms. Also these models make it easier to obtain closed-form mathematical expressions for signal processing problems which include the channel matrix expression [77–79].

The major drawback of these types of channel model is that the antenna effects and the propagation effects are not dissociated. The channel depends on the type of antenna that has been used in the measurements and will not be applicable if other types of antenna with other characteristics are used.

Geometry-based stochastic channel models

Geometry-Based Stochastic Channel Models (GBSCM) are a family of statistic channel models where the channel is considered to be the sum of multipath propagation components. In GBSCM, the different propagation paths are characterized. The channel itself will be modeled by adding up all the propagation paths. In this way the channel model implicitly contains all the channel characteristics such as fading, path-loss, etc.

All the parameters representing the propagation paths such as the angles of transmission and the angles of reception of the propagation paths are statistically characterized. For a given propagation path k, some of the parameters used in GBSCM to represent the propagation path are the angles of departure at the transmitter side $\mathbf{\Omega}_{t,k}$, the angles of arrival at the receiver side $\mathbf{\Omega}_{r,k}$, the propagation delay τ_k and the propagation complex attenuation γ_k. The *directional channel* $h(\mathbf{\Omega}_t, \mathbf{\Omega}_r, \tau)$ is given by the sum of the different propagation paths:

$$h(\mathbf{\Omega}_t, \mathbf{\Omega}_r, \tau) = \sum_{k=1}^{K} \gamma_k \delta(\tau - \tau_k)\delta(\mathbf{\Omega}_t - \mathbf{\Omega}_{t,k})\delta(\mathbf{\Omega}_r - \mathbf{\Omega}_{r,k}) \tag{1.23}$$

By appropriately modeling the different parameters describing the propagation paths such as $\mathbf{\Omega}_{t,k}$, $\mathbf{\Omega}_{r,k}$, τ_k, γ_k and K the channel characteristics can implicitly be obtained.

A major avantage in GBSCM is that the antenna effects are not included in the model. The antenna effects are dissociated with the propagation paths and the propagation paths only includes the propagation effects. The model can then be applied for different types of transmit and receive antennas.

1.4.3 Polarization in wireless channel modeling

The polarization of Electromagnetic waves could also be included in the two categories of channel models described above:

Polarization in deterministic and geometry-based models

As in both deterministic and geometry-based models, the channel is characterized by modeling the different propagation paths, the polarization of the propagation paths can be included in the study. This is done through the γ matrix which contains the attenuation of the transmitted waves and the depolarization of the transmitted $\vec{1_\theta}$ and $\vec{1_\phi}$ components into the received $\vec{1_\theta}$ and $\vec{1_\phi}$ components. Equation 1.23 becomes then:

$$h(\mathbf{\Omega}_t, \mathbf{\Omega}_r, \tau) = \sum_{k=1}^{K} \begin{pmatrix} \gamma_{k,\theta\theta} & \gamma_{k,\theta\phi} \\ \gamma_{k,\phi\theta} & \gamma_{k,\phi\phi} \end{pmatrix} \delta(\tau - \tau_k)\delta(\mathbf{\Omega}_t - \mathbf{\Omega}_{t,k})\delta(\mathbf{\Omega}_r - \mathbf{\Omega}_{r,k}) \tag{1.24}$$

Polarization in system-based statistical channel model

In system-based statistical channel models, the antenna is considered to be an indissociable part of the channel. As a result, the polarization is included in the model by considering the power imbalance between the different elements of the cross-polarized channel matrix. This is done by characterizing the leakage occurring in cross-polar channels (e.g. vertical to vertical channel) and co-polar channels (e.g. vertical to horizontal channel). As explained in previous sections, the power imbalance between the elements of the cross-polarized multi-antenna channel matrix are caused by three phenomena: the polarization leakage occurring in the antenna, the depolarization due to the orientation mis-match of the antennas, and the depolarization occurring through the propagation in the channel. As these three phenomena cannot be dissociated in system-based statistical channel models, it is crucial to consider a realistic general scenario and to integrate all these three phenomena in a same characterization.

1.5 Contribution and outline of the thesis

The depolarization occurring through the propagation of the waves in the channel is studied for two cognitive radio scenarios in chapter 2. The depolarization of the transmitted waves has a significant impact on the performances of cognitive radio systems. Two important parameters which characterize the radiowave polarization are characterized: Cross-Polar-Discrimination (XPD) and Co-Polar-Ratio (CPR). XPD quantifies the amount of leakage from one polarization to another and CPR describes the link quality of one polarization compared to the other one. These two parameters are characterized separately at three different scales: small scale variation of XPD and CPR in a local zone, XPD and CPR mean fitting vs. distance, and large-scale variations of XPD and

CPR around the mean fitting.

The study of the depolarization in the channel for different kinds of propagation environment has been addressed in many previous works [46, 80–95]. The experimental results carried out in these works give an order of magnitude of the values of XPD and CPR for different propagation environments. The small-scale variation of XPD and CPR has been analyzed in [96, 97] for outdoor-to-outdoor scenarios and in [98, 99] for an indoor-to-indoor scenario.

The fitting of the mean XPD vs. distance between transmitter (Tx) and receiver (Rx) has been studied for an outdoor-to-outdoor scenario in [64, 68, 80, 100–102] and for an indoor-to-indoor scenario in [98, 103].

While all of these works aim at characterizing the overall XPD mean-fitting, little attention has been paid to model the different spatial variation scales separately. Furthermore, there are presently no results characterizing the XPD and CPR in outdoor-to-indoor environments. In most of these works, no distinction has been made between the depolarization from the vertical to horizontal components and from the horizontal to vertical ones. Moreover most of the previous works characterizing XPD has used a set of two cross-polarized antennas: one vertical and one horizontal. However, in order to obtain all the incident polarizations, a third orthogonal horizontal antenna is needed.

In this work, the XPD and CPR parameters can be separately characterized at three different scales: small scale variation of XPD and CPR in a local zone, XPD and CPR mean fitting vs. distance, and large-scale variations of XPD and CPR around the mean fitting.

For this purpose an extensive measurement campaign has been realized in two outdoor-to-indoor and indoor-to-indoor cognitive radio scenarios.

In section 2.1 an introduction to the impact of radio waves depolarization on the performance of cognitive radio systems is presented and the importance of its characterization is highlighted. An overview of the state of the art of the existing works on the characterization of the depolarization is given and the contribution of the proposed model of the XPD and the CPR is presented.

In section 2.2, the drawbacks of the classical approach in modeling the XPD where only two perpendicularly polarized antennas are used are mentioned. A new approach is proposed where a set of three cross-polarized co-located antennas is used and the received signals on the two horizontally polarized antennas are combined in order to overcome the drawbacks of the classical approaches.

The measurement campaign is presented in section 2.3. The measurement setup is detailed and the two outdoor-to-indoor and indoor-to-indoor cognitive radio scenarios are presented. In the outdoor-to-indoor scenario the primary base station is deployed outside and the secondary network is deployed inside a building. In the indoor-to-indoor scenario both the primary and the secondary networks are deployed inside a building.

Based on the measurements, the XPD and CPR parameters are statistically characterized separately at three different spatial scales and under static environment. Models of small-scale variation, large-scale variations and distance variation of these two parameters are given in section 2.4 under the two investigated scenarios.

While in chapter 2, the spatial statistics of the multi-polarized channel is characterized, the time-dynamics of the multi-polarized channel is characterized in chapter 3. The temporal and the spatial variations of the channel are not two independent phenomena. In fact each spatial variation in the channel caused by a variation of the position of the receiver, the transmitter or the interacting objects in the propagation environment leads also to a temporal variation.

In the scenario considered in chapter 2, the spatial variation of the channel depolarization are due to the variation in the position of the receiver while the transmitter and the interacting objects stay static. In chapter 3 however, the time-dynamics of the multi-polarized channel is characterized based on a scenario where the position of the interacting objects changes with time while the position of the transmitter and the receiver stay static.

While a classical approach in modeling the multi-polarized MIMO channels is to consider the signals received at one vertical and one or two horizontal perpendicular antennas [68, 79, 98, 103–106], in chapter 3, the polarization of the received waves are characterized from an electromagnetic point of view. Previous works have been done in order to model the multi-polarized MIMO channel at different scales of variation . While these works tend at characterizing the signals received at one vertical and one or two horizontal perpendicular antennas, no work has been done in order to model the global polarization of the received fields from an electromagnetic point of view.

The time dynamics of the receive polarization ellipse is characterized for a particular scenario and in a statistical system based approach. This new approach has the advantage to be transposable to any orientation of a receiver with multi-polarized co-located antennas.

A theoretical formulation is proposed in section 3.2, in order to obtain the parameters describing the receive elliptical polarization, based on the signals received at three omnidirectional cross-polarized co-located antennas. The time dynamics of the different parameters describing the elliptical polarization in the 3D space are characterized based on a measurement campaign. This measurement campaign is described in section 3.3. The measurements are made in an indoor-to-indoor scenario and at a frequency of 3.6 GHz. Different measurement positions are considered in a LOS and a NLOS scenario. Based on the theoretical analysis and a measurement campaign, a time-varying statistical model of the polarization ellipse is developed in section 3.4.

The statistical distribution of the different parameters describing the polarization ellipse are proposed. In order to study the time-variant dynamics of the channel, the autocorrelation functions of all the parameters are analyzed and models of autocorrelation are given. An analytical formulation is also proposed in order to project the polarization ellipse onto an antenna system composed of three cross-polarized co-located antennas. Finally, the different steps needed in order to generate a time-varying multi-polarized channel series based on the proposed time-varying model of the polarization ellipse are given.

Compared to previous works treating multi-polarized channel modeling, the approach used in this chapter for modeling the multi-polarized channel could be applied to any orientation of the receive antenna system, by projecting the receive elliptical polarization to the receive antenna system

In chapter 4, the sensing performance of a cognitive radio system using a set of three cross-polarized antennas at the secondary terminal and in a real-world scenario is investigated. An energy detector is applied to a multi-polar antenna system and its detection performances are compared with a uni-polar single and multi antenna system. This analysis is based on the outdoor-to-indoor measurement campaign described in chapter 2. In this scenario, the secondary network is deployed indoor and senses the signals received from an outdoor primary base-station.

Several previous works have already treated the application of energy detector on a multiple antenna system [53–59]. It has been found that the poor sensing performances of a single antenna system are considerably improved by the use of spatial diversity at the Secondary Terminal (STE). However, the impact of the polarization of the electromagnetic waves on the spectrum sensing performances has not been treated yet.

A theoretical formulation is presented in order to analytically obtain the detection and false alarm probabilities of an energy detector applied to a multi-polarized antenna system, under correlated and uncorrelated Rayleigh fading channel. Based on this theoretical formulation and the results obtained from the measurement campaign of chapter 2, the sensing performance of an energy detector applied to a tri-polarized antenna where each antenna experiences different uncorrelated Rayleigh fading is studied and compared to the spatial diversity case where the secondary terminal is made of three co-polar spatially separated antennas. The detection probability as a function of distance between the primary transmitter and secondary terminal, and the inter-antenna correlation effect on the sensing performance are studied.

Energy detection has been widely used in the literature because of its simplicity and the good performances that are achieved with this method [37–39, 107]. If good sensing performances are obtained with the energy detection method it is mainly because it is assumed in this method that the variance of the noise is known. In fact, having the knowledge of the noise variance makes it possible to detect very weak signals by detecting any small increase in the power due to the sum of the noise and signal power [50, 108].

However, in practice the noise variance is not known exactly at the secondary terminal [38, 50, 108–110]. An uncertainty on the estimation of the noise variance affect considerably the detection performance of energy detection method [38, 50, 108–110]. In chapter 5, new spectrum sensing methods are proposed which do not require any a priori knowledge of the noise variance and are thus robust to the noise variance uncertainty. These methods, refered to as *blind spectrum sensing methods*, are based on a particularity of multi-polarized antenna systems and require at the secondary terminal, a set of three cross-polarized antennas. The performances of the proposed methods are compared with each other in two dynamic and static channel scenarios. The GLRT methods proposed which are proposed in the literature as blind spectrum sensing methods are extended to the case of multi-polarized systems. New blind spectrum sensing methods are also proposed based on particularities in multi-polarized systems. This analysis is based on an analytical formulation applied to the outdoor-to-indoor measurement campaign of chapter 2. The performances of the proposed methods are also compared with the energy detection method with an without noise variance uncertainty. Finally, the effect of antenna orientation on the spectrum sensing performances of the proposed blind spectrum sensing method and the energy detection method is studied. This is done by projecting the elliptical polarization model developed in chapter 3 onto a multi-polarized antenna system with different orientations.

Finally, chapter 6 presents the conclusion of this thesis. The results obtained in the previous chapters are highlighted and some future outlooks are presented.

In summary, the major contributions of the present thesis are:

- Characterization of the depolarization in two indoor-to-indoor and outdoor-to-indoor cognitive radio scenarios through the modeling of XPD and CPR separately at three different spatial scales: small-scale variations, large-scale variations and distance variations.
- Characterization of the polarization of the received waves from an electromagnetic point of view by modeling the time-dynamics of

the receive polarization ellipse in the 3D space and for different LOS and NLOS scenarios.

- Extension of energy detector to multi-polarized systems in a real-world cognitive radio scenario based on an analytical formulation and a measurement campaign and comparison of its performance with a uni-polar single and multi antenna system.

- Developing of new blind spectrum sensing methods based on particularity of multi-polarized systems. The proposed methods are robust to the noise variance uncertainty and outperform the energy detector in presence of noise variance uncertainty.

CHAPTER 2

Spatial statistics of the channel depolarization

2.1 Introduction

As already mentioned in the previous chapter, in a cognitive radio system, the polarization of the transmitted waves from the primary base station changes before arriving at the secondary terminal due to different phenomena such as the imperfection of the antennas or the interaction of the transmitted waves with the environment surrounding the transmitter and the receiver. Let us consider for instance that the transmit antenna at the primary base station transmits on a vertical polarization. The transmitted vertically polarized wave will be depolarized into its perpendicular horizontal polarization due to its interaction with the environment surrounding the transmitter and the receiver. If only one vertically polarized antenna is used at the secondary terminal, all the incident polarizations will not be received. On the other hand, in a practical implementation, the polarization of the primary transmit antenna may not be known at the secondary terminal. As a result, these depolarization phenomena allow the secondary terminal to detect the signals coming from the primary base station even if it does not use the same polarization as the primary transmit antenna.

If the proportion of leakage from one polarization to another is not very important, a mismatch between the polarization of the antennas of the primary base station and the secondary terminal could prevent the secondary terminal to detect the signals from the primary base station.

On the other hand, if the same polarization is used at the antennas of the secondary terminal and the primary base station, in case of high depolarization, the sensing performances of the secondary terminal could be significantly deteriorated.

The polarization orthogonality could also be used in order to enable the coexistence of multiple networks on the same frequency resources. Several works proposed the co-existence of primary and secondary networks by using diversity techniques [111–116]. The use of orthogonal codes such as Code Division Multiple Access (CDMA) [114] or the use of directional antenna [113] are some of the diversity techniques which allows the co-existence of multiple networks. Beside the different diversity techniques which could be used in order to allow the co-existence of primary and secondary networks, the polarization orthogonality could also be used. Several works have treated the implementation of multiple networks on the same frequency resources by using orthogonal polarization in each network [111, 114, 117, 118]. In fact in an idealistic case where there is no depolarization, two networks could coexist in the same frequency resource without interfering with each other by using orthogonal polarizations. However because of the depolarization phenomena, a perfect orthogonality between networks using orthogonal polarizations is not feasible.

Let us for instance consider two networks deployed on the same frequency resource where vertically polarized antennas are used in one of the networks and horizontally polarized antennas at the other. In an idealistic case where there is no depolarization these two networks could coexist in the same frequency resource without interfering with each other since the vertically and horizontally polarized waves use two orthogonal dimensions which do not interfere with each other. However in a realistic scenario, a fraction of the vertically polarized waves transmitted by the first network will leak to the orthogonal horizontal polarization and therefore will interfere with the second network. In [118], a probabilistic approach is used where by guaranteeing a minimum capacity to the licensed primary network, the co-existence of the primary and the secondary networks having orthogonal polarizations is studied based on the polarization leakage. It is shown that by deploying a secondary network which uses an orthogonal polarization than the primary network, the transmission rate of the primary network could be increased while, at the same time, the primary exclusive region could be reduced.

For these different reasons, it is thus important to characterize the proportion of leakage from one polarization to another for different cognitive radio scenarios based on a system approach. In the present work the polarization leakage is characterized for two cognitive-radio scenarios: *Outdoor-to-Indoor* and *Indoor-to-Indoor*:

- *Outdoor-to-indoor:*

  The outdoor-to-indoor scenario corresponds to a typical cognitive radio scenario where the primary base station is deployed outside and the secondary network is deployed inside a building. This could for instance correspond to a Wi-Fi secondary network deployed on the frequency resources of a WiMAX base station.

- *Indoor-to-indoor:*

  The indoor-to-indoor scenario corresponds to a cognitive radio scenario where both the primary and the secondary networks are deployed inside a same building. This scenario could correspond to a cognitive radio architecture where the principle goal is to make possible the co-existence of two or more different unlicensed networks sharing the same unlicensed spectrum resources in the best efficient way. This corresponds to the second type of cognitive radio architecture explained in section 1.1.1.

For this purpose, an extensive measurement campaign was realized in both of these scenarios. The principal aim of this measurement campaign was to characterize at different spatial scales and in a static environment, the depolarization phenomena occurring in the channel.

One important parameter which characterizes the radiowave polarization is the Cross-Polarization-Discrimination (XPD). It quantifies the amount of leakage from one polarization to another caused by the channel. Another relevant parameter is the Co-Polar-Ratio (CPR) that describes the link quality of one polarization compared to the other one (Figure 2.1). These parameters are defined as the power ratio between the different elements of the MIMO channel matrix:

$$\mathrm{XPD_V} = \frac{\left\langle |h_{VV}|^2 \right\rangle}{\left\langle |h_{HV}|^2 \right\rangle} \tag{2.1}$$

$$\mathrm{XPD_H} = \frac{\left\langle |h_{HH}|^2 \right\rangle}{\left\langle |h_{VH}|^2 \right\rangle} \tag{2.2}$$

$$\mathrm{CPR} = \frac{\left\langle |h_{VV}|^2 \right\rangle}{\left\langle |h_{HH}|^2 \right\rangle} \tag{2.3}$$

where $\left\langle |h_{VV}|^2 \right\rangle$ denotes the average $|h_{VV}|^2$ over some spatial or temporal scale.

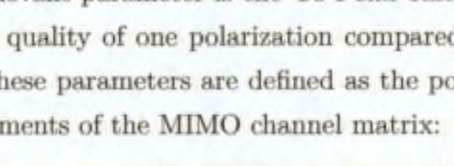

Figure 2.1: Cross-polarized sub channels

These parameters are included in some channel models (e.g. in the very popular *Kronecker* channel model [119–121]). Also the analytical expressions developed in the context of the co-existence of cross-polarized cognitive radio networks make use of these parameters [111, 114, 117, 118].

The XPD could be divided in two parts representing the two main phenomena which induce a depolarization in the channel [79]:

- The depolarization due to the imperfect antennas or *Cross Polar Isolation (XPI)*
- The depolarization due to the orientation mis-match of the antennas.
- The depolarization due to the propagation of the transmitted waves in the channel or *Cross Polar Ratio (XPR)*

The combination of these three phenomena yields to a global Cross-Polar Discrimination (XPD). The depolarization due to the imperfect antennas is a well known subject in the antenna theory and could be accounted for by means of the cross-polar antenna pattern [79]. The depolarization due to the orientation mis-match of the antennas depends on the implementation context and the spatial configuration of the transmitter and the receiver. The XPR depends on the propagation environment. In this work, the depolarization due to the orientation mis-match of the antennas is not studied separately and is included in the XPR.

The study of the depolarization in the channel for different kinds of propagation environment has been addressed in many previous works [46, 80–95]. The depolarization increases with the amount of scatterers in the propagation environment and as a result the XPD decreases [122]. The Non-Line-of Sight (NLOS) radio environments experience high multipath due to the high interaction of the transmitted waves with the environment. However, the LOS radio environments experience lower multipath since the interactions with the environment are less important. As a result, lower average values of XPD are reported for the NLOS scenarios compared to LOS scenarios [89, 123, 124].

Note that in most of the experimental studies on the XPD, experimental cross-polar co-located antennas with a high cross-polar isolation were used. As a result the global XPD is considered to be approximately equal to the XPR [79].

Previous works have already provided models of the XPD in different kinds of environments. The small-scale variation of XPD and CPR has been experimentally analyzed in [96,97] for outdoor-to-outdoor scenarios and in [98] for an indoor-to-indoor scenario and it has been found that it follows approximately a log-normal distribution. In [99], the small-scale variation of XPD is theoretically investigated for an indoor-to-indoor scenario and it has been shown that it follows a doubly non-central F distribution which could be approximated by a log-normal distribution. The time-variant statistics of the XPD has been analyzed in [104]. In this paper a time-varying statistical channel model is proposed for tri-polarized antenna systems. The temporal variations of the channel are separated into fast and slow channel variations.

The fitting of the mean XPD vs. distance between transmitter (Tx) and receiver (Rx) has been studied for an outdoor-to-outdoor scenario in [64, 68, 80, 100–102] and for an indoor-to-indoor scenario in [98, 103]. Some of the main results obtained in these works are highlighted in the following and summarized in Table 2.1:

- *Models of XPD for outdoor-to-outdoor scenarios:*

  In [64], based on a measurement campaign realized at the frequency of 2.48 GHz and in an outdoor-to-outdoor suburban area, the XPD is characterized as a function of distance between the transmitter and the receiver. In the proposed model of XPD, no distinction is made between XPD_V and XPD_H. The distant dependent model of XPD is proposed for the range of distance between

100 and 10000 meters:

$$XPD(dB) = -4.46\log_{10}(d/d_0) + 4.86 \tag{2.4}$$

where $d_0 = 1km$ denotes the distance of reference.

In this range of variation of the distance, the overall trend of XPD is reported to be descending with respect to the distance. The large-scale variations of XPD around its linear distance-dependent model is reported to have a log-normal distribution with standard deviation of 4.90 dB.

In [80], similar measurements are carried out at a frequency of 2.48 GHz in a outdoor-to-outdoor suburban area. Based on these measurements, a model of XPD as a function of distance is proposed:

$$XPD(dB) = -2.93\log_{10}(d/d_0) + 3.70 \tag{2.5}$$

The overall trend of XPD is reported to be descending with respect to the distance. The large-scale variations of XPD around its linear distance-dependent model is reported to have a log-normal distribution with standard deviation of 4.88 dB.

In [68], the distance-dependent trend of the XPD is studied by extending a stochastic geometry-based scattering model to multipolarized transmissions. The study is made for a frequency of 2.5 GHz and for an outdoor-to-outdoor scenario. The overall behaviour of XPD is reported to be descending with distance. The case of a cross-polarized antenna with $0°$ and $45°$ tilted angle is studied. The following models are obtained for each of these cases:

$$XPD_{0^\circ}(dB) = -0.31\log_{10}(d/1000) + 14.2 \tag{2.6}$$

$$XPD_{45^\circ}(dB) = -1.1\log_{10}(d/1000) + 12.3 \tag{2.7}$$

In [100–102], a three-dimensional geometry-based analytical model for XPD is presented for an outdoor-to-outdoor suburban scenario.

The distance-dependence of the XPD is studied based on this model. The theoretical model is compared with measurements in a similar environment. In the range of distance between 1.3 to 10 Km, close matching is obtained between the measured and the theoretical distance-dependent model of XPD. The overall trend of XPD is reported to be descending with respect to the distance and varying from 4 to 1 dB in the range of variation of the distance between 1.3 to 10 Km.

- *Models of XPD for indoor-to-indoor scenarios:*

  In [103], the XPD is characterized as a function of distance between the transmitter and the receiver in an indoor environment. The study is based on experimental measurements carried out at a frequency of 2.6 GHz. Two scenarios are investigated: LOS in a corridor and NLOS between a corridor and offices. No distinction is made between $\mathrm{XPD_V}$ and $\mathrm{XPD_H}$. For each scenario, the following distance dependent models are proposed:

  $$\text{LOS Scenario:} \quad \mathrm{XPD}(dB) = 5.5log_{10}(d) + 7.9 \tag{2.8}$$

  $$\text{NLOS Scenario:} \quad \mathrm{XPD}(dB) = 2.9log_{10}(d) + 2.6 \tag{2.9}$$

  In the studied range of distance $(2 < d(m) < 50)$The overall trend of the XPD is found to be ascending as a function of distance. The decay components are much higher for the NLOS case than in the LOS case.

  In [98], the XPD is characterized as a function of distance for an indoor WLAN scenario. The study is based on measurements which are carried out at a frequency of 5.25 GHz. Two scenarios are considered: An NLOS office scenario and a LOS hotspot type of environment. No distinction is made between $\mathrm{XPD_V}$ and $\mathrm{XPD_H}$. The XPD is reported to be independent with respect to the distance.

Table 2.1: A literature overview on XPD vs distance model - Freq : frequency, std: standard deviation, dist: distance

Scenario	Freq	distance dependent model	trend vs dist	std
Outdoor suburban [64]	2.48 GHz	$\mathrm{XPD}(dB) = -4.46\log_{10}(d(m)/10^3)+4.86$	descending	4.90 dB
Outdoor suburban [80]	2.48 GHz	$\mathrm{XPD}(dB) = -2.93\log_{10}(d(m)/10^3)+3.70$	descending	4.88 dB
Outdoor [68]	2.5 GHz	$\mathrm{XPD}_{0^\circ}(dB) = -0.31\log_{10}(d/10^3) + 14.2$ $\mathrm{XPD}_{45^\circ}(dB) = -1.1\log_{10}(d/10^3) + 12.3$	descending	
Outdoor suburban [100–102]	2.5 GHz	$1 < \mathrm{XPD}$ (dB)< 4 for $1.3 < d(\mathrm{km}) < 10$	descending	
Indoor LOS corridor & NLOS corridor to offices [103]	2.6 GHz	LOS: $\mathrm{XPD}(dB) = 5.5log_{10}(d) + 7.9$ NLOS: $\mathrm{XPD}(dB) = 2.9log_{10}(d) + 2.6$	ascending	
Indoor NLOS office & LOS hotspot [98]	5.25 GHz	XPD$\approx$ 6,7 dB for $5 < d(m) < 50$	invariable	

While all of these works aim at characterizing the overall XPD mean-fitting, little attention has been paid to model the different spatial variation scales separately. Furthermore, there are presently no results characterizing the XPD and CPR in outdoor-to-indoor environments. In most of these works, no distinction has been made between the $\mathrm{XPD_V}$ and $\mathrm{XPD_H}$ components. Moreover most of the previous works characterizing XPD has used a set of two cross-polarized antennas: one vertical and one horizontal. However, in order to obtain all the incident polarizations, a third orthogonal horizontal antenna is needed.

In this work, the XPD and CPR parameters can be separately characterized at three different scales: small scale variation of XPD and CPR in a local zone, XPD and CPR mean fitting vs. distance, and large-scale variations of XPD and CPR around the mean fitting. In fact as introduced in the general introduction, the wireless channel has different scales of variations and so has the XPD and CPR. Two scenarios will be investigated: outdoor-to-indoor and indoor-to-indoor. In each of these scenarios, a set of one vertically polarized and one horizontally polarized antennas is considered at the transmitted and a set of three perpendicularly polarized co-located antennas is considered at the receiver side.

2.2 Multi-polarized antenna system

When an antenna is illuminated by an electromagnetic wave, an electric current is induced in it. The relation between the incident electric field and the signal received in the antenna is given by the effective height of the antenna [125]. The effective height of an antenna is a complex vector representing the response of the antenna to an incident electric field in a given direction.

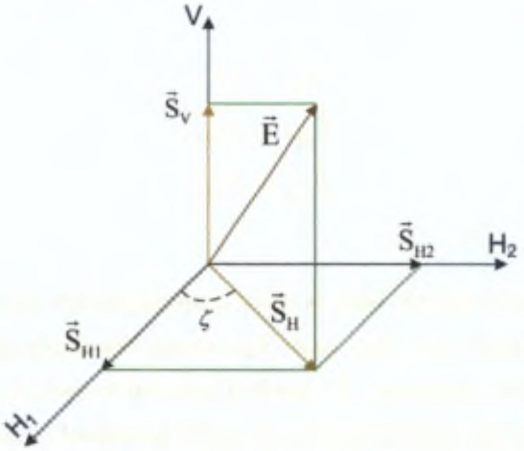

Figure 2.2: The incident electric field $\vec{E}$ and the received signals on three perpendicularly polarized antennas

Let us for instance consider the case of an incident electric field $\vec{E}$ to a cross-polarized antenna system made of three omnidirectionnal co-located cross-polarized linear wire antennas which is represented in figure 2.2. The induced signals S_V, S_{H1} and S_{H2} at respectively the vertically and the two horizontally polarized antennas are given by:

$$\begin{aligned} S_V &= \vec{L}_V \vec{E} \\ S_{H1} &= \vec{L}_{H1} \vec{E} \\ S_{H2} &= \vec{L}_{H2} \vec{E} \end{aligned} \tag{2.10}$$

where $\vec{L}_V$, $\vec{L}_{H1}$ and $\vec{L}_{H2}$ denote the equivalent height vectors of respectively the vertically and the two horizontally polarized antennas. By assuming the same amplitude L for the equivalent height of the three receive antennas we have:

$$\vec{L}_V = L\vec{1}_V$$
$$\vec{L}_{H1} = L\vec{1}_{H1}$$
$$\vec{L}_{H2} = L\vec{1}_{H2} \tag{2.11}$$
$$\tag{2.12}$$

The received electric field is thus represented by the three received signal components S_V, S_{H1} and S_{H2} along the three perpendicularly polarized receive antennas. A classical approach used in many previous works studding the depolarization in multi-polarized channels, is to consider the received signals at one vertically polarized and only one of the two horizontally polarized antennas. However there are two drawbacks in the use of this approach:

- First of all by considering only one horizontal signal component, all the signal components are not taken into account. Therefore all the depolarization possibilities are not taken into account as a depolarization may for instance occur between one of the considered signal components to the unconsidered horizontal component.
- In a practical case, the Rx antenna system does not remain in the same orientation all the time. As a result, the two horizontal signal component are not distinguishable if a rotation is occurred around the vertical antenna. Therefore the polarization model deduced from the results depends on the orientation of the Rx antenna system. A standard polarization model cannot be given without considering this ambiguity.

In order to overcome this problem, the three signal components are reduced to one vertical S_V and one overall horizontal signal component S_H. The overall horizontal signal component is obtained by combining the two horizontal signal components S_{H1} and S_{H2}:

$$\begin{aligned}
\vec{S}_H &= \vec{S}_{H1} + \vec{S}_{H2} \\
&= (L\vec{1}_{H1}\vec{E})\vec{1}_{H1} + (L\vec{1}_{H2}\vec{E})\vec{1}_{H2} \\
&= S_{H1}\vec{1}_{H1} + S_{H2}\vec{1}_{H2} \\
&= \sqrt{S_{H1}^2 + S_{H2}^2}(\vec{1}_{H1} + \vec{1}_{H2}) \\
&= \sqrt{S_{H1}^2 + S_{H2}^2}\vec{1}_H \\
&= S_H\vec{1}_H
\end{aligned} \tag{2.13}$$

The signal component S_H corresponds to the signal that would be received on an antenna placed in the direction $\vec{1}_H$ with equivalent height $\vec{L}_H = L\vec{1}_H$.

In the measurement campaign realized in this work and which is described in the next section, three omnidirectional cross-polarized co-located antennas were used at the receiver. The signals received on the two horizontally polarized antennas are combined as described above, in order to have a vertical and an overall horizontal signal components. The XPD and CPR values are obtained based on these signals.

2.3 Measurement Setup

2.3.1 Measurement equipment

The measurement was performed using a Vector Signal Generator (Rohde & Schwarz SMATE200A VSG) at the transmitter side and a Signal Analyzer (Rohde & Schwarz FSG SA) at the receiver side. An illustrative diagram of the Tx chain is given in figure 2.3. The Tx chain was composed of the VSG and a unipolar directional antenna (Rohde & Schwarz HE300, Figure 2.4). By rotating the module to the desired horizontal or vertical orientation, it could be operated either on vertical or horizontal polarizations. A typical azimuthal radiation pattern of this antenna on the vertical and the horizontal polarizations is given in figure 2.5.

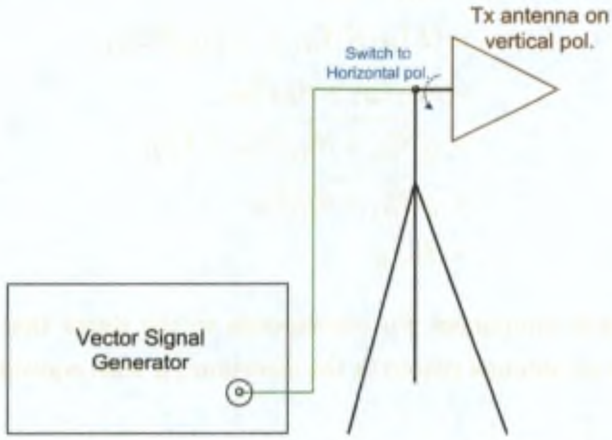

Figure 2.3: The transmitter chain

Figure 2.4: Transmitter antenna

An illustrative diagram of the Rx chain is given in figure 2.6. The Rx antenna (Satimo Insite Free 3–6 GHz [126]) was a tri-polarized antenna, made of three co-located perpendicular omnidirectional short linear antennas (Figure 2.7). As these are experimental cross-polarized antennas, high cross-polar isolation should exist between the different antennas.

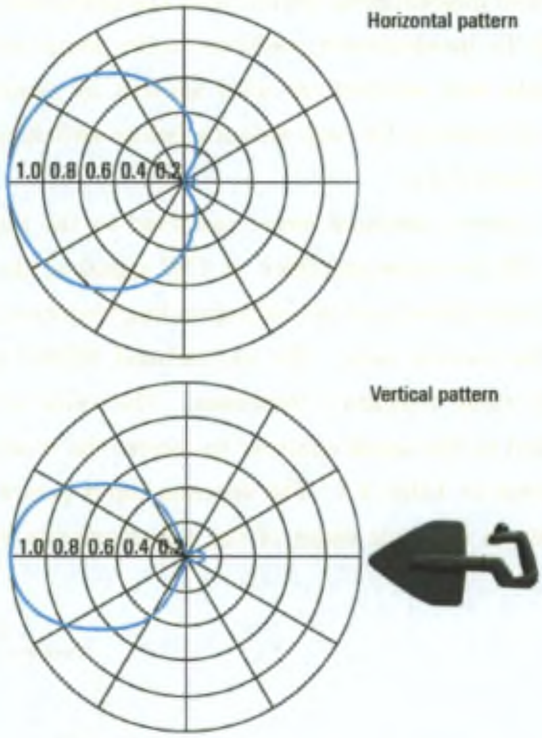

Figure 2.5: A typical azimuthal radiation pattern of the Tx antenna for the two horizontal and vertical polarizations and in frequency range from 500 MHz to 7.5 GHz

However, the XPI values of these antennas are not specified by their manufacturer. The axial radiation patterns of the Rx vertical and horizontal antennas are given in figure 2.8.

The three receive antennas were fixed on an automatic positioner (Vexta PK268) to create a virtual planar array. By doing this, the number of elements in the antenna arrays could be increased without any coupling between the different elements in the antenna arrays. However, in order to keep the same channel condition between the different positions in the planar array, the channel should stays as static as possible during the entire measurement period with the positioner.

At each of the measurement positions in the planar array, the three receive antennas were selected one after another by means of a switch. The duration of measure for each antenna before switching to the other antenna was about 0.2 s.

The three receive antennas were connected to the Signal Analyzer through a 25 dB low-noise amplifier. A CW signal at the frequency of 3.5 GHz was transmitted and the corresponding frequency response was recorded at the receiver side. The narrowband MIMO matrices were obtained from these frequency responses. The value of the different parameters used at the signal analyzer to receive the received frequency response is given in Table 2.2. The antenna input power was 19 dBm and the minimum dynamic range of the measurements was around 15 dB.

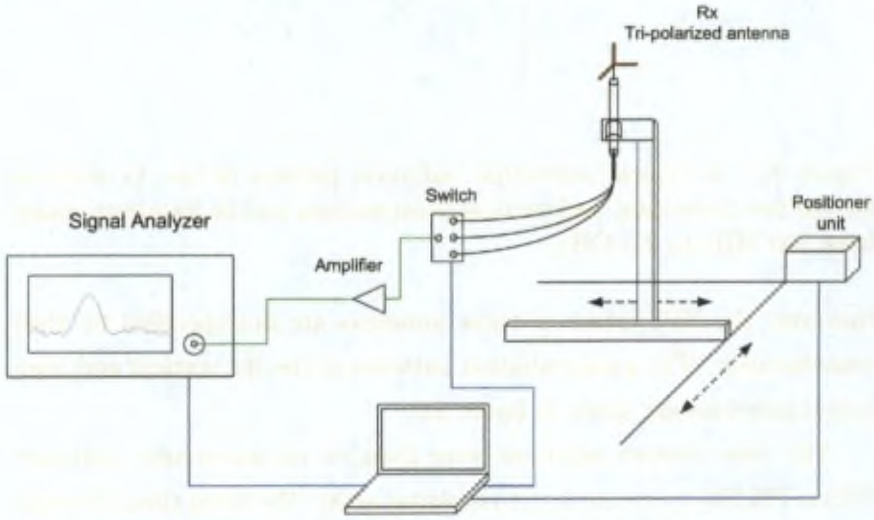

Figure 2.6: The receiver chain

Figure 2.7: Receiver antenna

Table 2.2: Signal analyzer parameters

Center frequency	3.5 GHz
Bandwidth	100 KHz
number of collected samples	625
IF Bandwidth	5 KHz

2.3.2 Measurement scenario

The measurement site was the third floor of Building U at Solbosch campus of Université Libre de Bruxelles (ULB). Two measurement scenarios were investigated:

- **Outdoor-to-Indoor Scenario**

  In the outdoor-to-indoor case (Figure 2.9), the transmitter was fixed on the rooftop of a neighboring building (Building L), at a total height of 15 m (Figure 2.10) and was directed toward the measurement site (Figures 2.12). A brick wall was separating the LOS direction between this measurement site and the transmit-

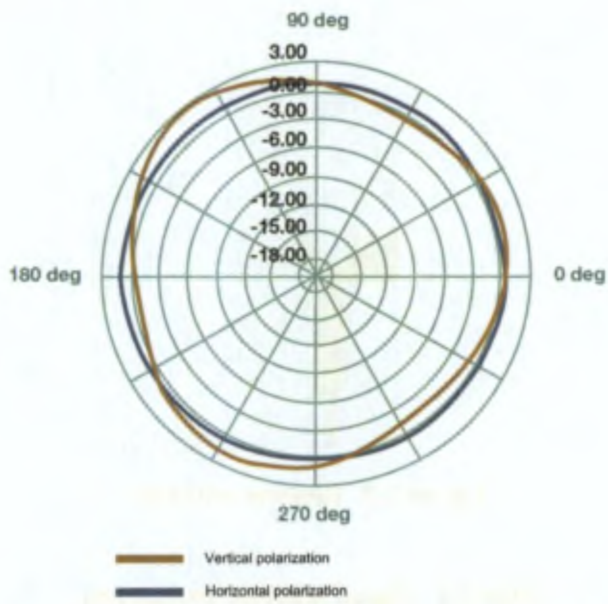

Figure 2.8: Axial radiation pattern of the Rx vertically and horizontally polarized antennas for the frequency of 3.6 GHz

ter. The measurements were performed in a total of 78 positions, located in seven successive rooms. The rooms were separated by brick walls and closed wooden doors. The distance between the transmitter and the measurement points was in the range of 30 to 80 meters.

- **Indoor-to-Indoor Scenario**

  In the indoor-to-indoor case (Figure 2.11), the Tx antenna was fixed in the first room (Figure 2.13) and was directed toward the seven next rooms, in which 65 measurement points were taken. The distance between the transmitter and the measurement points was for this case in the range of 8 to 55 meters.

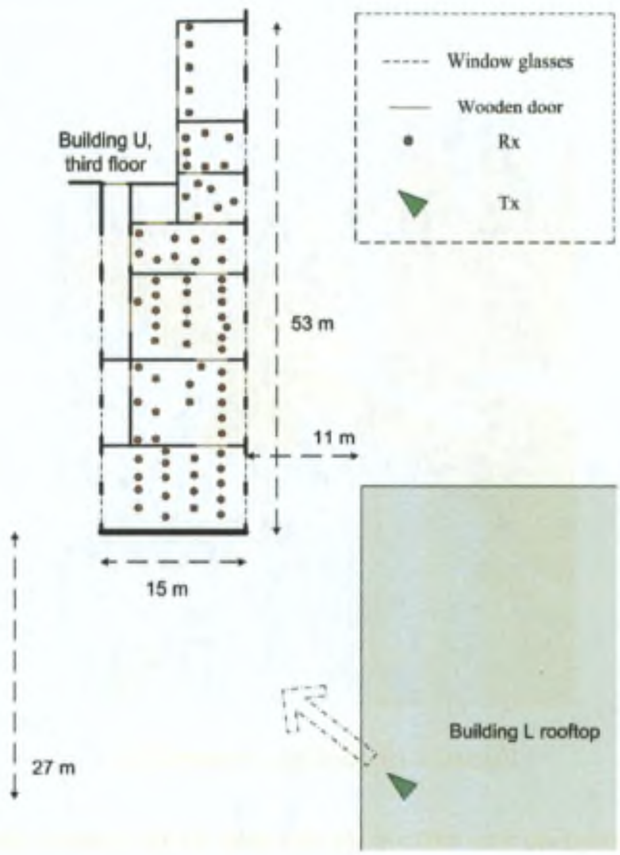

Figure 2.9: Outdoor-to-Indoor measurement setup

In both cases, in order to characterize the small scale statistics of XPD, a total of 64 spatially separated measurements were taken over an 8×8 grid at each Rx position. The spacing between grid points was $\lambda/2$ (4 cm). At each grid point, 5 snapshots of the received signal were sampled and averaged over to increase the Signal-to-Noise-Ratio (SNR). During the measurements the environment was kept as static as possible.

In the Rx chain, the signal analyzer, the positionner and the switch were all connected to a computer in order to control the measurements.

Figure 2.10: Outdoor transmitter

A matlab program was written for this sake which connect the different measurement devices to the computer and which coordinate the measurement process. All the devices used in the Rx chain were carried on a trolley in order to more easily move from one measurement position to another. As previously mentioned, the two polarizations used at the transmit antenna should have been changed manually. As a result at each measurement position, the whole measurement process was first done for the vertically polarized transmit antenna and then repeated for the horizontally polarized transmit antenna. In the outdoor-to-indoor scenario this coordination between the transmitter and the receiver sides was done by two persons at each sides, communicating by walkie-talkies. The Tx and Rx units are two distinct modules which are not synchro-

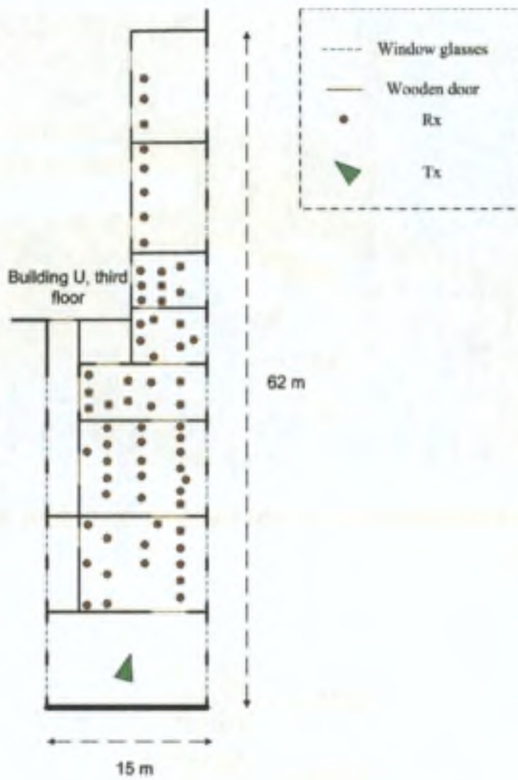

Figure 2.11: Indoor-to-Indoor measurement setup

nized to each other. As a result, the phase of the received signals is not measured and only the amplitude of the received signals is obtained.

2.4 Measurement Results

2.4.1 Small-scale variations

Theoretical distribution

Let $\tilde{\text{XPD}}$ and $\tilde{\text{CPR}}$ denote the instantaneous cross-polarization discrimination and co-polar ratio obtained by the ratio of the instantaneous channel powers:

Figure 2.12: Measurement site for the outdoor-to-indoor and indoor-to-indoor scenarios

$$\tilde{\mathrm{XPD}}_{\mathrm{V}} = \frac{|h_{VV}|^2}{|h_{HV}|^2} \quad (2.14)$$

$$\tilde{\mathrm{XPD}}_{\mathrm{H}} = \frac{|h_{HH}|^2}{|h_{VH}|^2} \quad (2.15)$$

$$\tilde{\mathrm{CPR}} = \frac{|h_{VV}|^2}{|h_{HH}|^2} \quad (2.16)$$

In the case of Ricean fading channels, the distribution of the amplitude of the sub-channels used, e.g for $\tilde{\mathrm{XPD}}_{\mathrm{V}}$ (h_{VV} and h_{HV}) can be written as:

$$|h_{VV}| \sim \mathrm{Rice}(\sigma, \nu) \quad (2.17)$$

$$|h_{HV}| \sim \mathrm{Rice}(\alpha_1\sigma, \alpha_0\nu) \quad (2.18)$$

where σ and ν are the Rice parameters of $|h_{VV}|$ ($2\sigma^2$ is the power of the scattered components and ν^2 the power of the coherent component), and $\alpha_1\sigma$ and $\alpha_0\sigma$ denote here the Rice parameters of the $|h_{HV}|$ Ricean

Figure 2.13: Indoor transmitter

distribution. The corresponding parameters for $\tilde{\mathrm{XPD}}_{\mathrm{H}}$ and $\tilde{\mathrm{CPR}}$ are defined in the same way as those of $\tilde{\mathrm{XPD}}_{\mathrm{V}}$.

The square of a random variable which follows a Ricean distribution with parameters $(1,\nu)$ follows a non-central chi-squared distribution with two degrees of freedom and the non-centrality parameter ν $(\chi_2^2(\nu))$ [127]. Therefore, we have:

$$\frac{|h_{VV}|^2}{\sigma^2} \sim \chi_2^2(\frac{\nu^2}{\sigma^2}) \tag{2.19}$$

$$\frac{|h_{HV}|^2}{\alpha_1^2\sigma^2} \sim \chi_2^2(\frac{\alpha_0^2\nu^2}{\alpha_1^2\sigma^2}) \tag{2.20}$$

As it was previously shown in [99], by assuming that the different sub-channels in a cross-polarized antenna system are independent, the quotient between $|h_{VV}|^2$ and $|h_{HV}|^2$ i.e. the $\tilde{\mathrm{XPD}}_{\mathrm{V}}$ variation around α_1^2 follows a doubly non-central F distribution:

$$\alpha_1^2 \tilde{\mathrm{XPD}}_{\mathrm{V}} \sim F''(2, 2, 2K_{VV}, 2K_{HV}) \tag{2.21}$$

where

$K_{VV} = \frac{\nu^2}{2\sigma^2}$ and $K_{HV} = \frac{\alpha_0^2\nu^2}{2\alpha_1^2\sigma^2}$

are the Ricean K factors for the VV and HV links respectively. Similarly to $\tilde{\mathrm{XPD}}_{\mathrm{V}}$, the theoretical distributions for $\tilde{\mathrm{XPD}}_{\mathrm{H}}$ and $\tilde{\mathrm{CPR}}$ are also obtained by a doubly non-central F distribution with the corresponding Rice factor parameters [99].

Experimental distributions:

As previously mentioned, from each measurement position, 64 measurement points were taken on a grid of 8×8 in order to characterize the small-scale variation of XPD and CPR in a local area. The experimental distribution was compared to the theoretical one in all positions and for both scenarios. The theoretical distribution for $\tilde{\mathrm{XPD}}_{\mathrm{V}}$ was obtained by filling in the corresponding α and Rice factors in equation 2.18. The theoretical distribution for $\tilde{\mathrm{XPD}}_{\mathrm{H}}$ and $\tilde{\mathrm{CPR}}$ were obtained in the same way.

An overview of the different Rice factors is given for the outdoor-to-indoor case in Table 2.3 and for the indoor-to-indoor case in Table 2.4.

Table 2.3: Measured K-factors for Outdoor-to-Indoor scenario

$\mathrm{Min}(K_{VV})$	-35,16 dB	$\mathrm{Min}(K_{HV})$	1,38 dB
$\mathrm{Max}(K_{VV})$	7,63 dB	$\mathrm{Max}(K_{HV})$	9 dB
$\mathrm{Mean}(K_{VV})$	1,62 dB	$\mathrm{Mean}(K_{HV})$	5,67 dB
$\mathrm{Min}(K_{HH})$	-0,37 dB	$\mathrm{Min}(K_{VH})$	-42,63 dB
$\mathrm{Max}(K_{HH})$	13,36 dB	$\mathrm{Max}(K_{VH})$	5,41 dB
$\mathrm{Mean}(K_{HH})$	6,15 dB	$\mathrm{Mean}(K_{VH})$	0,55 dB

Table 2.4: Measured K-factors for Indoor-to-Indoor scenario

$\mathrm{Min}(K_{VV})$	-64,76 dB	$\mathrm{Min}(K_{HV})$	0,91 dB
$\mathrm{Max}(K_{VV})$	7,93 dB	$\mathrm{Max}(K_{HV})$	8 dB
$\mathrm{Mean}(K_{VV})$	1,72 dB	$\mathrm{Mean}(K_{HV})$	5,19 dB
$\mathrm{Min}(K_{HH})$	-71,14 dB	$\mathrm{Min}(K_{VH})$	-37,33 dB
$\mathrm{Max}(K_{HH})$	12,12 dB	$\mathrm{Max}(K_{VH})$	8,66 dB
$\mathrm{Mean}(K_{HH})$	5,08 dB	$\mathrm{Mean}(K_{VH})$	0,92 dB

Figure 2.14 shows the good matching between the Cumulative Distribution Function (CDF) of the experimental $\tilde{\mathrm{XPD}}$ and the corresponding theoretical doubly non-central F distribution for a particular position in the indoor-to-indoor scenario.

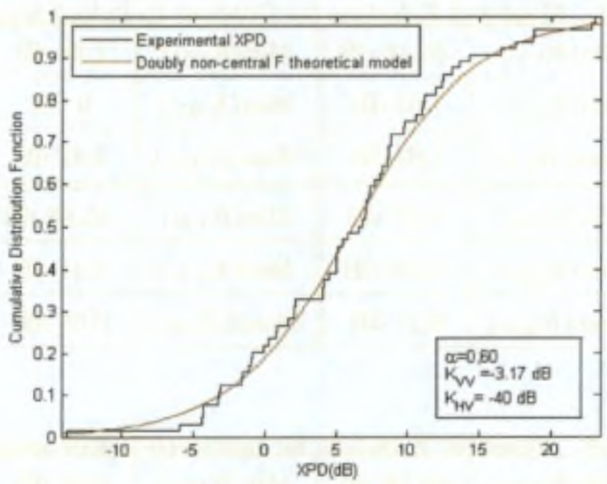

Figure 2.14: Comparison between the CDF of experimental $\tilde{\mathrm{XPD}}_{\mathrm{V}}$ and its theoretical model.

In order to confirm the good matching between theoretical and experimental distributions, a Kolmogorov-Smirnov (KS) test was applied for each measurement position. The KS test is a statistical hypothesis test that compares the theoretical CDF with the experimental one and is sensitive to both location and shape of the experimental CDF.

The null hypothesis H_0 is satisfied when the experimental data and the theoretical model have the same distribution. The hypothesis H_1 is satisfied when they do not have the same distribution. The significance level is set to 5%. For both outdoor-to-indoor and indoor-to-indoor scenarios and for the three parameters $\tilde{\mathrm{XPD}}_{\mathrm{V}}$, $\tilde{\mathrm{XPD}}_{\mathrm{H}}$, and $\tilde{\mathrm{CPR}}$, the null hypothesis has been satisfied for all the 78 (for outdoor-to-indoor case) and 65 (for indoor-to-indoor cases) tested zones.

2.4.2 Large Scale Variations

In order to separate the small-scale effects from the large-scale effects, at each measurement position, the 64 sub-channel power measurements over the 8 × 8 grid were averaged. From the averaged power per subchannel values, the values of XPD and CPR per measurement position were then computed:

$$\mathrm{XPD_V} = \frac{\left\langle |h_{VV}|^2 \right\rangle}{\left\langle |h_{HV}|^2 \right\rangle} \tag{2.22}$$

$$\mathrm{XPD_H} = \frac{\left\langle |h_{HH}|^2 \right\rangle}{\left\langle |h_{VH}|^2 \right\rangle} \tag{2.23}$$

$$\mathrm{CPR} = \frac{\left\langle |h_{VV}|^2 \right\rangle}{\left\langle |h_{HH}|^2 \right\rangle} \tag{2.24}$$

These values are no longer affected by the channel small-scale variations. Based on these values, a mean XPD/CPR vs. Tx-Rx distance model has been developed.

- *XPD_V large-scale variations*

  The $\mathrm{XPD_V}$ values vs Tx-Rx distance are plotted in figure 2.15 and 2.16 for respectively the outdoor-to-indoor and the indoor-to-indoor scenarios. The corresponding linear regression curves in a least squares sense are plotted in the same figures. For both scenarios, $\mathrm{XPD_V}$ is decaying with distance. In order to fully model the large scale variations of $\mathrm{XPD_V}$, its fading distribution around the linear model ($\Delta\mathrm{XPD_V}$), has been analyzed. It has been found that for both scenarios this later follows a zero mean normal distribution (when the difference is expressed in dB). The Standard Deviation (SD) of this zero-mean normal distributions is given, for both scenarios, in Table 2.5.

- *XPD_H large-scale variations*

  The $\mathrm{XPD_H}$ values vs Tx-Rx distance are plotted in figure 2.17 and 2.18 for respectively the outdoor-to-indoor and the indoor-to-indoor scenarios. The corresponding linear regression curves in a least squares sense are plotted in the same figures. In both scenarios, the global trends of XPD_H were found to be independent with respect to the distance. Furthermore, the samples of XPD_H follow a normal distribution with mean μ and standard deviation σ. These values are given in Table 2.6 for the Outdoor-to-Indoor and the Indoor-to-Indoor cases, respectively.

- *CPR large-scale variations*

  The CPR values vs Tx-Rx distance are plotted in figure 2.19 and 2.20 for respectively the outdoor-to-indoor and the indoor-to-indoor scenarios. The corresponding linear regression curves in a least squares sense are plotted in the same figures. For both scenarios, the overall behavior of CPR was found to be ascending with respect to the distance. The large scale variations of CPR around its linear model (ΔCPR) were found to follow a zero mean normal distribution. The Standard Deviation (SD) of this distribution is also given in Table 2.5.

Table 2.5: Standard deviation of the large scale normal distribution

Out-to-In	σ (dB)	In-to-In	σ (dB)
ΔXPD_V	1,96	ΔXPD_V	2,34
ΔCPR	2,45	ΔCPR	2,47

Table 2.6: Mean and standard deviation of the large scale normal distribution

Out-to-In	μ (dB)	σ (dB)	In-to-In	μ (dB)	σ (dB)
XPD_H	6,71	2,97	XPD_H	6,44	1,75

For ΔXPD_V and ΔCPR, we observe the close values of SD in the two scenarios, meaning that the dispersion of the depolarization of the vertical to the horizontal components is essentially occurring through the Indoor-to-Indoor path. As for the XPD_H , while we observe the same mean value for the two scenarios, the value of SD is larger in the Outdoor-to-Indoor case comparing to the Indoor-Indoor one. This shows that the dispersion of the depolarization of the horizontal components to the vertical ones is more important in Outdoor-to-Indoor case compared to the Indoor-to-Indoor one.

By comparing the figures of XPD_V and XPD_H , we may note that the depolarization from the vertical components to the horizontal ones increases more quickly with distance than the depolarization from the horizontal components to the vertical ones.

We also observe that for both scenarios, the CPR values remain negative on average which means that the overall transmission of the horizontal to horizontal link is better than the vertical to vertical one. Moreover, based on the ascending slope of the CPR mean model, the vertical to vertical transmission is getting better with distance to the detriment of the horizontal to horizontal one. However, in the distance interval studied in this chapter, the overall transmission of the horizontal to horizontal link is better than the vertical to vertical one.

Compared to the previous works characterizing the XPD, our new approach has the advantage to characterize the different spatial variation effects separately from each-other. Moreover, despite most of the previous works, a distinction is made between the XPD_V and XPD_H. Although some previous works have been made on the modeling of XPD for outdoor-to-outdoor and indoor-to-indoor scenarios, the proposed model is the first one which characterize XPD for an outdoor-to-indoor scenario. The use of three cross-polarized antennas instead of only two as classically used in multi-polarized channel studies has the advantage to include all the depolarization possibilities in the model and to make the model independent from the orientation of the antenna system.

As previous works have treated the modeling of XPD for indoor-to-indoor scenarios, a comparison between the results obtained in these works with the results of the proposed study should be done. However one should bear in mind that in all of these works, different frequencies are considered than the one used in this work and no distinction is made between XPD_V and XPD_H.

The values of XPD and CPR reported in [87] and [84] for different indoor-to-indoor environments are in accordance with the results obtained in this work. Higher values of XPD and CPR are obtained in [85, 86] which may be due to the difference in the used frequency or the studied environment. In [98] where the distance-dependence of XPD is characterized for an indoor-to-indoor scenario, the overall trend of XPD is reported not to depend on the distance between the transmitter and the receiver. In our work the same conclusion was drawn for the XPD_H. The mean and standard deviation values of XPD reported in this work are very close to the ones obtained in our work.

In [103], the XPD is characterized in an indoor environment. Despite in our work where a descending trend was observed for XPD_V and a constant trend was observed for XPD_H as a function of distance, in this work the distance-dependent trend of XPD is reported to be ascending with respect to the distance. This different trend may be due to the different definitions of XPD and the different measurement environment compared to our work. However despite this difference in the XPD vs distance trend, the values of XPD reported in this paper are in the same order of magnitude than in our work(around 6dB in the studied interval of distance).

As for the small-scale variation of XPD, the experimental analysis carried out in this work confirms the theoretical results obtained in [99], based on which the XPD small-scale variations follow a doubly non-central F distribution.

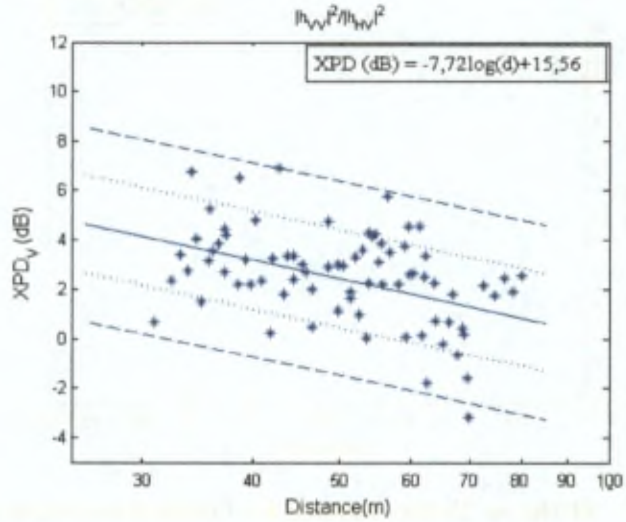

Figure 2.15: XPD_V vs Tx-Rx distance for Outdoor-to-Indoor scenario and the 1σ and 2σ confidence interval

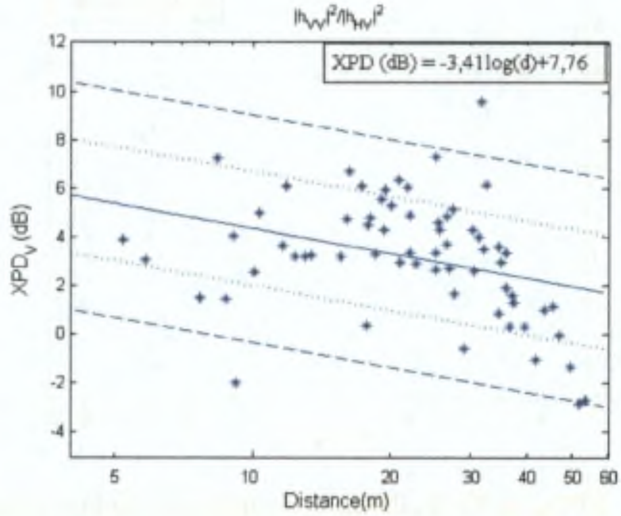

Figure 2.16: XPD_V vs Tx-Rx distance for Indoor-to-Indoor scenario and the 1σ and 2σ confidence interval

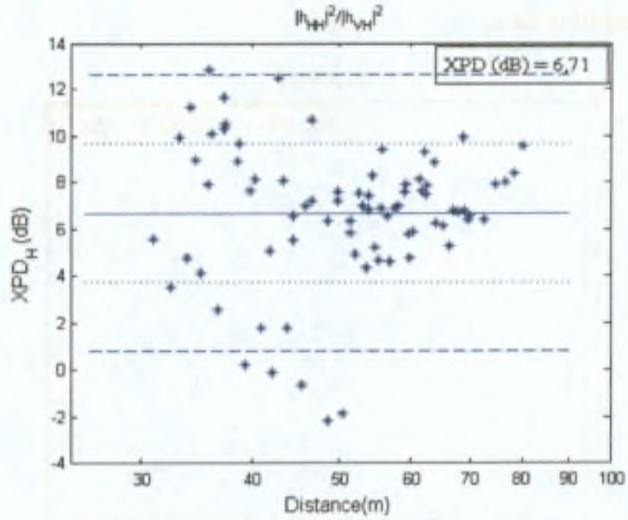

Figure 2.17: XPD_H vs Tx-Rx distance for Outdoor-to-Indoor scenario and the 1σ and 2σ confidence interval

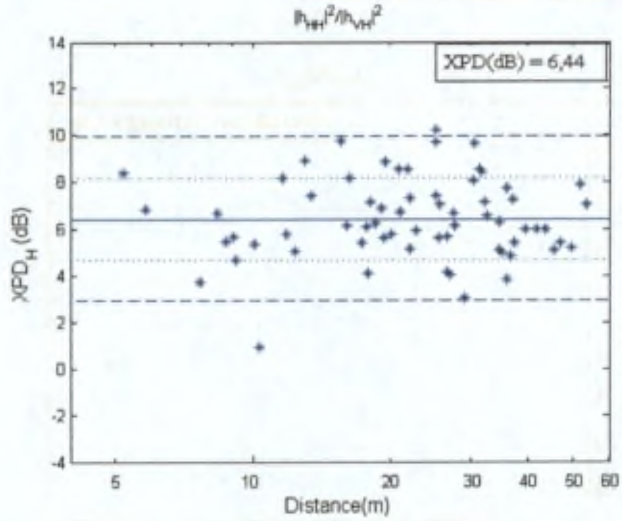

Figure 2.18: XPD_H vs Tx-Rx distance for Indoor-to-Indoor scenario and the 1σ and 2σ confidence interval

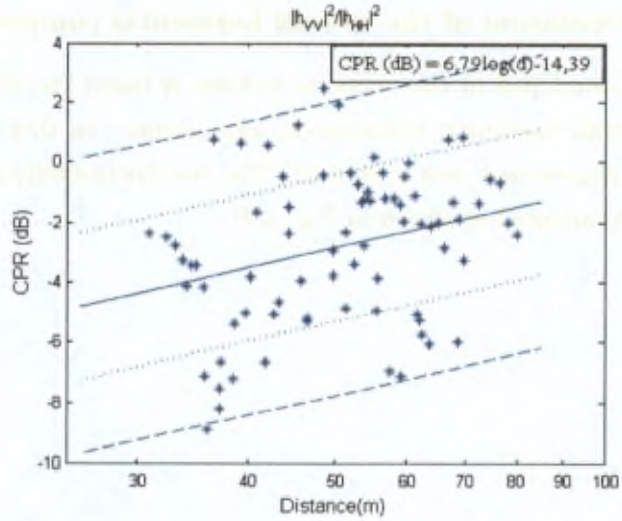

Figure 2.19: CPR vs Tx-Rx distance for Outdoor-to-Indoor scenario and the 1σ and 2σ confidence interval

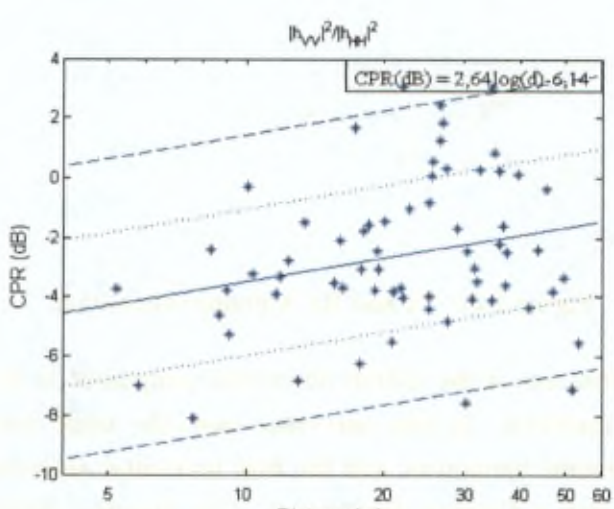

Figure 2.20: CPR vs Tx-Rx distance for Indoor-to-Indoor scenario and the 1σ and 2σ confidence interval

2.4.3 Orientation of the overall horizontal component

The model developed in the previous sections is based on the vertical and the overall horizontal polarization components. In this section a particular tri-polarized case is studied. The two horizontally polarized antennas are oriented as shown in Fig. 2.21.

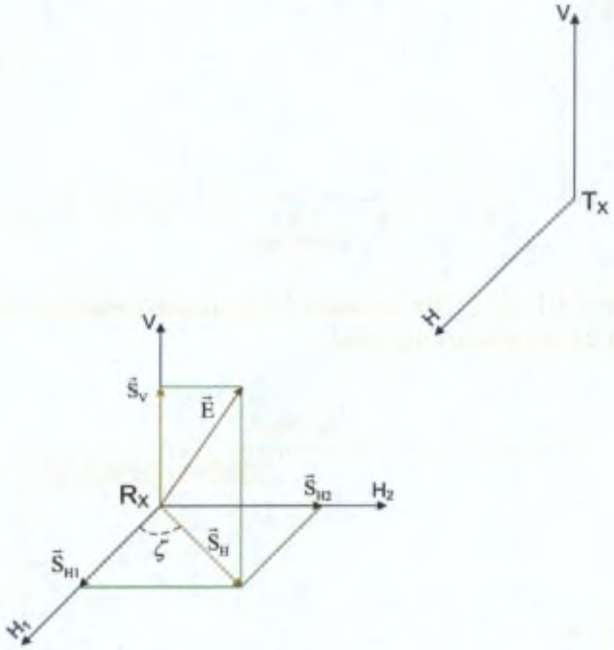

Figure 2.21: Tx and Rx Antenna orientation

The orientation of the overall horizontal component is studied for all the Rx positions. In this particular case, the angle between the overall horizontal component and the first horizontal antenna (ζ) was best fitted with a Gamma distribution. The Gamma distribution is a two parameter family of continuous probability distributions and is parametrized in terms of a shape parameter A and a scale parameter B [128]. An overview of the different Gamma parameters is given for both scenarios in Table 2.7 and Table 2.8. An exemple of the good agreement between the Cumulative Distribution Function (CDF) and the Probability Density Function (PDF) of the experimental ζ and the corresponding Gamma fitting is given in figure 2.22 for a particular position in the indoor-to-indoor scenario.

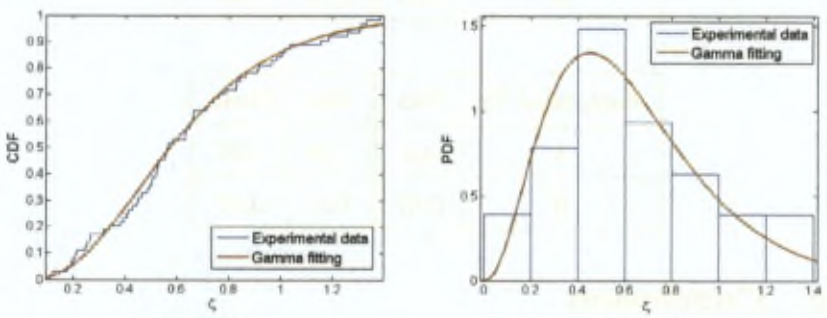

(a) CDF (b) PDF

Figure 2.22: Comparison between the CDF and the PDF of experimental ζ and the corresponding Gamma fitting for a particular position in the indoor-to-indoor scenario.

Table 2.7: Gamma parameters (Shape parameter A and scale parameter B) for the Outdoor-to-Indoor scenario

Vertical Tx	Max	Min	Mean
A	6,17	1,05	2,27
B	0,62	0,16	0,39

Horizontal Tx	Max	Min	Mean
A	4,87	0,78	1,96
B	0,59	0,16	0,38

We can notice the close values of gamma parameters between the two scenarios which show the homogeneity of the orientation of the overall horizontal polarization in the two scenarios.

Table 2.8: Gamma parameters (Shape parameter A and scale parameter B) for the Indoor-to-Indoor scenario

Vertical Tx	Max	Min	Mean
A	5,82	0,83	1,88
B	0,65	0,19	0,46

Horizontal Tx	Max	Min	Mean
A	4,4	0,54	1,27
B	0,67	0,1	0,37

2.5 Conclusion

In this chapter, the depolarization occurred in two cognitive radio scenarios was investigated. Two important parameters describing the radiowave polarization were analyzed: XPD and CPR. XPD quantifies the amount of leakage from one polarization to another caused by the channel. CPR describes the link quality of one polarization compared to the other one. The small scale variations, distance variations and large scale variations of these two parameters have been characterized. This analysis is based on an extensive measurement campaign realized in two different cognitive radio scenarios: outdoor-to-indoor and indoor-to-indoor. The outdoor-to-indoor scenario corresponds to a typical cognitive radio scenario where the primary base station is deployed outside and the secondary network is deployed inside a building. The indoor-to-indoor scenario corresponds to a cognitive radio scenario where both the primary and the secondary networks are deployed inside a same building.

The ambiguity of the orientation of the Rx antenna was resolved by considering the overall horizontal polarization. It has been experimentally shown that for both scenarios, small-scale variations of XPD and CPR follow a doubly non-central F distribution. The distance variations and large scale variations of XPD and CPR have been analyzed independently from the small scale variations. For both scenarios, while the mean variation of XPD_V with distance is linearly decaying, the mean variation of XPD_H is constant with distance. The CPR mean variation was found to be ascending with distance. The large scale variations of all the three parameters around their mean distance model follow a zero-mean normal distribution.

CHAPTER 3

Time-dynamics of wave polarization

3.1 Introduction

Let us consider a MIMO system where the receive antenna is a tri-polarized antenna system made of three co-located perpendicular omni-directionnal antennas. In an idealistic case where there are no Interacting Objects (IOs) in the environnement surrounding the transmitter and the receiver, the polarization of the wave transmitted from the transmitter antenna stays the same at the receiver side. However in a realistic scenario where the environnement is made of many IOs, the polarization of the transmitted wave will change: each multi-path component at the receiver will have different polarization properties. A fraction of a linearly polarized wave will for instance be depolarized, into its perpendicular component leading to an elliptical polarization [129, 130].

The superposition of the different multi-path components having each a different elliptical polarization scheme will lead to another elliptical polarization scheme. In a dynamic scenario, the IOs could change their position and/or shape over time, leading to a dynamic receive scheme where the global receive polarization ellipse changes over time.

In the context of system-based statistical channel modeling, a classical approach in modeling the multi-polarized MIMO channel is to consider the signals received at one vertical and two horizontal perpendicular antennas. Previous works have been done in order to model the multi-polarized MIMO channel at different scales of variation [68, 79, 98, 103–106]. While these works tend at characterizing the signals received at one vertical and one or two horizontal perpendicular antennas, no work has been done in order to model the global polarization of the received fields from an electromagnetic point of view.

The aim of this chapter is to characterize the time dynamics of the receive polarization ellipse for a particular scenario and in a statistical system based approach. This new approach has the advantage to be transposable to any orientation of a receiver with multi-polarized co-located antennas.

In previous works treating multi-polarized MIMO channels, no attention has been paid to fix a particular orientation for the receive antenna system. While this approach has the advantage to model the channel in a situation where the orientation of the receive antenna system does not stay the same all the time, it does not let the model to be transposable to a particular orientation of the receive antenna system. In fact the receive antenna system is made of three perpendicular co-located antennas and as the orientation of this antenna system changes, the channel changes as well. The approach used in this work for modeling the multi-polarized channel could be applied to any orientation of the receive antenna system, by projecting the receive elliptical polarization to the receive antenna system.

With this new approach, the performance of wireless communications could be improved, by adapting the receive antenna system based on the informations on the receive elliptical polarization.

Based on a theoretical analysis and a measurement campaign, a statistical model of the polarization ellipse is developed. The measurements are made in an indoor-to-indoor scenario and at a frequency of 3.6 GHz. Different measurement positions are considered in a LOS and a NLOS scenario.

3.2 Theoretical formulation of the elliptical polarization

An elliptically polarized wave may be resolved in two linearly polarized waves having different phases and amplitudes and being perpendicular to each-other. Different set of parameters may be used in order to characterize an elliptical polarization in the three dimensional (3D) space. In the two dimensional (2D) case, the passage from the received signals on two perpendicular antennas to the elliptical polarization parameters is immediate [131]. In a more realistic 3D scenario, this passage is less intuitive and requires the knowledge of the orientation of the polarization plane (characterized by the vector normal to its surface (Figure 3.1)).

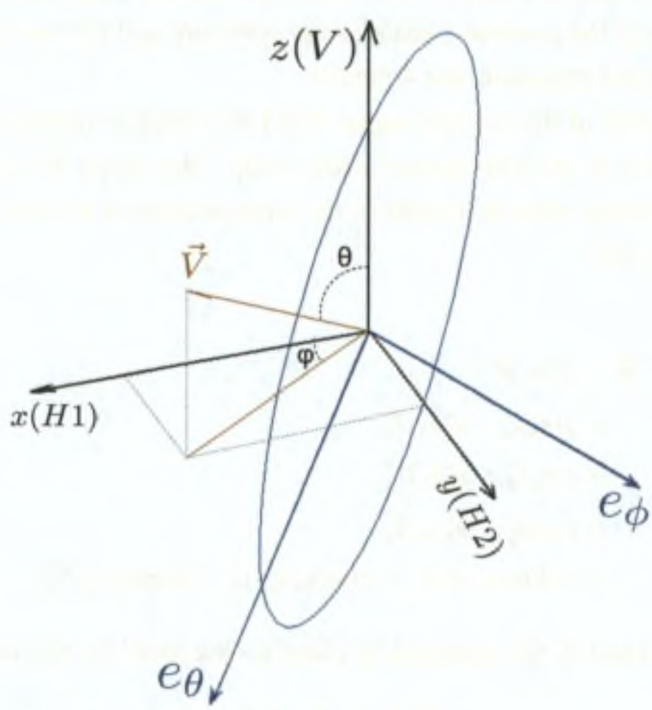

Figure 3.1: The 3D representation of the received polarization ellipse

Let consider $\vec{E}(t)$, the electric field at the receiver. As explained in section 2.2, this electric field will induce a signal at the three receive perpendicularly polarized omnidirectional antennas through the respective equivalent height of each antenna. Let $s_V(t)$, $s_{H1}(t)$ and $s_{H2}(t)$ denote the received signals at the vertical and the two horizontally polarized antennas respectively. The phasors associated with these signals are given by:

$$\vec{s} = \begin{pmatrix} s_x \\ s_y \\ s_z \end{pmatrix} = \begin{pmatrix} s_{H1}e^{j\phi_{H1}} \\ s_{H2}e^{j\phi_{H2}} \\ s_V e^{j\phi_V} \end{pmatrix} \tag{3.1}$$

where s_V,s_{H1} and s_{H2} are the amplitudes and ϕ_V, ϕ_{H1} and ϕ_{H2} are the phases of the received signals at the vertically and the two horizontally polarized perpendicular antennas.

The vector of the received signal $\vec{s}$ and its complex conjugate $\vec{s^*}$ are both located in the polarization plane [132]. The vector $\vec{\mathbf{V}}$ normal to the polarization plane is parallel to the cross product of the two vectors $j\vec{s}$ and $\vec{s^*}$ [132]:

$$\begin{aligned}
\vec{\mathbf{V}} &= j\vec{s} \times \vec{s^*} \\
&= j(s_y s_z^* - s_y^* s_z)\vec{1_x} \\
&+ j(s_z s_x^* - s_z^* s_x)\vec{1_y} \\
&+ j(s_x s_y^* - s_x^* s_y)\vec{1_z} \\
&= -2\mathrm{Im}(s_y s_z^*)\vec{1_x} - 2\mathrm{Im}(s_z s_x^*)\vec{1_y} - 2\mathrm{Im}(s_x s_y^*)\vec{1_z}
\end{aligned} \tag{3.2}$$

The normal to the polarization plane is thus given by the vector $\vec{\mathbf{V}}$:

$$\vec{\mathbf{V}} \equiv (V_x, V_y, V_z) \tag{3.3}$$

where

$$\begin{aligned} V_x &= -2\,\mathrm{Im}\{s_y s_z^*\} \\ V_y &= -2\,\mathrm{Im}\{s_z s_x^*\} \\ V_z &= -2\,\mathrm{Im}\{s_x s_y^*\} \end{aligned} \tag{3.4}$$

$\vec{\mathbf{V}}$ is characterized by its azimuthal and elevation angles ϕ and θ, defined in the Cartesian coordinate system OC_1 formed by the three receive antennas. The normal to the polarization plane belongs to the half space defined by: $0 \leq \phi \leq \pi$ and $0 \leq \theta \leq \pi$. In fact as only the normal to the polarization plane is known but the direction of arrival of the global incident wave is not known and has no meaning, the normal vectors situated in the half space defined by $\pi \leq \phi \leq 2\pi$ and $0 \leq \theta \leq \pi$ are equivalent to their corresponding parallel and opposite vectors in the other half space defined by $0 \leq \phi \leq \pi$ and $0 \leq \theta \leq \pi$. This is illustrated in figure 3.2.

Let us consider $OC2$ the spherical coordinate system defined by the vector $\vec{\mathbf{V}}$ and its orientation angles θ and ϕ (Figure 3.3). Let $\vec{e_\theta}$, $\vec{e_\phi}$ and $\vec{e_r}$ be the orthogonal axes of $OC2$ defined in the direction of increasing θ, ϕ and r. In this way, the $\vec{e_r}$ axis is parallel to the direction of the normal to the polarization plane and the two axes $\vec{e_\theta}$ and $\vec{e_\phi}$ define a transverse 2D basis containing the polarization plane. As a result, the signal components in the coordinate system OC_1 are transformed into the coordinate system OC_2 by the following transformation [133]:

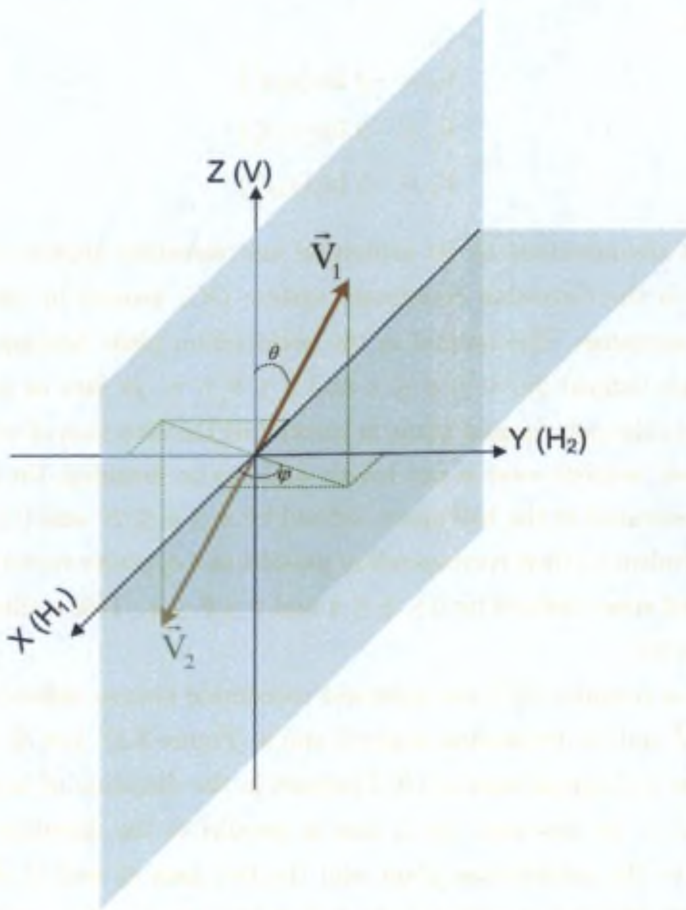

Figure 3.2: A given vector V_2 situated in the half space defined by $\pi \leq \phi \leq 2\pi$ and $0 \leq \theta \leq \pi$ and representing the normal to the polarization plane and its equivalent vector V_1 situated in the other half space defined by $0 \leq \phi \leq \pi$ and $0 \leq \theta \leq \pi$

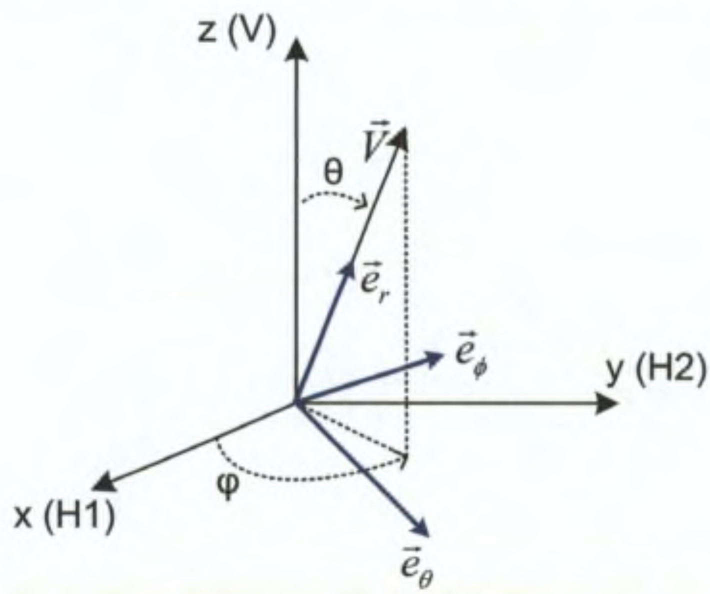

Figure 3.3: The two coordinate systems OC_1 (in black) and OC_1 (in blue) for a given normal to the polarization plane $\vec{V}$

$$\begin{pmatrix} s_r \\ s_\theta \\ s_\phi \end{pmatrix} = \begin{pmatrix} \sin\theta\cos\phi & \sin\theta\sin\phi & \cos\theta \\ \cos\theta\cos\phi & \cos\theta\sin\phi & -\sin\theta \\ -\sin\phi & \cos\phi & 0 \end{pmatrix} \cdot \begin{pmatrix} s_x \\ s_y \\ s_z \end{pmatrix} \tag{3.5}$$

where the radial component s_r will be zero.

Having the two transverse components s_θ and s_ϕ, the elliptical polarization parameters in the polarization plane are obtained by the classical 2D relations (Figure 3.4).

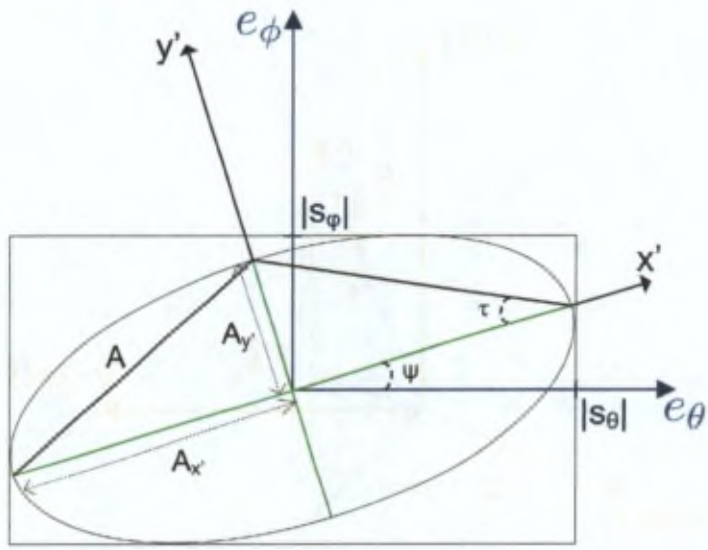

Figure 3.4: The representation of the polarization ellipse in the polarization plane

The phase difference between the two transverse components is defined by:

$$\delta = \text{phase}(s_\phi) - \text{phase}(s_\theta) \tag{3.6}$$

The orientation of the polarization ellipse in the polarization plane is determined by the tilt angle of the ellipse in the transverse basis. The tilt angle is defined as the angle between the major axis of the polarization ellipse and the e_θ axis and is confined in the interval $[-\frac{\pi}{2}, +\frac{\pi}{2}]$. Let us define, κ, the quotient between the amplitudes of the two transverse components:

$$\kappa = \frac{|s_\theta|}{|s_\phi|}. \tag{3.7}$$

Let us define the angle $\hat{\psi}$ as:

$$\hat{\psi} = \frac{1}{2} \arctan \frac{2|s_\theta||s_\phi| \cos(\delta)}{|s_\theta|^2 - |s_\phi|^2}. \tag{3.8}$$

In the case where $\kappa > 1$, the tilt angle ψ is given by equation 3.8: $\psi = \hat{\psi}$.

In the case where $\kappa < 1$, the tilt angle is given by:

- $\psi = \hat{\psi} + \frac{\pi}{2} \quad \text{if} \quad \hat{\psi} < 0$
- $\psi = \hat{\psi} - \frac{\pi}{2} \quad \text{if} \quad \hat{\psi} > 0$

The ellipticity angle τ is given by:

$$\tau = \frac{1}{2} \arcsin \frac{2|s_\theta||s_\phi| \sin(\delta)}{|s_\theta|^2 + |s_\phi|^2} \tag{3.9}$$

The ellipticity rate e represents the degree of ellipticity of an electromagnetic wave. The value $|e| = 1$ corresponds to a circularly polarized wave and the value $|e| = 0$ corresponds to a linearly polarized wave. The ellipticity rate e is given by:

$$e = \tan(\tau) \tag{3.10}$$

The amplitude of the wave A is given by :

$$A = \sqrt{|s_\theta|^2 + |s_\phi|^2} \tag{3.11}$$

Finally, the length of the semi-minor and the semi-major axis are given by:

$$\begin{aligned} A_{y'} &= |A \sin(\tau)| \\ A_{x'} &= |A \cos(\tau)| \end{aligned} \tag{3.12}$$

Five parameters are used in order to obtain the receive polarization ellipse in the 3D space. Different set of parameters could be used for this purpose. A particular set of parameters which could be used is for instance given by the orientation of the normal to the polarization plane (θ and ϕ), the orientation of the polarization ellipse in the polarization plane (ψ) and the length of the semi-major and the semi-minor axes. Another set of parameters could be given by the orientation of the normal to the polarization plane (θ and ϕ), the orientation of the polarization ellipse in the polarization plane (ψ), the amplitude of the wave A and the ellipticity angle τ.

In the following, the temporal variations of the polarization ellipse are characterized based on an indoor-to-indoor measurement campaign.

3.3 Measurements

A measurement campaign has been performed using the ULB/UCL Elektrobit MIMO channel sounder.

Electrobit channel sounder

The channel sounder is a device which measures the complex baseband response of the channel. The channel sounder is made of two transmit and receive units. The two units can be separated without any cables between the two units. Each unit has a rubidium clock. By synchronizing the two rubidium clocks, the two units stay synchronized separately. To avoid the phase drift, the two units could also be synchronized by a connecting cable using only one of the rubidium clocks. As the clock signal is at low frequency (10 MHz), it could be transmitted over long cables without any significant attenuation. The Electrobit channel sounder transmits and receives long pseudo-noise sequences to determine the channel impulse response.

The transmit and receive units are each connected to a switch which enables very fast switching between 8 antennas at the transmitter and 8 antennas at the receiver. This capability of the sounder is crucial if the temporal variation of the channel is studied in a dynamic channel scenario. The sounder covers the frequencies between 3.4 to 4.2 GHz with a maximum of 200 MHz Bandwidth. In the single clock mode, before starting the measurements, the absolute time of Tx and Rx should be synchronized and the system should be calibrated. Then the two units could be connected to the Tx and Rx antennas and separated while keeping the synchronisation cable between the two units.

The two units of the channel sounder are heavy and bulky devices (see figures. 3.5 and 3.6). This complicates the practical implementation of the measurement campaigns. Some of these complications could be summarized as follow: Each unit has to be carried on a trolley, narrow doors should be avoided, the connection of the channel sounder with other measurement devices such as positioner increases the size of the measurement devices and complicates the measurements, the impact of the channel sounder itself on the propagation channel, etc.

Experimental setup

The measurement parameters which are introduced in the sounder are summarized in Table 3.1. These parameters are chosen in a way to satisfy some criteria such as a good dynamic range in all the measurement positions (around 25 dB), an adequate temporal resolution, a sufficient number of temporal samples during a sufficient period of time, to respect the technical constraints related to the sounder including its stored data rate, etc. The working frequency was 3.6 GHz with a 200 MHz bandwidth. The transmitter and receiver units of the sounder (Figures. 3.5 and 3.6) were connected using a 32-meter N-cable, to run the sounder on a unique clock to avoid phase drift. Both the transmitter and the receiver were tri-pole antennas, composed of three perpendicular co-located short linear antennas. these antenna are the same type than the one used in the previous measurement campaign described in section 2.3. Although the used antennas are experimental measurement antennas, similar compact patch-antenna systems have already been developed for mobile applications [134]. The transmitter and the receiver were at about the same height. Each cycle recorded the complete 3×3 channel matrix. The channel sample rate was 281.171 Hz and a total of 30000 cycles were recorded (over 106 s recording time). An illustrative diagram of the measurement setup is presented in figure 3.7.

The receiver and the transmitter modules were each carried on a separate trolley in order to facilitate the movement of the sounder and the measurement in different positions (figures 3.5 and 3.6). A fixation system was built in order to carry the Data Acquition Unit(DAQ), the receiver unit, the switching system, and the receiver laptop on a same trolley.

Table 3.1: Sounder measurement parameters

Center frequency	3.6 GHz
Bandwidth	200 MHz
Transmit power	23 dBm
Channel sample rate	281.171 Hz
Samples/chip	4
Code length	511
Number of measured cycles	3000 cycles (106.7 sec)
Stored data rate	13.154 MB/s

Three scenarios are investigated:

- *LOS Dynamic:* There is a LOS between the transmitter and the receiver which are both in the same room (Figure 3.12). Both the transmitter and the receiver are static during the measurements while people are randomly moving around (figure 3.8). The measurements are made at a total of 4 different positions. The floor plan of the measurements is given in figure 3.11.
- *LOS Back-Dynamic:* There is a LOS between the transmitter and the receiver which are both in the same room. Both the transmitter and the receiver are static during the measurements while people

Figure 3.5: The transmitter unit

are randomly moving around without blocking the LOS between the transmitter and the receiver (figure 3.9). The measurements are made at a total of 4 different positions. The floor plan of the measurements is given in figure 3.11.

- *NLOS Dynamic:* There is non LOS between the transmitter and the receiver. A Lab-to-Lab scenario is considered where the trans-

Figure 3.6: The receiver unit

mitter is in a first room at the same place than the LOS scenario. The measurements are carried out in two successive rooms at a total of 12 different positions. At each position, the receiver and the transmitter were static during the measurement while people were randomly moving around (figure 3.10). The floor plan of the measurements is given in figure 3.11.

In each scenario and for each measurement position, a static measurement was also made in order to compare the static and the dynamic

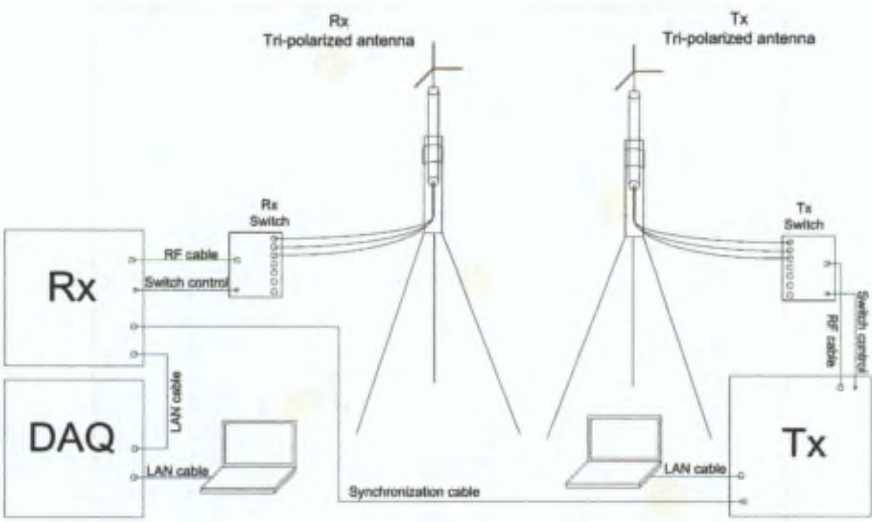

Figure 3.7: The measurement setup

behaviors of the channel. To allow the reproduction of the model and to have the same orientation of the basis, in all the measurement positions, the same orientation was imposed for the transmitter and the receiver tri-pole antennas. The measured impulse responses were averaged over 3 successive impulse responses to increase the measurement SNR, yielding a final channel sampling rate of 93.72 Hz. Finally, the narrowband MIMO matrices were obtained by summing the wideband impulse responses in the delay domain. While only the vertically polarized antenna is considered at the transmitter side, all the three antennas are considered at the receiver side.

3.4 Results

Based on the measurements and the theoretical expressions presented earlier in this chapter, the temporal variations of the parameters describing the receive polarization ellipse in the 3D space are analyzed and a statistical model is deduced.

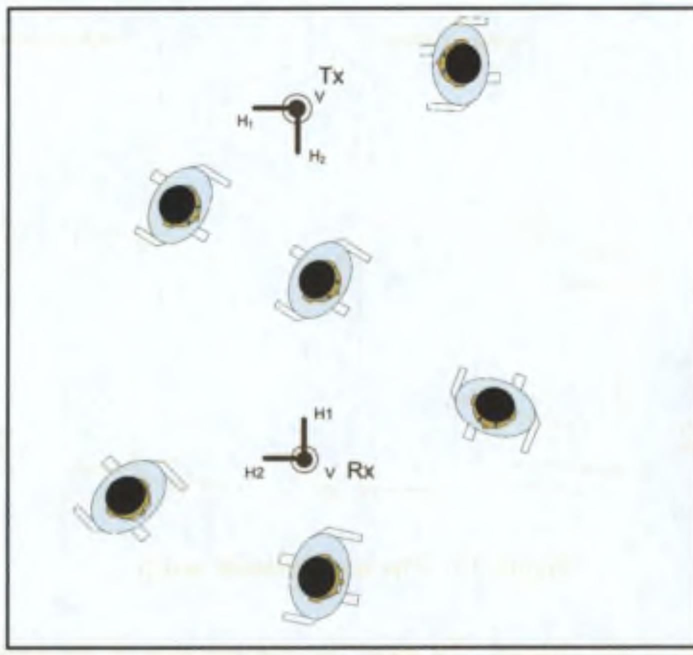

Figure 3.8: The movement around the Rx and the Tx in the LOS dynamic scenario

In order to obtain the statistical distribution of each parameter, the temporal samples of each parameter are first averaged over ten successive samples yielding a total number of 984 samples. Based on these temporal samples, the statistical distribution that each parameter follows at each position is obtained. The following distributions were tested: Beta, Exponential, Gamma, Gaussian, Generalized extreme value, Lognormal, Nakagami, Rayleigh, Ricean, T location-scale and Weibull. Among these distributions, A, $A_{x'}$, $A_{y'}$, e and ψ were best fitted with a Gaussian distribution. The best fitting for the ϕ parameter was obtained by the Gaussian and the Generalized extreme value distributions [135]. As for the θ parameter, the best fitting is obtained by the Gaussian and the T location-scale distributions [136]. As explained later in this chapter, the time-variant dynamics of the channel is also studied based on the

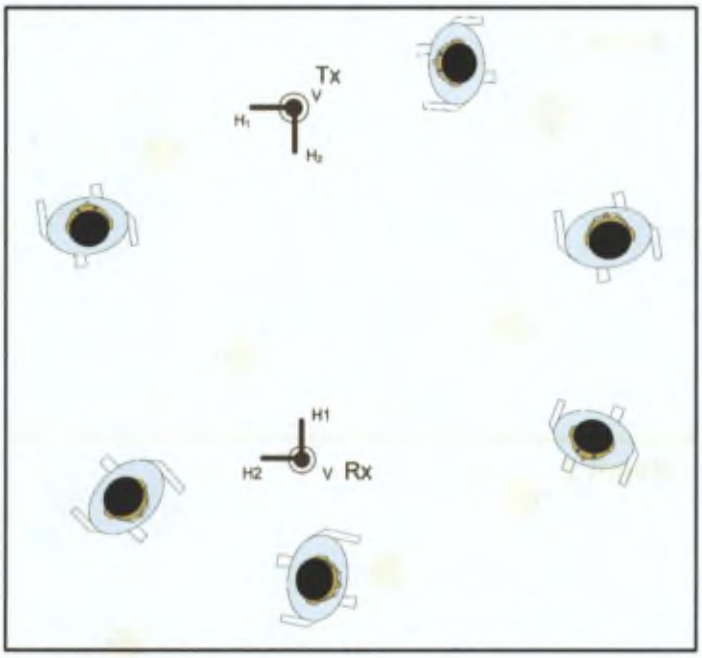

Figure 3.9: The movement around the Rx and the Tx in the LOS Back-dynamic scenario

autocorrelation functions of each parameter. During the generation step of the model, in order to be able to generate statistical temporal samples which are correlated with each other, a Gaussian (or related Gaussian-family) distribution is required for the temporal samples [137]. For this reason the Gaussian distribution is selected for the θ and the ϕ parameters as well.

An overview of these Gaussian distributions and their respective parameters is given in Tables 3.2, 3.3 and 3.4 for the NLOS Dynamic, the LOS Dynamic and the LOS Back-Dynamic scenarios respectively. The distributions of $A_{x'}$, $A_{y'}$ and A are normalized with respect to the average between the different positions of the mean value of the Gaussian distribution of the wave amplitude A.

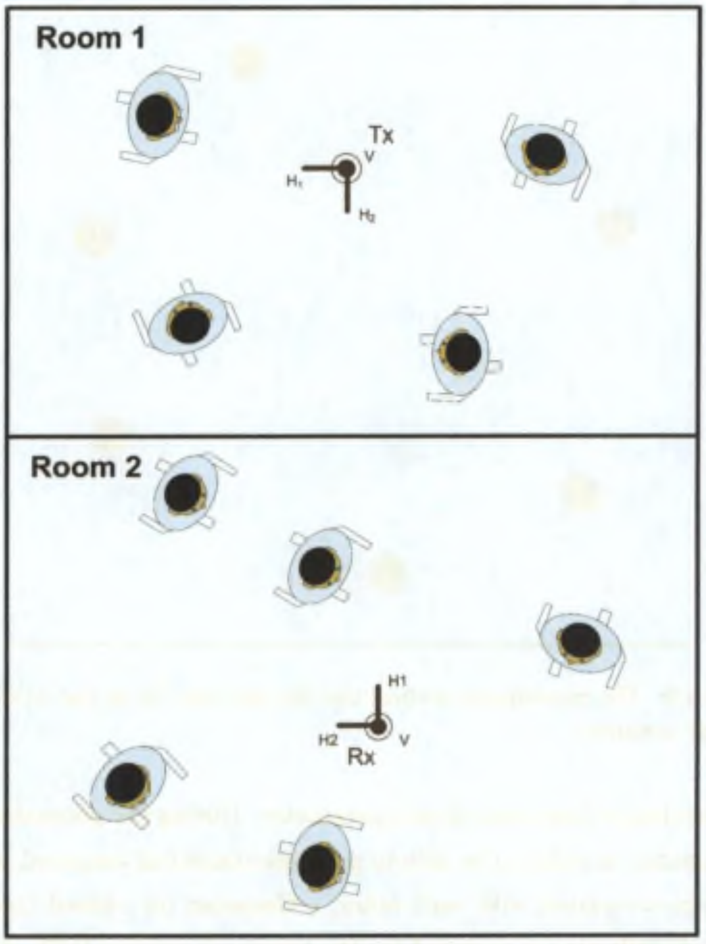

Figure 3.10: The movement around the Rx and the Tx in the NLOS scenario

For all three scenarios, the mean elevation angle θ is on average around 90 degree which corresponds to the horizontal plane and is consistent with the measurements setup where the transmitter and the re-

[2] μ and σ denote respectively the mean and the standard deviation of the Gaussian distribution for each parameter and min, max and mean denote respectively the minimum, the maximum and the mean value of μ or σ between the different measurement positions.

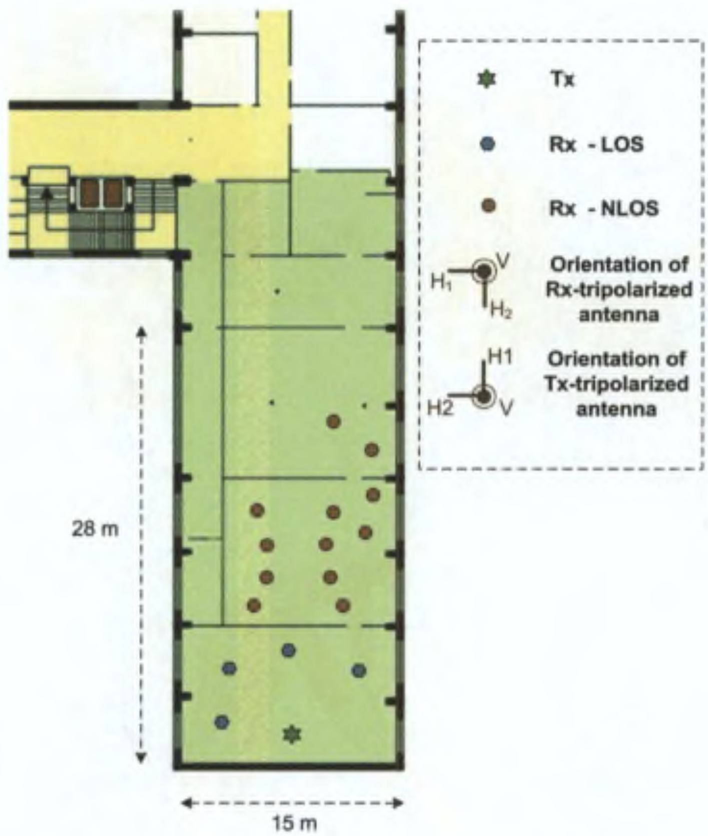

Figure 3.11: Floor plan of the measurements

ceiver were more or less at the same height. However, a system approach was considered in the measurement setup. The antenna effects are thus included in the channel measurements. As omni-directional antennas with high XPI were used in the measurements, the antenna effects are minimized. Moreover, the tri-polarized antennas used at the transmitter and the receiver were made of three cross-polarized co-located antennas. Each antenna was connected to a cable of about 2 meters. The connecting cables could not be disconnected from the antennas. As a result during the calibration phase, the phase shift and the attenuation gener-

Figure 3.12: A particular position in the LOS scenario

ated in these cables were not taken into account. Therefore, the normal to the polarization plane does not necessarily represent the physical direction of arrival of the main beam. In Figure 3.13, the directions of the normal to the polarization plane are presented in 3D space and for the first measurement position in the LOS-Dynamic scenario. We notice the concentration of these vectors in a privileged direction. In other words, the direction of arrival of the measured elliptical polarization is concen-

Table 3.2: Overview of the statistical distributions of the parameters describing the polarization ellipse for the NLOS Dynamic scenario [2]

Parameters	μ			σ		
of the ellipse	min	max	mean	min	max	mean
$A_{x'}$	0.152	1.731	0.942	0.014	0.327	0.165
$A_{y'}$	0.034	0.635	0.269	0.012	0.192	0.074
A	0.157	1.75	1	0.015	0.301	0.166
e	-0.460	0.464	-0.085	0.074	0.270	0.156
ψ $(radian)$	-0.689	-0.043	-0.3	0.046	0.734	0.315
ϕ $(radian)$	0.3133	2.2048	1.0989	0.3004	1.1110	0.6345
θ $(radian)$	1.2960	2.3254	1.9592	0.0692	0.5212	0.2509

Table 3.3: Overview of the statistical distributions of the parameters describing the polarization ellipse for the LOS Dynamic scenario

Parameters	μ			σ		
of the ellipse	min	max	mean	min	max	mean
$A_{x'}$	0.707	1.362	0.925	0.149	0.276	0.207
$A_{y'}$	0.299	0.437	0.351	0.069	0.149	0.103
A	0.776	1.442	1	0.144	0.288	0.213
e	-0.325	0.300	-0.013	0.150	0.312	0.261
ψ $(radian)$	0.174	0.858	0.543	0.244	0.436	0.372
ϕ $(radian)$	0.8109	2.7449	1.8462	0.4134	0.9088	0.6547
θ $(radian)$	1.4898	2.0490	1.8186	0.1716	0.6456	0.4172

trated in a privileged direction. This concentration is more obvious in case of a static channel as shown in figure 3.14. Similar observations were made for the other measurement positions.

Table 3.4: Overview of the statistical distributions of the parameters describing the polarization ellipse for the LOS Back-Dynamic scenario

Parameters	μ			σ		
of the ellipse	min	max	mean	min	max	mean
$A_{x'}$	0.621	1.379	0.932	0.063	0.095	0.079
$A_{y'}$	0.263	0.4	0.342	0.044	0.079	0.058
A	0.679	1.447	1	0.058	0.095	0.079
e	-0.447	0.301	0.009	0.071	0.289	0.168
ψ (*radian*)	0.225	1.067	0.695	0.111	0.324	0.214
ϕ (*radian*)	0.5463	2.9234	2.0212	0.2312	0.6221	0.4457
θ (*radian*)	1.5321	2.2711	1.8957	0.0823	0.7501	0.3205

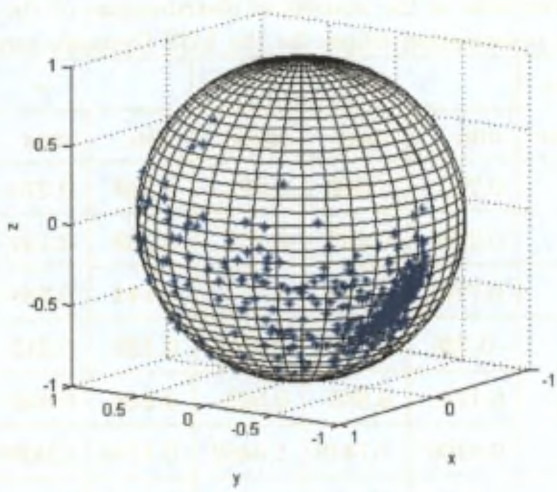

Figure 3.13: The directions of the normal to the polarization plane in 3D space and for a dynamic channel

A wide range of variation is obtained for the mean direction of the normal to the polarization plane. The mean direction of the normal to

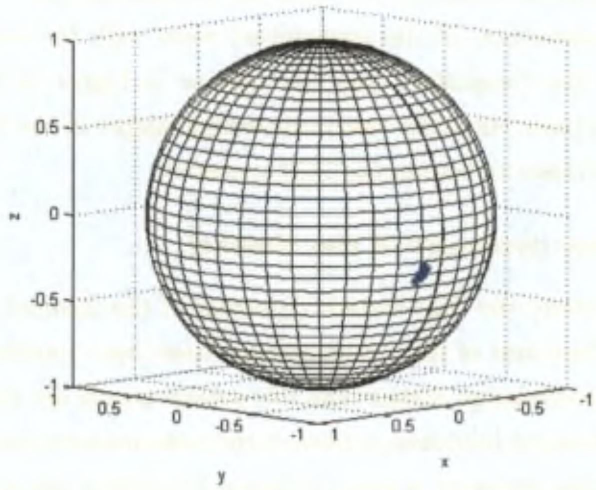

Figure 3.14: The directions of the normal to the polarization plane in 3D space and for a static channel

the polarization plane highly depends on the position of the receiver and the geometrical configuration of the environment.

We notice the close values of μ between the LOS Dynamic and LOS Back-Dynamic scenarios and higher values of σ in the LOS Dynamic scenario compared to the Los Back-Dynamic scenario. Regardless of how people move around the receiver, the elliptical polarization parameters stay the same on average. However the parameters will be much more deviated from the mean values in case of a total dynamic scenario.

We also note the wide range of variation of the mean ellipticity rate parameter between the different positions. As the ellipticity rate represents the degree of ellipticity of a wave, this means that the transmitted vertically polarized wave is received in many different polarization schemes at the receiver. This polarization variability is not exploited in classical MIMO systems where a set of spatially separated co-polarized antennas is used. This problem is solved by using three perpendicularly polarized antennas which receive all incident polarizations.

As the interaction of the transmitted wave with the environment surrounding the transmitter and the receiver is higher in the NLOS scenario, the mean ellipticity rate is on average higher in the NLOS case and remains closer to zero in the LOS scenarios.

3.4.1 Time dynamics of the channel

In order to study the time-variant dynamics of the channel, the autocorrelation functions of all the parameters have been analyzed. For a value of autocorrelation higher than 0.5, similar trends are obtained for the autocorrelation functions of most of the measurement positions. An exemple of this similarity is given in figure 3.15 where the autocorrelation functions of the ellipticity rate is presented for different positions in the NLOS-Dynamic and LOS Bac-Dynamic scenarios.

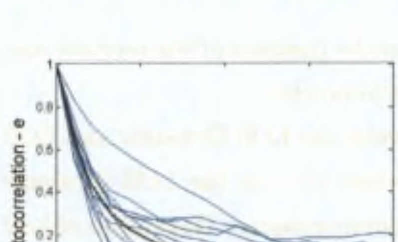

(a) NLOS Dynamic scenario

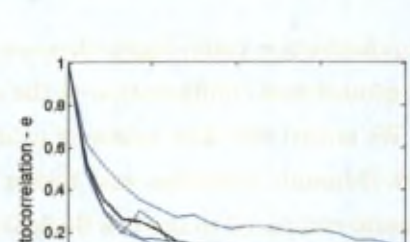

(b) LOS Back-Dynamic scenario

Figure 3.15: Autocorrelation functions of e for different measurement positions (blue thin line) and the mean autocorrelation function of e between the different positions (black bold line) in NLOS and LOS-Back Dynamic scenarios

For each scenario, the average autocorrelation function was obtained by averaging the autocorrelation functions of all the positions. For all the parameters the average autocorrelation functions have very similar trends between the three scenarios. This is shown in figure 3.16. Regardless of how people moves around the receiver and the presence or not of a LOS between the transmitter and the receiver, the temporal dynamics of the parameters describing the polarization ellipse are the same on average. The average autocorrelation functions were best fitted with a decaying exponential model. The parameters of these exponential models are presented in Table 3.5. The *coherence time* of each parameter represents the duration over which the parameter is considered to be not varying. In the literature, the coherence times is assumed to be the duration over which the autocorrelation function is above a certain pourcentage of its maximum value. During this period, the parameter is assumed to change only slightly. The *coherence times* of the different parameters are given in Table 3.6 for the level of 0.7 and 0.5 which correspond to the usual levels used in the literature [137].

For the sake of comparison, the coherence times of the received signals at the three receive antennas are given in Table 3.7. We notice the close values of the coherence time of received signals at the three receive antennas with the coherence times of $A_{x'}$, $A_{y'}$ and A and higher values of coherence time compared to the other parameters of the elliptical polarization.

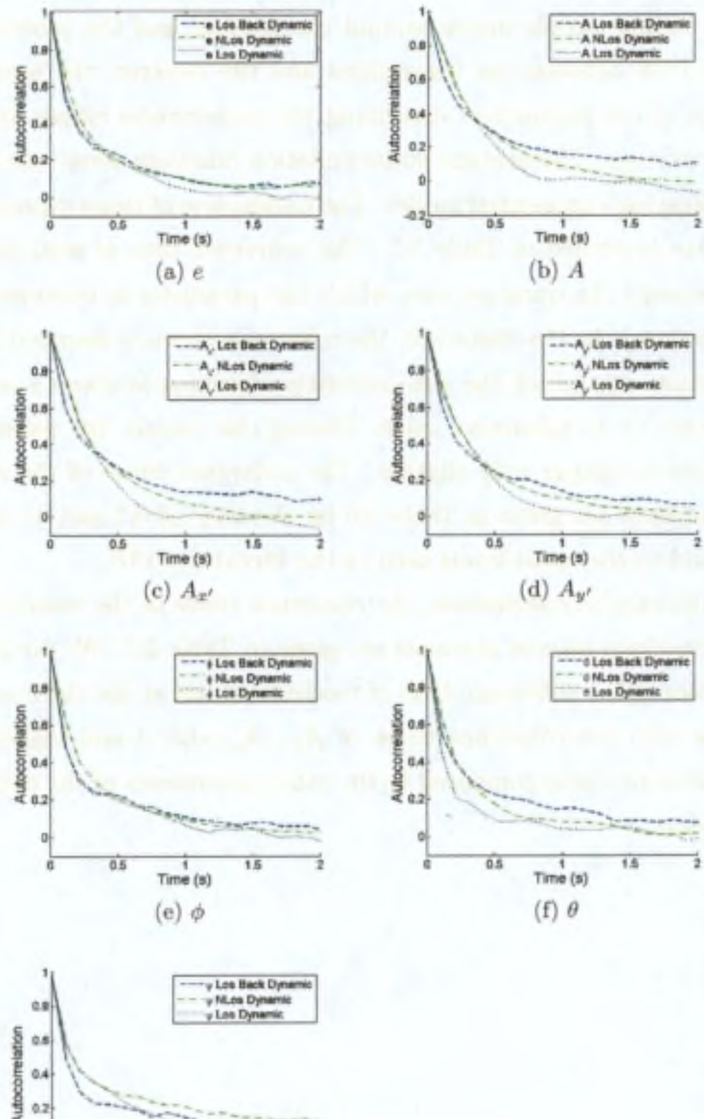

(a) e

(b) A

(c) $A_{x'}$

(d) $A_{y'}$

(e) ϕ

(f) θ

(g) ψ

Figure 3.16: Average autocorrelation functions of the different parameters for the NLOS, LOS Dynamic and LOS Back-Dynamic scenarios

Table 3.5: Exponential models of the autocorrelation functions

$y = exp(-bt)$	b (s^{-1})
$A_{x'}$	3
$A_{y'}$	3.52
A	2.88
e	4.63
ψ	4.81
θ	5.31
ϕ	5.27

Table 3.6: Coherence time in seconds of the different parameters at 0.7 and 0.5 levels

Coherence time (s)	level=0.5	level=0.7
$A_{x'}$	0.231	0.119
$A_{y'}$	0.197	0.101
A	0.241	0.124
e	0.15	0.077
ψ	0.144	0.074
θ	0.13	0.067
ϕ	0.131	0.068

3.5 Projection of the elliptical polarization

In previous sections, the multi-polarized MIMO channel was characterized from an electromagnetic point of view by modeling the receive elliptical polarization. In this section, the theoretical formulation needed in order to project the receive polarization ellipse into the system axis

Table 3.7: Coherence time in seconds of the received signals at the three receive antennas at 0.7 and 0.5 levels

Coherence time (s)	level=0.5	level=0.7
Vertical Rx	0.235	0.121
Horizontal Rx 1	0.209	0.108
Horizontal Rx 2	0.241	0.124

composed of three cross-polarized antennas are obtained. Having a given combination of 5 parameters characterizing the polarization ellipse in the 3D dimension, the multi-polarized channel could be obtained by projecting the polarization ellipse to the receive antenna system.

Let us first consider the polarization ellipse in its polarization plane as presented in figure 3.4. The parametric equations of the elliptical polarization in the $x'y'$ axis are given by:

$$x' = A_{x'} \cos(t) \tag{3.13}$$

$$y' = A_{y'} \sin(t) \tag{3.14}$$

where $t \in [0, 2\pi]$.

The parametric equations of the polarization ellipse in the $e_\theta e_\phi$ axis could be obtained from its parametric equations in the $x'y'$ axis by the following transformation:

$$\begin{pmatrix} e_\theta \\ e_\phi \end{pmatrix} = \begin{pmatrix} \cos\psi & -\sin\psi \\ \sin\psi & \cos\psi \end{pmatrix} . \begin{pmatrix} x' \\ y' \end{pmatrix} \tag{3.15}$$

By combining the equations 3.13, 3.14 and 3.15, the parametric equations of the polarization ellipse along the e_θ and e_ϕ are given by:

$$e_\theta = A_{x'} \cos(\psi)\cos(t) - A_{y'} \sin\psi \sin(t) \tag{3.16}$$

$$e_\phi = A_{x'} \sin(\psi)\cos(t) + A_{y'} \cos\psi \sin(t) \tag{3.17}$$

The amplitude of the two transverse components $|s_\theta|$ and $|s_\phi|$ are obtained by maximizing as a function of t, the parametric equations of the polarization ellipse along the e_θ and the e_ϕ axes respectively:

For $|s_\theta|$ for instance, first the value of t which maximizes the parametric equation of the polarization ellipse along the e_θ axis is found by equalizing to zero the derivate of the e_θ component as a function of t:

$$\begin{aligned}
&\frac{\partial e_\theta}{\partial t} = 0 \\
&\Rightarrow \frac{\partial}{\partial t}\left(A_{x'}\cos(\psi)\cos(t) - A_{y'}\sin\psi\sin(t)\right) = 0 \\
&\Rightarrow -A_{x'}\cos(\psi)\sin(t) - A_{y'}\sin\psi\cos(t) = 0 \\
&\Rightarrow t = \arctan\left[-\frac{A_{y'}}{A_{x'}}\tan(\psi)\right]
\end{aligned} \tag{3.18}$$

The $|s_\theta|$ component is found by replacing equation 3.18 in 3.16:

$$\begin{aligned}
|s_\theta| = \Bigg| &A_{x'}\cos(\psi)\cos\left(\arctan\left[-\frac{A_{y'}}{A_{x'}}\tan(\psi)\right]\right) \\
&-A_{y'}\sin\psi\sin\left(\arctan\left[-\frac{A_{y'}}{A_{x'}}\tan(\psi)\right]\right)\Bigg|
\end{aligned} \tag{3.19}$$

For a given variable x we have [138]:

$$\sin\left(\arctan(x)\right) = \frac{x}{\sqrt{1+x^2}} \tag{3.20}$$

$$\cos\left(\arctan(x)\right) = \frac{1}{\sqrt{1+x^2}} \tag{3.21}$$

As a result the equation 3.19 could be simplified to:

$$|s_\theta| = \left|\frac{A_{x'}\cos(\psi) + \frac{A_{y'}^2}{A_{x'}}\sin(\psi)\tan(\psi)}{\sqrt{1+\frac{A_{y'}^2}{A_{x'}^2}\tan^2(\psi)}}\right| \tag{3.22}$$

The same process is followed in order to obtain the amplitude of transverse component along the e_ϕ axis, $|s_\phi|$. First the value of t which maximizes the parametric equation of the polarization ellipse along the e_ϕ axis is found by equalizing to zero the derivate of the e_ϕ component as a function of t:

$$\begin{aligned}
&\frac{\partial e_\phi}{\partial t} = 0 \\
&\Rightarrow \frac{\partial}{\partial t}\left(A_{x'}\sin(\psi)\cos(t) + A_{y'}\cos\psi\sin(t)\right) = 0 \\
&\Rightarrow -A_{x'}\sin(\psi)\sin(t) + A_{y'}\cos\psi\cos(t) = 0 \\
&\Rightarrow t = \arctan\left[\frac{A_{y'}}{A_{x'}}\cot(\psi)\right]
\end{aligned} \tag{3.23}$$

The $|s_\phi|$ component is found by replacing the equation 3.23 in the equation 3.17:

$$\begin{aligned}
|s_\phi| = \Bigg| &A_{x'}\sin(\psi)\cos\left(\arctan\left[\frac{A_{y'}}{A_{x'}}\cot(\psi)\right]\right) \\
&+ A_{y'}\cos\psi\sin\left(\arctan\left[\frac{A_{y'}}{A_{x'}}\cot(\psi)\right]\right)\Bigg|
\end{aligned} \tag{3.24}$$

Using, the relation 3.20 and 3.21, the equation 3.24 could be simplified to:

$$|s_\phi| = \left|\frac{A_{x'}\sin(\psi) + \frac{A_{y'}^2}{A_{x'}}\cos(\psi)\cot(\psi)}{\sqrt{1 + \frac{A_{y'}^2}{A_{x'}^2}\cot^2(\psi)}}\right| \tag{3.25}$$

Having the ellipticity angle τ, and the amplitude of the two transverse components $|s_\theta|$ and $|s_\phi|$, the phase difference between the two transverse components could be obtained by inversing the equation 3.9:

$$\hat{\delta} = \arcsin\left[\frac{\left(|s_\theta|^2 + |s_\phi|^2\right) sin(2\tau)}{2\,|s_\theta|\,|s_\phi|}\right] \quad -\pi/2 < \hat{\delta} < \pi/2 \tag{3.26}$$

For a given angle x, $\sin(x) = \sin(\pi - x)$. Therefore, given the equation 3.26, $\hat{\delta}$ does not necessarily represent the phase difference δ in all its interval of variation $[0, 2\pi]$. Depending on the value of the tilt angle ψ, the phase difference δ between the two transverse components could be obtained based on $\hat{\delta}$ by the following relations:

- $\delta = \hat{\delta}$ if $\psi \geq 0$
- $\delta = \pi - \hat{\delta}$ if $\psi < 0$.

Finally, having the amplitude of the two transverse components $|s_\theta|$ and $|s_\phi|$, the phase difference, δ, between these two components and the angles θ and ϕ defining the direction of the normal to the polarization plane, the received signals at the three receive antennas could be obtained by inversing the equation 3.5:

$$\begin{pmatrix} s_x \\ s_y \\ s_z \end{pmatrix} = \begin{pmatrix} \sin\theta\cos\phi & \sin\theta\sin\phi & \cos\theta \\ \cos\theta\cos\phi & \cos\theta\sin\phi & -\sin\theta \\ -\sin\phi & \cos\phi & 0 \end{pmatrix}^{-1} \cdot \begin{pmatrix} 0 \\ |s_\theta| \\ |s_\phi|e^{j\delta} \end{pmatrix} \tag{3.27}$$

where for a given matrix A, A^{-1} denotes the inverse of A.

3.6 Generating the model

In this section the process of generating a time-varying multi-polarized channel model based on the time-varying model of the polarization ellipse is explained. A particular combination of 5 parameters are needed in order to completely obtain the polarization ellipse in the 3D dimension. The following set of parameters could for instance be used: A, τ, ψ, θ and ϕ.

The objectif is to produce time-series which follow a given Gaussian distribution while keeping a given correlation between them [137]. First, i.i.d. random samples of the elliptical polarization parameters are generated using zero-mean unit-variance Gaussian distributions. The correlation between the temporal samples are then included in the model using a statistical method based on the Cholesky factorization of the correlation coefficient matrix. The mean and the standard deviation of each parameter are then included in the time-varying model using the Gaussian distributions given in Tables 3.2-3.4.

For each of the 5 parameters, the different steps in order to generate time-varying statistical series are summarized in the following:

1. Generating i.i.d random samples $X = (X_1 X_2, ..., X_m)$ using a zero-mean unit-variance Gaussian distribution $N(0,1)$. The size of the generated samples depends on the duration of the time-series and the sampling frequency.

2. For the duration of the time series, developing a vector of autocorrelation, by sampling the autocorrelation functions given in Table 3.5 at the sampling frequency.

3. Developing the "*covariance*" matrix **Cov** by performing a Toeplitz operation on the vector of autocorrelation [139]. Let the vector of autocorrelation be: $\rho = (1\ \rho_2\ \rho_3\ ...\ \rho_m)$ where ρ_i corresponds to the i^{th} element of the autocorrelation function.

   In this case, the covariance matrix, **Cov**, is obtained by:

$$\mathbf{Cov} = \mathrm{Toeplitz}(\rho) = \begin{pmatrix} 1 & \rho_2 & \rho_3 & \rho_4 & \cdots & \rho_m \\ \rho_2 & 1 & \rho_2 & \rho_3 & \cdots & \rho_{m-1} \\ \rho_3 & \rho_2 & 1 & \rho_2 & \cdots & \rho_{m-2} \\ . & . & . & . & . & . \\ . & . & . & . & . & . \\ . & . & . & . & . & . \\ \rho_m & \rho_{m-1} & \rho_{m-2} & \rho_{m-3} & \cdots & 1 \end{pmatrix} \tag{3.28}$$

4. Performing a Cholesky factorization of the matrix **Cov**, whereby lower triangular matrix **C** is obtained such that $\mathbf{Cov} = \mathbf{C}\mathbf{C}'$ where $(.)'$ denotes the transpose operation.

5. The zero-mean unit-variance correlated samples $Z = (Z_1, Z_2, ..., Z_m)$ are obtained by the following operation:

$$Z = \mathbf{C}X \tag{3.29}$$

6. Finally, considering the mean μ and the standard deviation σ for the Gaussian distribution of the considered elliptical polarization parameter, the vector of correlated samples P, following a Gaussian distribution $N(\mu, \sigma)$, are obtained by the following operation:

$$P = \mu + \sigma Z \tag{3.30}$$

By performing this operation for each of the 5 elliptical polarization parameters, the polarization ellipse is generated based on the time-varying statistical model developed in this chapter. In order to obtain the received signal at each of the cross-polarized receive antennas the generated polarization ellipses should be projected onto the multi-polarized antenna system by using the operations explained in section 3.5.

An example of the time-series obtained by measurements is given for a particular position and for the particular case of the A parameter in figure 3.17a. The corresponding times-series obtained by simulation using the process explained in section 3.6 is given in figure 3.18b. In figure 3.18, the time-series are given during one second of time-interval. Given the order of magnitude of the correlation times, the correlation between the temporal samples is more obvious in these figures.

A comparison between the CDF of the measured and simulated time-series is given in figure 3.19. As expected, we notice the close matching between these two CDF.

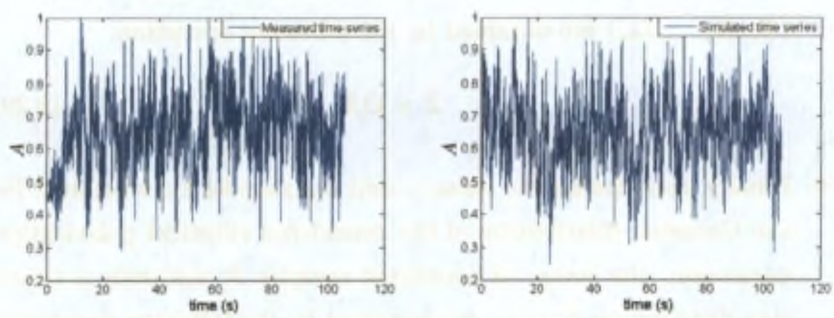

(a) Measured time-series (b) Simulated time-series

Figure 3.17: Time series of the measured and simulated normalized A parameter for a particular position in the NLOS scenarios

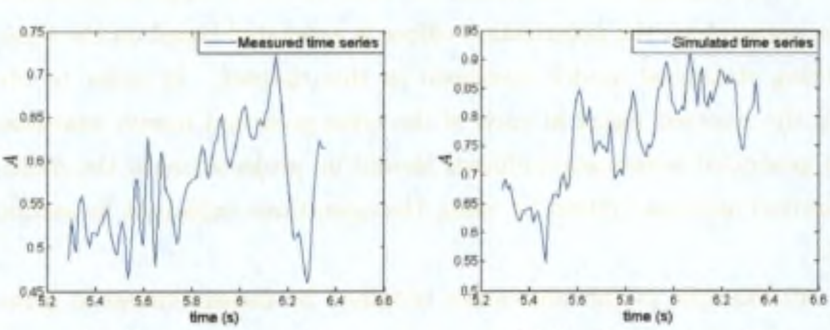

(a) Measured time-series (b) Simulated time-series

Figure 3.18: Time series during 1 sec of the measured and simulated normalized A parameter for a particular position in the NLOS scenarios

3.7 Conclusion

In this chapter, a time varying statistical model of the elliptical polarization of the received waves was presented for a particular indoor-to-indoor scenario. The proposed model was based on a theoretical formulation which was applied to the results obtained from an indoor-to-indoor measurement campaign. The statistical distributions of the parameters describing the polarization ellipse in the 3D space were obtained.

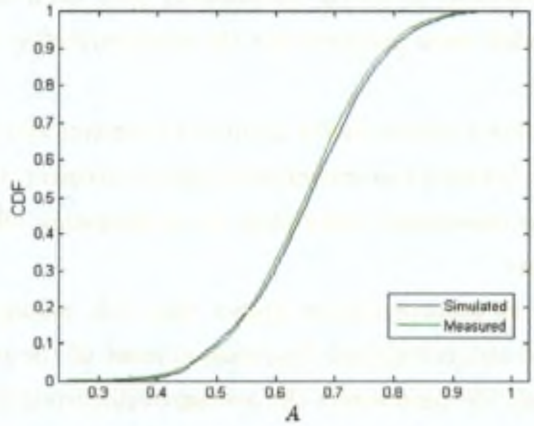

Figure 3.19: comparison between the CDF of the measured and simulated time-series of the normalized A parameter for a particular position in the NLOS scenario

Regardless of how people move around the receiver, the elliptical polarization parameters stay the same on average. However the parameters will be much more deviated from the mean values in case of a total dynamic scenario.

We also noted the wide range of variation of the mean ellipticity rate parameter between the different positions. The transmitted vertically polarized wave is received in many different polarization schemes at the receiver. This polarization variability is not exploited in classical MIMO systems where a set of spatially separated co-polarized antennas is used. This problem is solved by using three perpendicularly polarized antennas which receive all incident polarizations.

As the interaction of the transmitted wave with the environment surrounding the transmitter and the receiver is higher in the NLOS scenario, the mean ellipticity rate is on average higher in the NLOS case and remains closer to zero in the LOS scenarios.

In order to study the time-variant dynamics of the channel, the autocorrelation functions of all the parameters have been analyzed and exponential models were proposed for the autocorrelation functions of the parameters.

Regardless of how people moves around the receiver and the presence or not of a LOS between the transmitter and the receiver, the temporal dynamics of the parameters describing the polarization ellipse are the same on average.

For a value of autocorrelation higher than 0.5, similar trends are obtained for the autocorrelation functions of most of the measurement positions. For all the parameters the average autocorrelation functions have very similar trends between the three scenarios.

An analytical formulation was also proposed in order to project the polarization ellipse onto an antenna system composed of three cross-polarized co-located antennas. Finally, the different steps needed in order to generate a time-varying multi-polarized channel series based on the proposed time-varying model of the polarization ellipse are given. This analytical framework will be further used in chapter 5 in order to study the effect of the antenna orientation and the time-dynamics of the channel on the spectrum sensing performances of a proposed spectrum sensing method.

CHAPTER 4

Multi-polarized Spectrum Sensing by Energy-Detection

4.1 Introduction

In order to satisfy the primordial non-interfering condition in a cognitive radio system, the secondary user must be able to detect reliably and quickly the presence of a primary user in a frequency band [15]. Among the different spectrum sensing techniques which have been proposed so far in the literature Energy Detection (ED) has been widely applied since it does not require any a priori information about the primary signal and has much lower complexity [38, 39, 107].

However in practice, spectrum sensing is considerably deteriorated by the fading nature of wireless channels so that a primary user could be completely hidden from a secondary user. Multi-antenna sensing has been proposed as an interesting way to reduce channel fading effects by introducing spatial diversity into the spectrum sensing scheme. Several previous works have already treated the application of energy detector on a multiple antenna system [53–59]. It has been found that the poor sensing performances of a single antenna system are considerably improved by the use of spatial diversity at the Secondary Terminal (STE). However, there are two limiting issues in the use of spatial diversity which could be resolved by the use of co-located cross-polarized MIMO antennas at the STE.

First of all it is shown in [55] that in correlated channels the sensing performance of a multi-antenna CR system using spatial diversity is deteriorated; hence, to benefit from diversity, a large inter-antenna spacing is required to lower the inter-antenna correlation, which tends to increase the terminal size. The use of three perpendicularly polarized co-located antennas on the other hand, would let the STE be almost as compact as a single antenna system while enjoying the benefits of diversity by the low inter-antenna correlation which exists between cross-polarized antennas [60, 61, 63].

Secondly, the STE may not be aware of the polarization used at the primary base-station (PTx) antenna. Moreover, the polarization of the transmitted primary wave is randomized owing to the different interactions with the surrounding environment so that the signal received at the STE is composed of many waves with different polarizations. This polarization variability is not exploited in the spatial diversity case, and depending on the primary transmitted polarization and the orientation of the STE, the sensing performance could be deteriorated. This issue could be solved by the use of three perpendicularly polarized antennas which receive all incident polarizations.

The problem of multi-polarized spectrum sensing has been previously addressed in [140, 141] where only two perpendicularly polarized antennas are considered at the STE. However, the received wave can not be completely obtained by only 2 of its three polarization components and a third orthogonal antenna is needed in order to receive all the incident polarization components. Moreover, the received polarization state is not obtained based on a real scenario where the real channel depolarization is taken into account but only randomly and uniformly generated. While the depolarization is mainly happening through the propagation in the channel, the channel effect is not studied neither.

In this chapter, the sensing performance of a CR system using a tri-polarized antenna at the STE and in a real-world scenario is investigated. This analysis is based on the outdoor-to-indoor measurement campaign described in chapter 2. In this scenario, the secondary network is deployed indoor and senses the signals received from an outdoor primary base-station.

Based on the results obtained from the measurement campaign of chapter 2 and a theoretical formulation described later in the present chapter, the sensing performance of an energy detector applied to a tri-polarized antenna where each antenna experiences different uncorrelated Rayleigh fading is studied and compared to the spatial diversity case where the STE is made of three co-polar spatially separated antennas. The detection probability as a function of distance between PTx and STE, and the inter-antenna correlation effect on the sensing performance are studied.

4.2 Problem formulation

Let us consider a typical outdoor-to-indoor CR scenario where a secondary network is deployed indoor and senses the signals received from an outdoor primary base station (Figure 4.1). Three cases are considered: a)A STE with a single antenna b)A STE with three co-polar antennas and c)A STE with three perpendicularly polarized antennas. The principal aim of this chapter is to analyze and compare the sensing performances of these three cases and to determine how the polarization of the received electromagnetic waves could influence the spectrum sensing of a CR device. The analysis is based on a theoretical formulation applied to a real outdoor-to-indoor CR scenario through the measurement campaign of chapter 2.

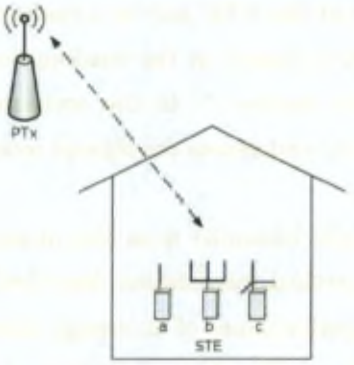

Figure 4.1: Considered outdoor-to-indoor CR scenarios

We consider a CR receiver made of M antennas (with $M = 3$ for the particular case of three cross-polarized antennas). Considering the signal bandwidth $2W$ (the signal is located in [-W,W]) and the observation time T over which signal samples are collected (chosen so that the time-bandwidth product $2TW$ be an integer), the goal is to determine whether a signal is present (hypothesis H_1) or not (hypothesis H_0).

Under H_1, the primary transmitted signal $s(t)$ is received at the i^{th} CR receive antenna over channel h_i and additive zero mean white Gaussian noise $n_i(t)$. The signal $s(t)$ is assumed to be unknown deterministic signal. The received signal $r_i(t)$ at the i^{th} receive antenna is then obtained under the two hypotheses by:

$$\begin{cases} H_1 \; : \; r_i(t) \; = \; h_i s(t) + n_i(t) \\ H_0 \; : \; r_i(t) \; = \; n_i(t) \end{cases} \tag{4.1}$$

In the unrealistic scenario where the received signals on each antenna are uncorrelated, by combining the signals received on each antenna, the channel fading effects could be reduced and the sensing performance is thus improved. In this chapter, two combining methods are considered. First the (MRC) method is presented since it maximizes the sensing performance [142] and the SNR at the output of the combiner, ρ_{output} [45]:

$$\rho_{output} = \sum_{i=1}^{M} \rho_i \tag{4.2}$$

where ρ_i is the SNR on branch i.

However, this optimal combining method requires the knowledge of the Channel State Information (CSI) from primary base station at the secondary terminal. Since in a realistic CR scenario the secondary user is not aware of the CSI from the primary base station, this method is only given as an optimal combining method for the sake of comparison with a second method, the Square Law Combining (SLC) method, where the knowledge of CSI from the primary base station is not required.

A modified energy detector is considered in order to differentiate the two hypothesis H_0 and H_1. With this detector the decision is based on the normalized quantity $E{=}2E_r/N_0$ where E_r is the Base-Band (BB) representation of the energy of the signal denoted $y(t)$ at the combiner output and N_0 is the one-sided noise PSD:

$$E = \frac{2}{N_0}\int_0^T |y(t)|^2\,dt = \frac{1}{N_0 W}\sum_{k=1}^{N} |y[k]|^2 \tag{4.3}$$

where $y[k]$ denotes the samples obtained by sampling $y(t)$ at the Nyquist frequency $2W$ and $N = 2TW$ is the total number of samples.

A signal will be considered as detected in the bandwidth $2W$ and during the observation time T, if the resulting modified energy at the combiner output is higher than a fixed threshold. Considering a detection threshold, η, the probability of detection, P_d, and the probability of false alarm, P_{FA}, are defined by :

$$P_d = P[E > \eta | H_1] \tag{4.4}$$

$$P_{FA} = P[E > \eta | H_0]. \tag{4.5}$$

In the following analysis, the case of a deterministic channel h_i between the primary transmitter and the i^{th} CR receive antenna is first investigated. Then, the case of a Rayleigh fading channel is studied where two diversity cases will be considered: Multipolar and Multi-antenna unipolar cases. In the multi-antenna unipolar reception scenario, all the sub channels experience a Rayleigh fading process with the same Rayleigh distribution parameter σ_h:

$$|h_i| \sim Rayleigh(\sigma_h). \tag{4.6}$$

On the other hand, in the multi-polar reception scenario, each subchannel h_i experiences a Rayleigh fading process with a different Rayleigh distribution parameter σ_{hi},

$$|h_i| \sim Rayleigh(\sigma_{hi}) \tag{4.7}$$

due to the cross-polar discriminations (XPD) which exists between the three polarizations. The XPD denotes the amount of leakage from one polarization to another caused by the channel. This leads to different path-loss patterns for each polarization. The measurement campaign described in chapter 2 characterizes for an outdoor-to-indoor scenario, the path-loss as a function of distance for each of the three receive polarizations. These results are used in this chapter.

In the following, analytical expressions of P_d and P_{FA} are given for MRC and SLC techniques and in a general case where each subchannel experiences a different Rayleigh fading process. In this context, this analytical development has already been made in [58] for the SLC technique but is new for the MRC technique. The application of the analytical expressions in a real-world scenario is then given, based on the measurement campaign.

4.3 Deterministic channel

Let us first consider a deterministic channel h_i between the PTx and each of the CR antennas.

4.3.1 MRC

Under the null hypothesis H_0, the combined signal $y(t)$ at the combiner output is given by:

$$y(t) = \sum_{i=1}^{M} h_i^* n_i(t) \tag{4.8}$$

where h_i^* is the complex conjugate of channel h_i.

Equation (4.3) gives:

$$E = \frac{1}{N_0 W} \sum_{k=1}^{N} |y[k]|^2 = \frac{1}{N_0 W} \sum_{k=1}^{N} \left| \sum_{i=1}^{M} h_i^* n_i[k] \right|^2. \tag{4.9}$$

This can be rewritten as:

$$E = \alpha_h^2 \frac{\sum_{k=1}^{N} \left| \sum_{i=1}^{M} h_i^* n_i[k] \right|^2}{N_0 W {\alpha_h}^2} = \alpha_h^2 E' \tag{4.10}$$

where $\alpha_h^2 = \sum_{i=1}^{M} |h_i|^2$.

Considering i.i.d. $n_i[k]$ with distribution $N(0, N_0W) + jN(0, N_0W)$, the variable $\sum_{i=1}^{M} h_i^* n_i[k] \sim N(0, N_0W \ \alpha_h^2) + jN(0, N_0W\alpha_h^2)$. As a result, E' follows a Chi-square distribution with $2N$ degrees of freedom (χ_{2N}^2) .The cumulative distribution function (cdf) of E is then given by :

$$cdf_E(y) = cdf_{E'}(\frac{y}{\alpha_h^2}) = \frac{\gamma(N, y/2\alpha_h^2)}{\Gamma(N)} \tag{4.11}$$

where $\gamma(..,..)$ is the lower incomplete gamma function and $\Gamma(..)$ denotes the Gamma function [143].

The probability of false-alarm is then given by:

$$\begin{aligned} P_{FA} = P[E > \eta|H_0] &= 1 - P[E < \eta|H_0] \\ &= 1 - cdf_E(\eta) = 1 - \frac{\gamma(N, \eta/2\alpha_h^2)}{\Gamma(N)} \\ = \frac{\Gamma(N) - \gamma(N, \eta/2\alpha_h^2)}{\Gamma(N)} &= \frac{\Gamma(N, \eta/2\alpha_h^2)}{\Gamma(N)} \end{aligned} \quad (4.12)$$

where $\Gamma(..,..)$ is the upper incomplete gamma function [143].

Under the hypothesis H_1 :

$$y(t) = \sum_{i=1}^{M} h_i^* r_i(t) = \sum_{i=1}^{M} h_i^*(h_i s(t) + n(t)) \quad (4.13)$$

and

$$E = \frac{1}{N_0 W} \sum_{k=1}^{N} y[k]^2 = \frac{1}{N_0 W} \sum_{k=1}^{N} \left| \sum_{i=1}^{M} |h_i|^2 s[k] + h_i^* n_i[k] \right|^2. \quad (4.14)$$

This can be rewritten as:

$$E = \alpha_h^2 \frac{\sum_{k=1}^{N} \left| \sum_{i=1}^{M} |h_i|^2 s[k] + h_i^* n_i[k] \right|^2}{\alpha_h^2 N_0 W} = \alpha_h^2 E''. \quad (4.15)$$

Considering i.i.d. $n_i[k]$ with distribution $N(0, N_0 W) + jN(0, N_0 W)$, E" follows a non central chi square distribution with $2N$ degrees of freedom and the non centrality parameter $\lambda = 2\sum_{i=1}^{M} \rho_i = 2\rho_{output}$ ($E'' \sim \chi_{2N}^2(2\rho_{output})$).

The probability of detection is then obtained by :

$$\begin{aligned} P_d = P(E > \eta|H_1) &= P(\alpha_h^2 E'' > \eta|H_1) \\ &= P(E'' > \frac{\eta}{\alpha_h^2}|H_1). \end{aligned} \quad (4.16)$$

Using [144], we can obtain the following closed-form expression:

$$P_d = Q_N(\sqrt{2\rho_{output}}, \sqrt{\frac{\eta}{\alpha_h^2}}) \tag{4.17}$$

where $Q_N(.,.)$ is the generalized Marcum Q function [145].

4.3.2 SLC

Using the SLC method, the combined signal $y(t)$ at the combiner output is given by:

$$y(t) = \sqrt{\sum_{i=1}^{M} r_i^2(t)}. \tag{4.18}$$

Using the same approach than the one used above in the MRC case, as done in [58], the analytical expressions of P_d and P_{FA} for the SLC method and in a deterministic channel scenario are given by :

$$P_{FA} = \frac{\Gamma(NM, \eta/2)}{\Gamma(NM)} \tag{4.19}$$

$$P_d = Q_{NM}(\sqrt{2\rho_{output}}, \sqrt{\eta}). \tag{4.20}$$

4.4 Rayleigh fading channel

The mean probability of detection $\overline{P_d}$ for correlated Rayleigh fading channels is obtained by averaging the probability of detection for deterministic channels (4.20) and (4.17) over the pdf of ρ_{output} referred to as $f(\rho_{output})$:

$$\overline{P_d} = \int_0^{\infty} P_d(\rho_{output}) f(\rho_{output}) d\rho_{output}. \tag{4.21}$$

It is shown in Appendix 1, how we obtain the analytical expressions of the pdf of ρ_{output} for correlated channels and in a multi-polar reception scenario. The final result of this development is given in the following.

The pdf of ρ_{output} for correlated Rayleigh fading channels is given by:

$$f(\rho) = \frac{1}{\gamma}[\frac{e^{Z_1\rho}}{(Z_1 - Z_2)(Z_1 - Z_3)} + \frac{e^{Z_2\rho}}{(Z_2 - Z_3)(Z_2 - Z_1)} + \frac{e^{Z_3\rho}}{(Z_3 - Z_1)(Z_3 - Z_2)}] \tag{4.22}$$

where Z_1, Z_2 and Z_3 are the poles of $\frac{1}{(Z^3+\frac{\beta}{\gamma}Z^2+\frac{\alpha}{\gamma}Z+\frac{1}{\gamma})}$ where:

$$\alpha = \overline{\rho}_1 + \overline{\rho}_2 + \overline{\rho}_3$$

$$\beta = \overline{\rho}_1\overline{\rho}_2 - |\rho_{12}|^2\,\overline{\rho}_1\overline{\rho}_2 + \overline{\rho}_1\overline{\rho}_3 - |\rho_{13}|^2\,\overline{\rho}_1\overline{\rho}_3 + \overline{\rho}_2\overline{\rho}_3 - |\rho_{23}|^2\,\overline{\rho}_2\overline{\rho}_3$$

$$\gamma = \overline{\rho}_1\overline{\rho}_2\overline{\rho}_3 - |\rho_{12}|^2\,\overline{\rho}_1\overline{\rho}_2\overline{\rho}_3 - |\rho_{13}|^2\,\overline{\rho}_1\overline{\rho}_2\overline{\rho}_3 - |\rho_{23}|^2\,\overline{\rho}_1\overline{\rho}_2\overline{\rho}_3 + \rho_{12}\rho_{23}\rho_{13}^*\overline{\rho}_1\overline{\rho}_2\overline{\rho}_3 + \rho_{13}\rho_{12}^*\rho_{23}^*\overline{\rho}_1\overline{\rho}_2\overline{\rho}_3$$

where $\overline{\rho}_i$ is the mean SNR received on the i^{th} antenna and ρ_{ij} is the complex correlation coefficient between the i^{th} and j^{th} antenna.

4.5 Results

4.5.1 The implementation context

The measurement campaign of chapter 2 is used in order to implement the theoretical results obtained in the previous sections. An outdoor-to-indoor cognitive radio scenario is considered where the secondary network is deployed indoor and senses the signals received from an outdoor primary base station. The outdoor-to-indoor measurement campaign described in chapter 2 is used in order to obtain the path-loss models between the different polarized antennas at the transmitter and the receiver.

By fitting the mean power values of the sub-channels obtained by averaging the 64 received power values in the 8×8 grid, a path-loss model was established for each of these sub-channels. The different path-loss models obtained from the measurements and in a least squares sense are presented in figures 4.2-4.7. The standard deviations of the shadowing around the path-loss models are given in Table 4.2. An overview of the different path-loss equations is given in Table 4.1. The theoretical expressions found in the previous sections are simulated using these path-loss models. The mean received power and SNR of the three polarizations at the receive antennas and for different distances between the primary transmitter and the secondary terminal are obtained from these path-loss models. These values are used for the simulation of the analytical relations.

As assumed in previous sections, it has been verified through the measurements that the distribution of the channel could be approached by a Rayleigh fading distribution. A KS test confirmed this assumption. For a significance level of 5% the null hypothesis has been satisfied on 75 out of the 78 positions.

The simulations were made using a pre-specified probability of false alarm $P_{FA} = 0.01$ and a fixed value of the time bandwidth product $TW = 5$ ($N = 10$). The transmit power was the one used in the measurements (19 dBm). The noise variance N_0W was fixed to -70dBm.

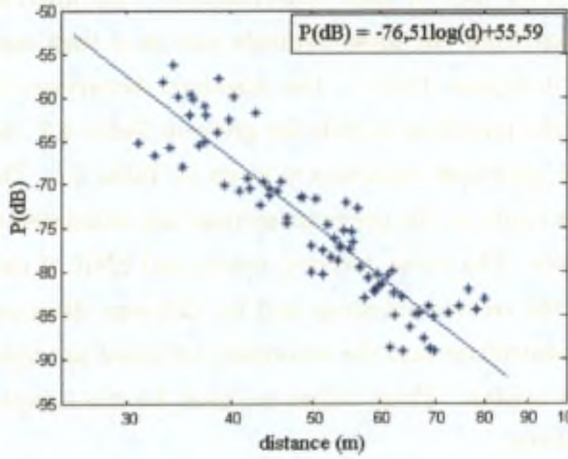

Figure 4.2: Path loss fitting for TX_V - RX_V

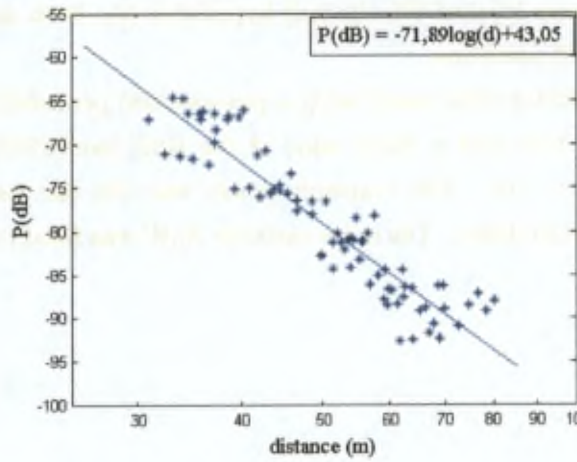

Figure 4.3: Path loss fitting for TX_V - RX_{H1}

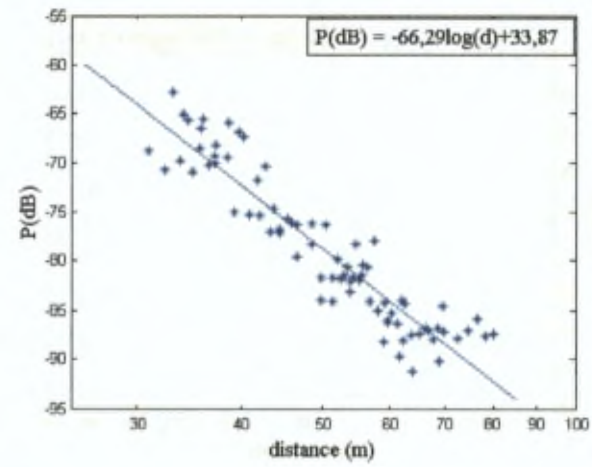

Figure 4.4: Path loss fitting for TX_V - RX_{H2}

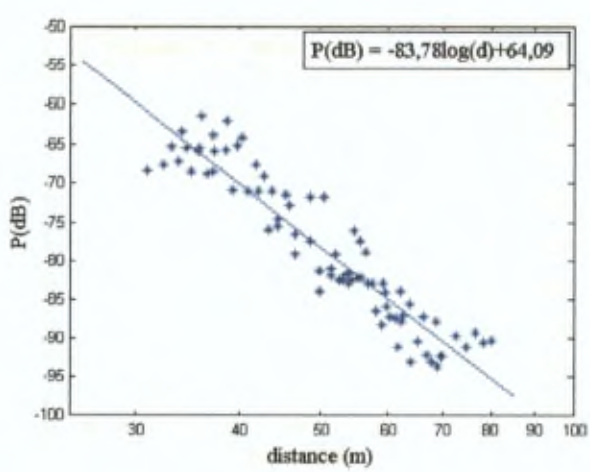

Figure 4.5: Path loss fitting for TX_H - RX_V

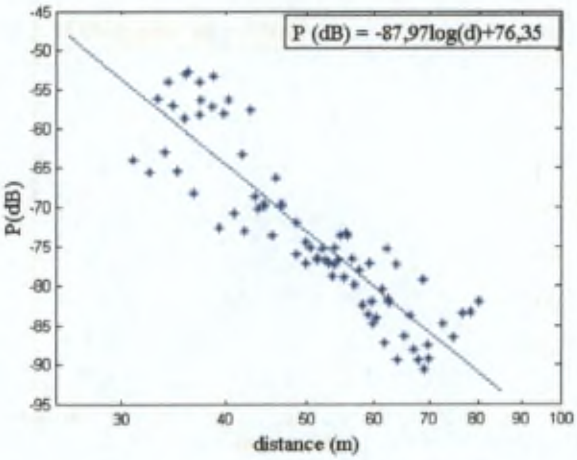

Figure 4.6: Path loss fitting for TX_H - RX_{H1}

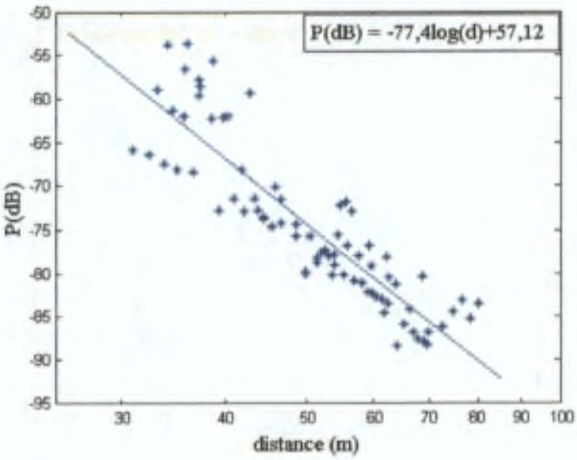

Figure 4.7: Path loss fitting for TX_H - RX_{H2}

Table 4.1: Path-loss equations[1]

$TX_V\ RX_V$	$P(dB) = -76.51\log_{10}(d(m)) + 55.59$
$TX_V\ RX_{H1}$	$P(dB) = -71.89\log_{10}(d(m)) + 43.05$
$TX_V\ RX_{H2}$	$P(dB) = -66.29\log_{10}(d(m)) + 33.87$
$TX_H\ RX_V$	$P(dB) = -83.78\log_{10}(d(m)) + 64.09$
$TX_H\ RX_{H1}$	$P(dB) = -87.97\log_{10}(d(m)) + 76.35$
$TX_H\ RX_{H2}$	$P(dB) = -77.40\log_{10}(d(m)) + 57.12$

Table 4.2: Standard deviations of the shadowing around the path-loss models

	Standard Deviation (dB)
$TX_V\ RX_V$	3.53
$TX_V\ RX_{H1}$	2.93
$TX_V\ RX_{H2}$	2.73
$TX_H\ RX_V$	3.21
$TX_H\ RX_{H1}$	4.69
$TX_H\ RX_{H2}$	4.21

4.5.2 Polarization and space diversity for uncorrelated channels

The probability of detection versus both the distance between the PTx and the STE, and the SNR at the receive horizontal antenna (RX_{H1}) is shown for different diversity cases in figure 4.8. The sensing performance

[1] $TX_H\ RX_V$ denotes the link between the horizontally polarized antenna at the Primary base station and the vertically polarized antenna at the secondary terminal receiver. RX_{H1} and RX_{H2} stand for the two horizontally polarized antenna at the secondary terminal receiver. P denotes in dB scale, the received power relative to the transmit power of 19 dBm. d denotes the distance in meter between the primary base station and the secondary terminal receiver

of the single-antenna case, the polarization diversity case and the space diversity case ($M = 3$) are compared with each other. The probability of detection is obtained by numerically integrating (4.21) for each distance. The threshold η is numerically obtained for each distance to meet the false-alarm probability constraint.

As shown in this figure, in a single antenna case, the orientation of the secondary CR antenna has a significant negative impact on the detection performance when it differs with the orientation of the primary transmitter antenna. In a practical case where the orientation of the STE does not stay the same all the time, the sensing performance could then be significantly deteriorated. As shown in this figure, the use of diversity considerably improves the sensing performance. By considering a minimum acceptable detection probability of 0.95, the use of diversity increases the range of acceptable sensing up to 18 meters. The minimum acceptable SNR is reduced up to 14 dB. Although in figure 4.8 the horizontally polarized antenna is considered at the transmitter side, similar conclusions are obtained for the vertically polarized transmit antenna.

As expected, the best performances are obtained by the MRC method. However this optimal method requires the knowledge of the primary to secondary CSI which is not practical in a realistic CR scenario. The detection performances are slightly decreased by using the SLC method where the knowledge of the primary to secondary CSI is not required anymore. For example for the multi-polar reception scenario, the SLC method increases the minimum acceptable SNR by less than 2 dB and decreases the range of acceptable sensing by less than 3 meters.

For the same combining method, the best performance is obtained when using three separated receive antennas with the same orientation as the orientation of the PTx. The performance of the tri-polarized sensing lies between the spatial diversity cases with co and cross-orientation

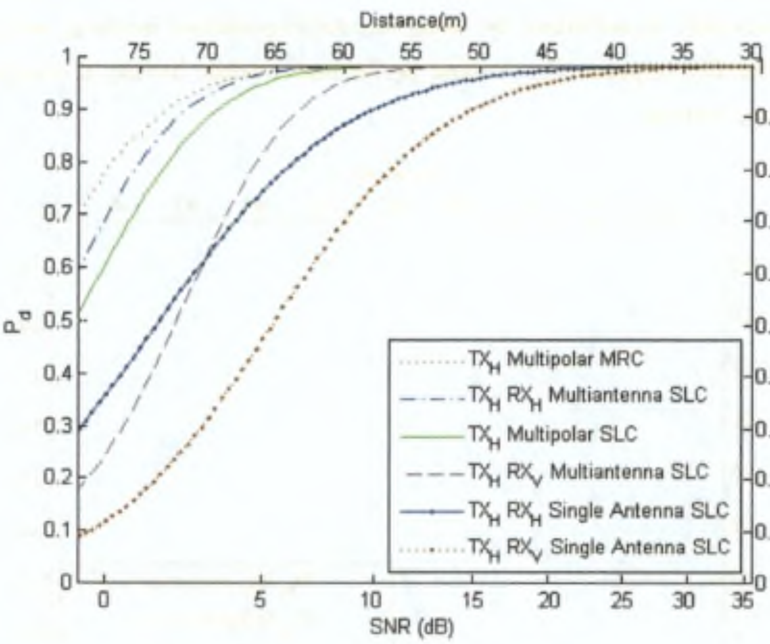

Figure 4.8: Multi-antenna Multi-polar and single antenna comparison, $M = 3$, $P_{FA} = 0.01$, $N = 10$, Horizontal polarization used at transmitter side(TX_H), SNR refers to as SNR obtained on the first horizontal receive antenna.

between PTx and STE. At lower SNR and in case of cross orientation between the PTx and the STE, the sensing performance of a CR system using spatial diversity could even become worse than a single antenna system having the same orientation than the PTx. In a practical case, where the orientation of the secondary terminal does not stay the same all the time, the use of a tri-polarized antenna scheme at the secondary terminal is a good trade-off of performance.

Also as shown in figure 4.9, in a practical case where the orientation of the PTx is unknown, the use of a tri-polarized antenna scheme at the secondary terminal is a good trade-off of performance compared to the spatial diversity case, since all the receive polarizations are taken into account. In addition, by using the multi-polarized sensing, we can considerably improve the sensing performance while having a compact antenna system.

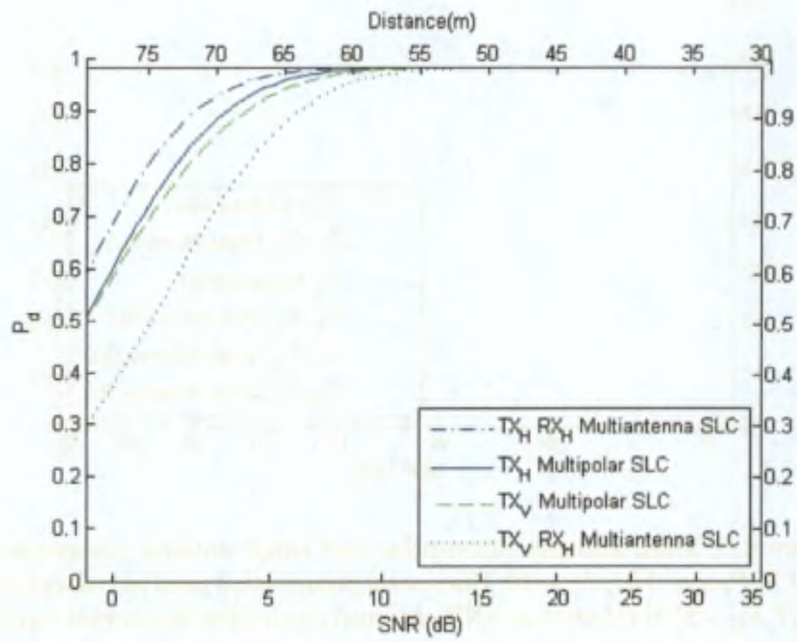

Figure 4.9: Multi-antenna and Multi-polar performance when the TX orientation is unknown, $M = 3$, $P_{FA} = 0.01$, $N = 10$, SNR refers to as SNR obtained on the first horizontal receive antenna.

The results given in the previous figures correspond to the mean probability of detection. In figure 4.10, the standard deviation of the instantaneous probability of detection around the mean probability of detection is given for the case of multi-polarized detection with SLC. The standard deviation is low at high SNR and increases as the SNR is reduced. For a SNR of 0 dB, the standard deviation of the instantaneous probability of detection becomes as high as 0.3. This high range of variation around the mean probability of detection, decreases the reliability of the system at low SNR. However, by increasing the number of samples, N, used for sensing, the values of low SNRs for which, high standard deviations are obtained for the instantaneous probability of detection could be reduced. By fixing the value of acceptable probability of detection to 0.9, the probability that the probability of detection be above 0.9 is given in figure 4.11. By comparing the figures 4.8 and 4.11, we notice that both performance metrics start decreasing at around 10 dB. However, by the reducing the SNR, the mean probability of detection decreases less quickly than the probability that the probability of detection be above 0.9.

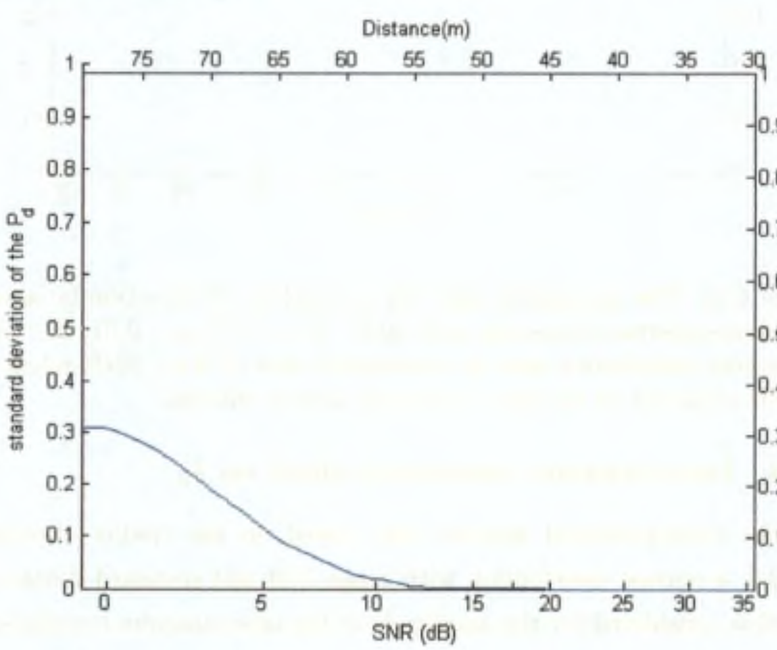

Figure 4.10: The standard deviation of P_d around the mean P_d, Multi-polarized detection with SLC, $M = 3$, $P_{FA} = 0.01$, $N = 10$, Horizontal polarization used at transmitter side (TX_H), SNR refers to as SNR obtained on the first horizontal receive antenna.

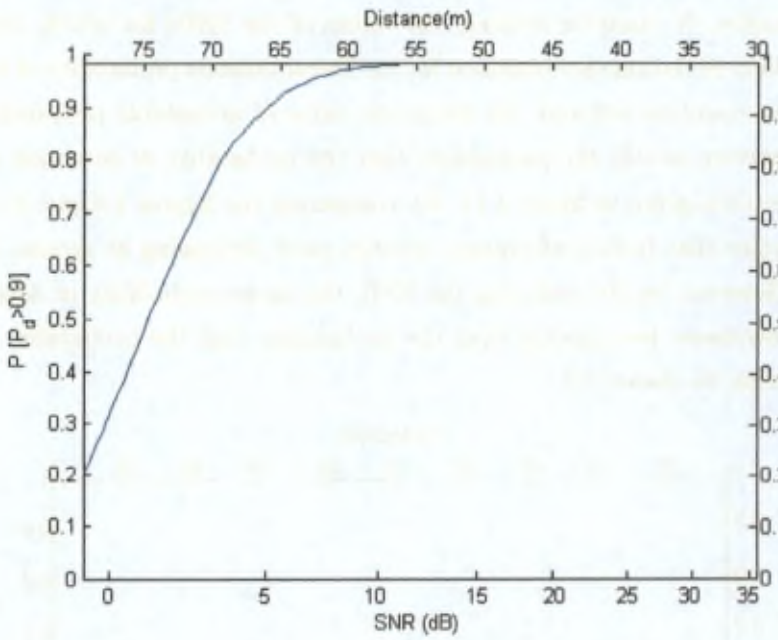

Figure 4.11: The probability that the probability of detection be above 0.9, Multi-polarized detection with SLC, $M = 3$, $P_{FA} = 0.01$, $N = 10$, Horizontal polarization used at transmitter side (TX_H), SNR refers to as SNR obtained on the first horizontal receive antenna.

4.5.3 Inter-antenna correlation effect on P_d

For the multi-polarized sensing case, based on the results obtained in [104], a normal distribution with mean 0.36 and standard deviation of 0.19 is considered for the amplitude of the inter-antenna correlation. Based on the same paper, the phase of the inter-antenna correlation parameters is considered to be uniformly distributed between 0 and 2π. Figure 4.12 shows that, as expected, by increasing the amplitude of correlation between the antennas, the sensing performances are deteriorated. However even with a high inter-antenna correlation, the performances of tri-polarized sensing remains considerably better than single antenna sensing.

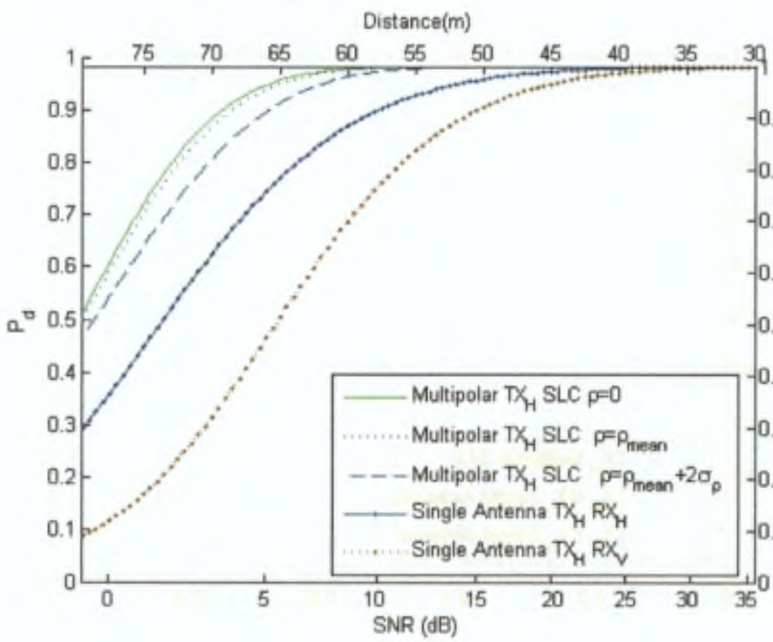

Figure 4.12: Inter-antenna correlation effect on the tri-polarized sensing and comparison with the single antenna case, SLC, $M = 3$, $P_{FA} = 0.01$, $N = 10$, Horizontal polarization used at transmitter side (TX_H), SNR refers to as SNR obtained on the first horizontal receive antenna.

In figure 4.13, the probability of detection is presented for different levels of the inter-channel correlation amplitude $|\rho|$ and for the multipolar and the single antenna cases. The sensing performances of tri-polarized sensing are slightly decreased with the correlation amplitude. However even in case of high correlated channels, the sensing performance of tri-polarized sensing remains better than the single antenna case. In case of a mismatch between the polarization of the STE and the PTx, the sensing performances of a single antenna system are much more deteriorated than if a high inter-antenna correlation exists in a tri-polarized system.

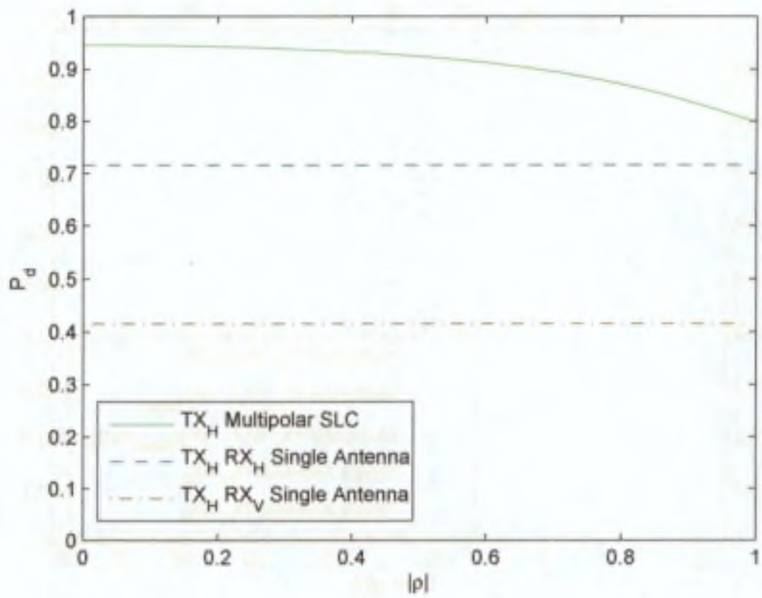

Figure 4.13: Probability of detection vs inter-antenna correlation coefficient $|\rho|$, Horizontal polarization used at transmitter side (TX_H), SNR at the first horizontal receive antenna = 4.4 dB, $M = 3$, $P_{FA} = 0.01$, $N = 10$

4.6 Conclusion

In this chapter the performance of multi-polarized spectrum sensing based on energy detection was studied and compared to a multi-antenna co-polar system. A theoretical formulation was derived and applied to a real-world scenario, based on an outdoor to indoor measurement campaign. The detection probability versus the distance between the PTx and the STE was analyzed for the different cases. It was shown that the poor sensing performance of a single antenna system could be significantly improved by the use of polarization and spatial diversity. It has been found that in a multi-path environment, the performance of spectrum sensing by spatial diversity could be significantly deteriorated depending on the matching between the orientation of the PTx and the STE. In a practical case where the orientation of the STE is not the same all the time and the orientation of the PTx is not known by the secondary user, the spectrum sensing by polarization diversity scheme takes into account all the received polarizations and is thus a good compromise of performance. Moreover the space diversity scheme requires large spacing between antennas. By using co-located tri-polarized antennas, the STE could be almost as compact as a single antenna system while having a significant better performance. As expected, the inter-antenna correlation was found to have a negative impact on the sensing performance. However, even with high inter-antenna correlation, the performance of tri-polarized sensing remains considerably better than the single antenna case.

APPENDIX 1

The analytical expressions of the pdf of ρ_{output} for correlated channels and in a multi-polar scenario using MRC and energy detector are derived by using the process used in [146]. The Laplace transform of $f(\rho_{output})$ is first deduced by:

$$\begin{aligned} F(Z) &= \mathscr{L}(f(\rho_{output})) \\ &= \int_0^{\infty} f(\rho_{output}) e^{-Z\rho_{output}} d\rho_{output} = |\mathbf{I} + Z\mathbf{L}|^{-1} \end{aligned} \tag{4.23}$$

where $\mathbf{I}$ is the identity matrix and $|..|$ denotes the determinant of the matrix and:

$$\mathbf{L} = \begin{pmatrix} \overline{\rho}_1 & \rho_{12}^* \sqrt{\overline{\rho}_1 \overline{\rho}_2} & \rho_{13}^* \sqrt{\overline{\rho}_1 \overline{\rho}_3} \\ \rho_{12} \sqrt{\overline{\rho}_1 \overline{\rho}_2} & \overline{\rho}_2 & \rho_{23}^* \sqrt{\overline{\rho}_2 \overline{\rho}_3} \\ \rho_{13} \sqrt{\overline{\rho}_1 \overline{\rho}_3} & \rho_{23} \sqrt{\overline{\rho}_2 \overline{\rho}_3} & \overline{\rho}_3 \end{pmatrix} \tag{4.24}$$

where ρ_{ij} is the complex correlation coefficient between the i^{th} and j^{th} antenna.

The $f(\rho_{output})$ is then obtained by the inverse Laplace transform of $F(Z)$:

$$f(\rho_{output}) = \mathscr{L}^{-1}(F(Z)) = \frac{1}{2\pi j}\oint e^{ZS}F(Z)dZ. \tag{4.25}$$

By developing $|\mathbf{I}+Z\mathbf{L}|^{-1}$, the following expression is obtained :

$$\begin{aligned} |\mathbf{I}+Z\mathbf{L}|^{-1} &= \frac{1}{1+\alpha Z+\beta Z^2+\gamma Z^3} \\ &= \frac{1}{\gamma(Z^3+\frac{\beta}{\gamma}Z^2+\frac{\alpha}{\gamma}Z+\frac{1}{\gamma})} \end{aligned} \tag{4.26}$$

where :

$$\alpha = \overline{\rho}_1+\overline{\rho}_2+\overline{\rho}_3$$

$$\beta = \overline{\rho}_1\overline{\rho}_2 - |\rho_{12}|^2\overline{\rho}_1\overline{\rho}_2 + \overline{\rho}_1\overline{\rho}_3 - |\rho_{13}|^2\overline{\rho}_1\overline{\rho}_3 + \overline{\rho}_2\overline{\rho}_3 - |\rho_{23}|^2\overline{\rho}_2\overline{\rho}_3$$

$$\begin{aligned}\gamma = \overline{\rho}_1\overline{\rho}_2\overline{\rho}_3 - |\rho_{12}|^2\overline{\rho}_1\overline{\rho}_2\overline{\rho}_3 - |\rho_{13}|^2\overline{\rho}_1\overline{\rho}_2\overline{\rho}_3 - |\rho_{23}|^2\overline{\rho}_1\overline{\rho}_2\overline{\rho}_3 + \\ \rho_{12}\rho_{23}\rho_{13}^*\overline{\rho}_1\overline{\rho}_2\overline{\rho}_3 + \rho_{13}\rho_{12}^*\rho_{23}^*\overline{\rho}_1\overline{\rho}_2\overline{\rho}_3.\end{aligned}$$

Let Z_1,Z_2 and Z_3 be the three poles of

$\frac{1}{(Z^3+\frac{\beta}{\gamma}Z^2+\frac{\alpha}{\gamma}Z+\frac{1}{\gamma})}$:

$$\begin{aligned} F(Z) = |\mathbf{I}+Z\mathbf{L}|^{-1} &= \frac{1}{\gamma(Z^3+\frac{\beta}{\gamma}Z^2+\frac{\alpha}{\gamma}Z+\frac{1}{\gamma})} \\ &= \frac{1}{\gamma(Z-Z_1)(Z-Z_2)(Z-Z_3)}. \end{aligned} \tag{4.27}$$

The inverse Laplace transform of $F(Z)$ is then obtained by :

$$f(\rho_{output}) = \mathbf{L}^{-1}(F(Z)) = \frac{1}{\gamma}[\frac{e^{Z_1\rho}}{(Z_1 - Z_2)(Z_1 - Z_3)} + \frac{e^{Z_2\rho}}{(Z_2 - Z_3)(Z_2 - Z_1)} + \frac{e^{Z_3\rho}}{(Z_3 - Z_1)(Z_3 - Z_2)}]. \quad (4.28)$$

CHAPTER 5

Blind Spectrum Sensing in Cognitive Radios

5.1 Introduction

In the previous chapter we extended the Energy detection method to the multi-polarized antenna systems. However a limiting issue in the use of Energy Detector is that it requires the knowledge of the noise variance at the STE. In practice, the noise variance is not known exactly at the STE [108]. An uncertainty on the estimation of the noise variance could then considerably affect the detection performance of ED method. Cyclostationary feature detection has been proposed as a solution to this problem since it does not require any a priori knowledge of the noise variance [16, 17]. However, although the Cyclostationary feature method performs better than the ED method due its robustness to the noise variance uncertainty, it requires high computational load [147].

Different *Blind Spectrum Sensing* methods are proposed in the literature which do not require any a priori knowledge neither on the primary user signal nor on the noise variance.

In [148], a "blind spectrum sensing" method is proposed which is based on the use of a set of multiple antennas where the antenna separation is less than half wavelength. In this way, in presence of a primary signal (hypothesis H_1), the sub-channels between the primary transmitter and each of the secondary receive antennas are correlated so that the receive signals at the different receive antennas are correlated with each other. In the absence of any primary signals however (hypothesis H_0), only uncorrelated noises are received at the secondary receive antennas. This different behavior under the H_1 and the H_0 hypotheses are used in order to sens the presence of a primary signal under correlated channels.

Generalized-Likelihood Ratio Test (GLRT)-based spectrum sensing methods have been proposed as blind spectrum sensing methods [149–152]. These methods uses a set of multiple antennas at the secondary terminal and are robust to the noise variance uncertainty. These methods were proposed for a static channel scenario and a uni-polar multi-antenna case. We'll see later in this chapter that in case of a dynamic channel, these methods will not work anymore if all the receive antennas are polarized in the same way. In this chapter, the GLRT-based spectrum sensing methods are extended to the case of cross-polarized multi-antenna systems where a set of three co-located cross-polarized antennas are used at the secondary terminal. The performances of a GLRT-based spectrum sensing method is studied in a multi-polarized cognitive radio scenario. The analysis is based on a static and a dynamic channel scenario. Two new multi-polarized blind spectrum sensing methods are also proposed which do not require any a priori knowledge of the noise variance and are thus robust to the noise variance uncertainty. These new methods are based on a particularity of multi-polarized systems.

The performances of these methods are compared with the ED method and in a real-world scenario. This analysis is based on the outdoor-to-indoor measurement campaign of chapter 2, where the secondary network is deployed indoor and senses the signals received from an outdoor primary base-station. Based on the results obtained from this measurement campaign and the theoretical formulation described later, the sensing performance of an energy detector applied to a three-polarized antenna system is studied and compared to the different proposed blind spectrum sensing methods.

5.2 The particularity in cross-polarized multi-antenna systems

Cross-polarized multi-antenna systems have a particularity which is not present in unipolar multi-antenna systems. As previously said in chapter 4.2 in presence of a Rayleigh flat fading channel between the primary transmitter and the secondary terminal while in the multi-antenna unipolar reception scenario, all the sub channels experience a Rayleigh fading process with the same Rayleigh distribution parameter σ_h, in the multi-polar reception scenario, each subchannel $h_i[k]$ experiences a different Rayleigh fading process with a different Rayleigh distribution parameter σ_{hi}. This is due to the XPD which exists between the three polarizations which leads to different path-loss patterns for each polarization. The different path-loss models for each of the three receive polarizations will be here obtained in a real-world scenario from the outdoor-to-indoor measurement campaign of chapter 4.5.1.

While in a multi-polar reception scenario, the different sub-channels $h_i[k]$ corresponding to the different receive antennas have different variances, the background noise $n[k]$ is assumed to have the same variance at all the three receive antennas.

5.3 GLRT-based spectrum sensing

GLRT-based spectrum sensing methods are based on the singular value decomposition of the covariance matrix of the received signals [149–152]. Let us consider the received signal:

$$\mathrm{r} \triangleq r_i[k] \tag{5.1}$$

where

- $x(i)[k]$ is a matrix where i is its line's index and k its column's index.

- $0 < i < M-1$ and i denotes the index of receive antenna between M receive antennas.
- $0 < k < N-1$ and k denotes the sample index out of N total number of samples used for the sensing.

Let us define the covariance matrix $\hat{R}$ as:

$$\hat{R} \triangleq \frac{1}{N} r r^{*} \tag{5.2}$$

where $(.)^{*}$ denote the conjugate transpose. Let us assume that it is feasible to perform an eigenvalue decomposition of the matrix $\hat{R}$ in order to obtain for each block of N samples, the unitary eigenvector matrix $\hat{\mathbf{U}}$ and the diagonal eigenvalue matrix $\hat{\mathbf{\Lambda}}$:

$$\hat{R} = \hat{\mathbf{U}} \hat{\mathbf{\Lambda}} \hat{\mathbf{U}}^{*} \tag{5.3}$$

where $\hat{\mathbf{\Lambda}} \triangleq \mathrm{Diag}\{\hat{\lambda}_i\}$, for $0 < i < M-1$ and $\{\hat{\lambda}_i\}$ is the set of eigenvalues of $\hat{R}$. Let us suppose that the eigenvalues of $\hat{R}$, $\{\hat{\lambda}_i\}$ are sorted in a descending order. In this case, a GLRT spectrum sensing method is proposed in [149, 151] where the test statistic is given by the quotient between the Maximum to the Minimum Eigenvalue (MME):

$$T_{GLRT} = \frac{\hat{\lambda}_0}{\hat{\lambda}_{M-1}} \tag{5.4}$$

Two cases should be considered:

5.3.1 Static Channel

The first case to consider is when the channel between the primary transmitter and each of the secondary terminal antennas stays static during each observation time for sensing. The received signal $r_i[k]$ is then obtained under the two hypotheses H_0 and H_1 by:

$$\begin{cases} H_1 \ : \ r_i[k] \ = \ h_i s[k] + n_i[k] \\ H_0 \ : \ r_i[k] \ = \ n_i[k] \end{cases} \tag{5.5}$$

Under H_1 and in absence of noise the received signal r_s is given by:

$$r_s \triangleq h_i s[k] \qquad 0 < i < M-1, \quad 0 < k < N-1 \tag{5.6}$$

Let us define the covariance matrix $\hat{R}_s$ as:

$$\hat{R}_s \triangleq \frac{1}{N}\{r_s\}\{r_s\}^* \tag{5.7}$$

Let us consider three perpendicularly polarized co-located antennas at the secondary terminal.

Under H_1, in the case of static channel, $\hat{R}_s$ is *rank-deficient*. In other words, the rank $N_s = 1 < M = 3$, the dimension of the received signal space. In this case, it is shown in [150] that the smallest $M - N_s = 2$ eigenvalues of $\hat{R}$ will be approximately equal to the noise variance σ_n^2, while the $N_s = 1$ largest eigenvalue of $\hat{R}$ will be approximately the sum of an eigenvalue of $\hat{R}_s$ and the noise variance σ_n^2. These approximations become exact in the limit $N \to \infty$.

Under H_0, $\hat{R}$ is a full-rank diagonal matrix with approximately the same eigenvalues. In this case the three eigenvalues of $\hat{R}$ are approximately equal to the noise variance σ_n^2.

In the absence of a primary signal, the test statistic is then approximately given by the quotient between two equal positive number (the variance of noise σ_n^2) and is then approximately equal to one. In the presence of a primary signal the test statistic is approximately given by the quotient between the sum of the noise variance and a positive number (one of the eigenvalues of $\hat{R}_s$) and the noise variance and is then greater than one. In this way, this test statistic distinguish then between the two hypotheses of presence or the absence of a primary signal under static channel.

5.3.2 Dynamic channel

The second case to consider is when the channel between the primary transmitter and the secondary terminal is dynamic and thus changes between two samples. The received signal $r_i[k]$ is then obtained under the two hypotheses H_0 and H_1 by:

$$\begin{cases} H_1 \ : \ r_i[k] \ = \ h_i[k]s[k] + n_i[k] \\ H_0 \ : \ r_i[k] \ = \ n_i[k] \end{cases} \tag{5.8}$$

Under H_1 and in absence of noise, the received signal r_s is given by:

$$r_s \triangleq h_i[k]s[k] \qquad 0 < i < M-1, \quad 0 < k < N-1 \tag{5.9}$$

The covariance matrix $\hat{R}_s$ is then given by:

$$\hat{R}_s \triangleq \frac{1}{N}\{r_s\}\{r_s\}^* \tag{5.10}$$

Let us consider three perpendicularly polarized co-located antennas at the secondary terminal. Let N_s denote the rank of the matrix $\hat{R}_s$: $\text{Rank}(\hat{R}_s) = N_s$.

Under H_1, in the case of dynamic channel, $\hat{R}_s$ is *full-rank*. In other words, $\text{Rank}(\hat{R}_s) = N_s = M = 3$, the dimension of the received signal space. In this case, it is shown in [150] that each eigenvalue of $\hat{R}$ will be approximately the sum of an eigenvalue of $\hat{R}_s$ and the noise variance σ_n^2.

Let $x_c[k]$ and $x_s[k]$ denote respectively the I and Q components of the BB signal x[k]. The sub-channel $h_i[k]$, the transmitted signal $s[k]$ and the noise $n_i[k]$ on the i^{th} antenna could then be expressed as: $h_i[k] = h_{ci}[k] + jh_{si}[k]$, $s[k] = s_c[k] + js_s[k]$ and $n_i[k] = n_{ci}[k] + jn_{si}[k]$.

Let us consider:

- iid $n_{ci}[k]$ and $n_{si}[k]$ with same distribution $\forall\ i$ $N(0, \sigma_n^2/2)$ where $\sigma_n^2 = 2N_0W$.

- iid $h_{ci}[k]$ and $h_{si}[k]$ with same distribution $N(0,\sigma_{hi}^2/2)$: $h_{ci}[k], h_{si}[k] \sim N(0,\sigma_{hi}^2/2)$
- $s_c[k]$ and $s_s[k]$ be independent random variables with zero mean and variance of $1/2$.

In this case, the eigenvalues of $\hat{R}_s$ are given by the channel variances $\sigma_{h_i}^2$ and each eigenvalue of $\hat{R}$ is then given by the sum of a channel variance $\sigma_{h_i}^2$ and the noise variance σ_n^2.

In the unipolar multi-antenna case where all the sub-channels experience the same Rayleigh fading, the channel variances $\sigma_{h_i}^2$ are equals to each other. As a result, the eigenvalues of $\hat{R}$ will be approximately equals as well and the quotient between the largest to the smallest eigenvalues of $\hat{R}$ will approximately be equal to one. In this case, the test statistic will not be able to distinguish between the hypothesis H_0 and H_1.

However as previously said, in the cross-polarized multi-antenna case, because of the XPD between polarized antennas, each subchannel experiences a different Rayleigh fading and the channel variances $\sigma_{h_i}^2$ are thus different to each other. As a result the eigenvalues of $\hat{R}$ will be different and the quotient between the largest to the smallest eigenvalues of $\hat{R}$ will be greater than one. Therefore, in the multi-polarized case, the GLRT test statistic can distinguish between the two hypotheses H_0 and H_1.

5.4 Spectrum sensing based on the difference of the variance of received signals

In this section two new multi-polarized spectrum sensing methods are proposed which are based on the difference of variance of received signals in multi-polarized antenna systems. Two cases should be considered:

5.4.1 Static channel

In this case, under H_1, the received signal $r_i[k]$ can be expressed as:

$$\begin{aligned} r_i[k] &= h_i s[k] + n_i[k] \\ &= h_{ci} s_c[k] - h_{si} s_s[k] + n_{ci}[k] + j\left(h_{ci} s_s[k] + h_{si} s_c[k] + n_{si}[k]\right) \quad (5.11) \\ &\triangleq r_{ci}[k] + j r_{si}[k] \quad (5.12) \end{aligned}$$

By assuming that all the variables in equation (5.11) are independent with respect to each others, the variance of $r_{ci}[k]$ can be expressed as:

$$\begin{aligned} \mathrm{Var}(r_{ci}[k]|H_1) =& |h_{ci}|^2 \mathrm{Var}(S_c[k]) + |h_{si}|^2 \mathrm{Var}(S_s[k]) + Var(n_{ci}[k]) \\ =& \frac{|h_i|^2 + \sigma_n^2}{2} \end{aligned} \quad (5.13)$$

By analogy to equation (5.13), the same result holds for the variance of $r_{si}[k]$:

$$\mathrm{Var}(r_{si}[k]|H_1) = \frac{|h_i|^2 + \sigma_n^2}{2} \quad (5.14)$$

In cross-polarized antenna systems, the sub-channels are uncorrelated with respect to each other. As a result during each observation time, the amplitude of each subchannel $|h_i|$ is generated from an independent Rayleigh distribution with different Rayleigh parameter $\sigma^2_{h_i}$. It is thus highly likely that the generated values of $|h_i|$ during each observation time be different at each receive antenna. As a result it can be deduced from equation 5.14 that the corresponding variances of the real and the imaginary parts of the received signals are different at each receive antenna.

Under H_0, the received signal $r_i[t]$ can be expressed as:

$$\begin{aligned} r_i[k] =& n_i[k] \\ =& n_{ci}[k] + j n_{si}[k] = r_{ci}[k] + j r_{si}[k] \end{aligned} \quad (5.15)$$

It then follows that the variances of $r_{ci}[k]$ and $r_{si}[k]$ under H_0 are given by:

$$\mathrm{Var}(r_{ci}[k]|H_0) = \mathrm{Var}(n_{ci}[k]) = \frac{\sigma_n^2}{2} \tag{5.16}$$

$$\mathrm{Var}(r_{si}[k]|H_0) = \mathrm{Var}(n_{si}[k]) = \frac{\sigma_n^2}{2} \tag{5.17}$$

By comparing the equations (5.16) and (5.17) with the equations (5.13) and (5.14), it can be noticed that, while under H_1 the variance of the received signal is different on each receive antenna, under H_0, the same variance is obtained on all the three receive antennas. This behavior will be further used in this paper in order to define new test statistics which differentiate the two hypotheses H_0 and H_1.

5.4.2 Dynamic channel

In the case of dynamic channel and under H_1, the received signal $r_i[k]$ can be expressed as:

$$\begin{aligned} r_i[k] &= h_i[k]s[k] + n_i[k] && (5.18)\\ &= h_{ci}[k]s_c[k] - h_{si}[k]s_s[k] + n_{ci}[k] \\ &\quad + j\left(h_{ci}[k]s_s[k] + h_{si}[k]s_c[k] + n_{si}[k]\right) && (5.19)\\ &\triangleq r_{ci}[k] + jr_{si}[k] && (5.20)\end{aligned}$$

By assuming that all the variables in equation (5.19) are independent with respect to each others, the variance of $r_{ci}[k]$ can be expressed as:

$$\begin{aligned} \mathrm{Var}(r_{ci}[k]|H_1) =& \mathrm{Var}(h_{ci}[k]s_c[k]) + \mathrm{Var}(h_{si}[k]s_s[k]) + \mathrm{Var}(n_{ci}[k]) \\ =& [E(h_{ci}[k])]^2\,\mathrm{Var}(s_c[k]) + [E(s_c[k])]^2\,\mathrm{Var}(h_{ci}[k]) \\ &+ \mathrm{Var}(h_{ci}[k])\mathrm{Var}(s_c[k]) + [E(h_{si}[k])]^2\,\mathrm{Var}(s_s[k]) \\ &+ [E(s_s[k])]^2\,\mathrm{Var}(h_{si}[k]) + \mathrm{Var}(h_{si}[k])\mathrm{Var}(s_s[k]) \\ &+ \mathrm{Var}(n_{ci}[k]) \\ =& \frac{\sigma_{hi}^2 + \sigma_n^2}{2} \end{aligned} \tag{5.21}$$

By analogy to equation (5.21), the same result holds for the variance of $r_{si}[k]$:

$$\mathrm{Var}(r_{si}[k]|H_1) = \frac{\sigma_{hi}^2 + \sigma_n^2}{2} \tag{5.22}$$

Similarly to equation 5.16, the variances of $r_{ci}[k]$ and $r_{si}[k]$ under H_0 are given by:

$$\mathrm{Var}(r_{ci}[k]|H_0) = \mathrm{Var}(n_{ci}[k]) = \frac{\sigma_n^2}{2} \tag{5.23}$$

$$\mathrm{Var}(r_{si}[k]|H_0) = \mathrm{Var}(n_{si}[k]) = \frac{\sigma_n^2}{2} \tag{5.24}$$

By comparing the equations (5.23) and (5.24) with the equations (5.21) and (5.22), it can be noticed that in a multi-polar reception scenario and in a dynamic channel case, while under H_1 the variance of the received signal is different on each receive antenna, under H_0, the same variance is obtained on all the three receive antennas. This particularity in multi-polar systems is exploited in order to define a new test statistic which differentiates the two hypotheses H_0 and H_1.

Under H_0 and during an observation time T, the variance of the I or Q components of the received signals tends to be the same on all the three receive antennas as T becomes larger. In case of H_1 the variance of the I or Q components of the received signals is not the same on each receive antenna. This different behavior under H_1 and H_0 is exploited in order to differentiate the two hypotheses. Two methods are proposed: *Sensing Per Difference (SPD)* and *Bartlett's test.*

5.4.3 Sensing per difference

Let M_{bh}^{ai} be the statistic test of the SPD method defined between the I or Q components of the signal received on the i^{th} antenna and the I or Q components of the signal received on the h^{th} antenna and which is expressed as:

$$M_{bh}^{ai} = \frac{|V_{ai} - V_{bh}|}{max\left[V_{ai}, V_{bh}\right]} \qquad i \neq h \tag{5.25}$$

- where $a, b = 1$ stands for the I component and $a, b = 2$ stands for the Q component of the received signal:

  $V_{ai} = \mathrm{Var}(r_{ci}[k])$ and $V_{bh} = \mathrm{Var}(r_{ch}[k])$ for $a, b = 1$

  $V_{ai} = \mathrm{Var}(r_{si}[k])$ and $V_{bh} = \mathrm{Var}(r_{sh}[k])$ for $a, b = 2$

- $max[x1, x2]$ expresses the maximum between $x1$ and $x2$.

Under H_0 and during an observation time T, the test statistic M_{bh}^{ai} between different antennas tends to zero as T becomes higher, since the variance of the I or Q components of the received signals tends to be the same on all the three receive antennas. In case of H_1, the test statistic is different than zero as the variance of the I or Q components of the received signals is not the same on each receive antenna. This different behavior under H_1 and H_0 is exploited in order to differentiate the two hypotheses. The primary signal is considered as absent during an observation time T if the test statistic M_{bh}^{ai} obtained during T is lower than a given threshold, η. In the opposite case, the H_1 hypothesis is fulfilled and the primary signal is considered as present. The probability of detection and the probability of false alarm for the test statistic M_{bh}^{ai} obtained between the i^{th} and the h^{th} receive antennas are then given by:

$$P_d = P\left[M_{bh}^{ai} > \eta | H_1\right] \tag{5.26}$$

$$P_{FA} = P\left[M_{bh}^{ai} > \eta | H_0\right] \tag{5.27}$$

The equation (5.25) can be rewritten as:

$$\begin{aligned} M_{bh}^{ai} &= \frac{max(V_{ai}, V_{bh}) - min(V_{ai}, V_{bh})}{max(V_{ai}, V_{bh})} \quad i \neq h \\ &= 1 - \frac{min(V_{ai}, V_{bh})}{max(V_{ai}, V_{bh})} \quad i \neq h \\ &\triangleq 1 - {M'}_{bh}^{ai} \quad i \neq h \end{aligned} \tag{5.28}$$

where $min(x1, x2)$ expresses the minimum between $x1$ and $x2$.

The probability of false-alarm P_{FA} is given by:

$$\begin{aligned} P_{FA} &= P(M_{bh}^{ai} > \eta | H_0) \\ &= 1 - P(M_{bh}^{ai} < \eta | H_0) \\ &= 1 - cdf_{M_{bh}^{ai}}(\eta) \end{aligned} \tag{5.29}$$

where $cdf_{M_{bh}^{ai}}(\eta)$ is the cumulative distribution function of M_{bh}^{ai} under H_0 and can be expressed, by using equation (5.28), by:

$$\begin{aligned} cdf_{M_{bh}^{ai}}(\eta) &= P[M_{bh}^{ai} < \eta | H_0] \\ &= P[1 - M'^{ai}_{bh} < \eta | H_0] \\ &= P[M'^{ai}_{bh} > 1 - \eta | H_0] \\ &= 1 - P[M'^{ai}_{bh} < 1 - \eta | H_0] \end{aligned} \tag{5.30}$$

Equation (5.29) can then be rewritten as:

$$\begin{aligned} P_{FA} = 1 - (1 - P[M'^{ai}_{bh} &< 1 - \eta | H_0]) \\ = P[M'^{ai}_{bh} &< 1 - \eta | H_0] \\ = cdf_{M'^{ai}_{bh}}&(1 - \eta) \end{aligned} \tag{5.31}$$

In order to obtain the $cdf_{M'^{ai}_{bh}}(1-\eta)$ under H_0, let us first define M''^{ai}_{bh} the quotient between V_{ai} and V_{bh}: $M''^{ai}_{bh} = \frac{V_{ai}}{V_{bh}}$ for $i \neq h$.

For instance, the variance of $r_{ch}[k]$, V_{1h}, is estimated by:

$$V_{1h} = \mathrm{Var}(r_{ch}[k]) = \frac{1}{N} \sum_{k=1}^{N} (r_{ch}[k] - \mu)^2 \tag{5.32}$$

where μ is the mean of $r_{ch}[k]$.

This estimation of variance tends to the real value of variance for $N \to \infty$.

Under H_0, considering that $r_{ch}[k] \sim N(0, \sigma_n^2)$, the mean of $r_{ch}[k]$, μ, is assumed to be zero. Equation (5.32) can then be rewritten as:

$$\begin{aligned} V_{1h} = \mathrm{Var}(r_{ch}[k]) &= \frac{1}{N}\sum_{k=1}^{N}(r_{ch}[k])^2 \\ &= \frac{\sigma_n^2}{N}\sum_{k=1}^{N}\frac{(r_{ch}[k])^2}{\sigma_n^2} \\ &= \frac{\sigma_n^2}{N}V'_{1h} \end{aligned} \tag{5.33}$$

where $V'_{1h} = \sum_{k=1}^{N}\frac{(r_{ch}[k])^2}{\sigma_n^2}$ follows a Chi-square distribution with N degrees of freedom: $V'_{1h} \sim \chi_N^2$. The same conclusion is drawn for $r_{ci}[k]$, $r_{si}[k]$ and $r_{sh}[k]$. It then follows that M''^{ai}_{bh} follows a F distribution with two same parameters N: $M''^{ai}_{bh} \sim F(N, N)$.

As shown in appendix 1, the probability density function (*pdf*) of M'^{ai}_{bh} is related to the *pdf* of M''^{ai}_{bh} by the following relation:

$$pdf_{M'^{ai}_{bh}}(x) = pdf_{M''^{ai}_{bh}}(x) + \frac{1}{x^2}pdf_{M''^{ai}_{bh}}(\frac{1}{x}) \quad 0 < x \leq 1 \tag{5.34}$$

Considering that $M''^{ai}_{bh} \sim F(N, N)$, the *pdf* of M''^{ai}_{bh} is given by the following expression [153]:

$$pdf_{M''^{ai}_{bh}}(x) = \frac{1}{B(N/2, N/2)}x^{\frac{N}{2}-1}(1+x)^{-N} \tag{5.35}$$

where B(.,.) is the Beta function [153].

It then results from equations (5.35) and (5.34), that the *pdf* of M'^{ai}_{bh} is obtained by the following closed-form expression:

$$pdf_{M'^{ai}_{bh}}(x) = \frac{2}{B(N/2, N/2)}x^{\frac{N}{2}-1}(1+x)^{-N} \tag{5.36}$$

Considering that $0 \leq M'^{ai}_{bh} \leq 1$, the *cdf* of M'^{ai}_{bh} is given by:

$$cdf_{M'^{ai}_{bh}}(t) = \int_0^t pdf_{M'^{ai}_{bh}}(x)dx \tag{5.37}$$

The correctness of the theoretical distribution of ${M'}^{ai}_{bh}$, developped above has been verified by simulation. An exemple of the good agreement between the theoretical pdf of ${M'}^{ai}_{bh}$ and the pdf obtained by simulation is given in figure 5.1.

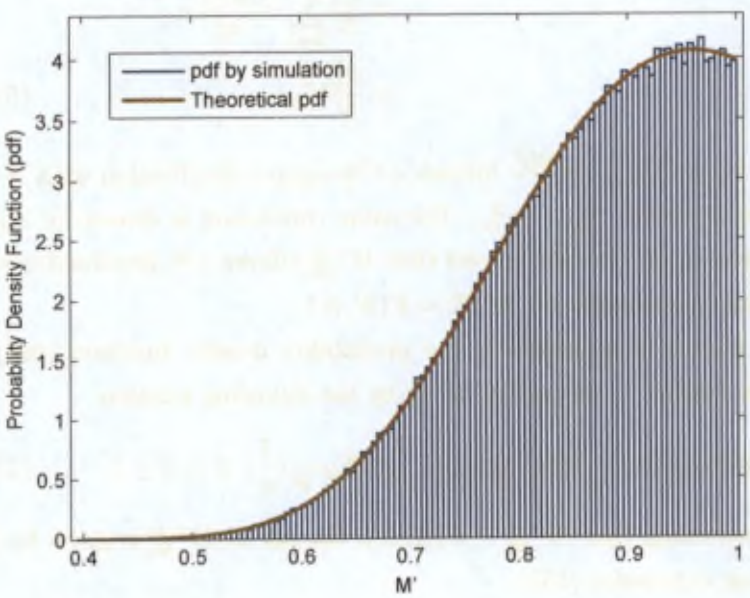

Figure 5.1: Comparison between the theoretical pdf of ${M'}^{ai}_{bh}$ and the pdf obtained by simulation

The expression of P_{FA} can then be obtained from equations (5.31), (5.36) and (5.37) by:

$$\begin{aligned} P_{FA} &= cdf_{{M'}^{ai}_{bh}}(1-\eta) \\ &= \int_0^{1-\eta} \frac{2}{B(N/2, N/2)}(1+x)^{-N} x^{\frac{N}{2}-1} dx \\ &= \frac{2}{B(N/2, N/2)}(-1)^{-\frac{N}{2}} B(\eta - 1, \frac{N}{2}, 1-N) \end{aligned} \quad (5.38)$$

where $B(.,.,.)$ is the incomplete Beta function [153].

Considering a multi-polarized antenna system made of three perpendicular antennas, a total of three independent test statistics M_{bh}^{ai} could be generated from the in-phase (I) and quadrature (Q) components of the signals received on these three antennas. Let us for instance consider the following set of test statistics: M_{12}^{11}, M_{23}^{22} and M_{13}^{21}, although other set of independent test statistics could also be considered. The primary signal will be considered as present if at least one of these three test statistics report the presence of a primary signal. This is equivalent to saying that the received signal will be considered as noise if all the three test statistics reports the absence of a primary signal and thus if all the three test statistics are under the threshold: $[(M_{12}^{11} < \eta)$ and $(M_{23}^{22} < \eta)$ and $(M_{13}^{21} < \eta)]$.

Under H_0, the final probability of detecting noise is then given by the product of probability of detecting noise for each of the test statistics. The probability of detecting noise under H_0 for each test statistic is given by one minus the probability of detecting a primary signal under H_0 for each test statistic, which is equivalent to the probability of false alarm for each test statistic. By considering the same probability of false alarm, P_{FA}, for each of the three test statistics, the final probability of detecting noise under H_0 is given by $(1 - P_{FA})^3$. The final probability of detecting a primary signal under H_0, $P_{FA,f}$ is obtained by one minus the final probability of detecting noise under H_0:

$$P_{FA,f} = 1 - (1 - P_{FA})^3 \tag{5.39}$$

where P_{FA} is given by equation (5.38).

5.4.4 Bartlett's test

The *Bartlett's test* ([154]) is also proposed as the test statistic to distinguish the two hypotheses. In statistics, the Bartlettt's test is used in order to verify the *homoscedasticity* or homogeneity of variances across different groups of samples. Here, the Bartlett's test is applied on the samples of the real and the imaginary parts of the received signals at the three receive antennas.

By assuming independent realizations for the I and Q components of the received signals, six groups of samples of size N are defined from the real and the imaginary parts of the received signals at the three receive antennas. The Bartlett's test is used in order to test the null hypothesis that all these six groups have the same variance against the alternative hypothesis that at least two of them have different variances.

The Bartlett's test is in this case defined by [154]:

$$\begin{aligned} T_B =& \frac{(6N-6)\ln(S_p^2) - (N-1)\sum_{i=1}^{3}\left[\ln(\text{Var}(r_{ci}[k])) + \ln(\text{Var}(r_{si}[k]))\right]}{1+\frac{1}{15}\left(\frac{6}{N-1}-\frac{1}{6N-6}\right)} \\ =& \frac{18(N-1)^2}{18N-11}\left[6\ln(S_p^2) - \sum_{i=1}^{3}\left[\ln(\text{Var}(r_{ci}[k])) + \ln(\text{Var}(r_{si}[k]))\right]\right] \end{aligned} \tag{5.40}$$

where $S_p^2 = \frac{1}{6}\sum_{i=1}^{3}\left[\text{Var}(r_{ci}[k]) + \text{Var}(r_{si}[k])\right]$.

For a block of observation of size N, all the real or imaginary parts of the received signals are considered to have the same variance on all the three receive antennas if the Bartlett's test is below a give threshold η. In this case the primary signal is considered to be absent. In the opposite case where the Bartlett's test is above the threshold, the primary signal is considered to be present.

The probability of detection and the probability of false alarm for the Bartlett's test are given by:

$$P_d = P\left[T_B > \eta | H_1\right] \tag{5.41}$$

$$P_{FA} = P\left[T_B > \eta | H_0\right] \tag{5.42}$$

Under H_0, the Bartlett's test defined for six groups of normally distributed samples follows approximately a chi-squared distribution with two degrees of freedom (χ_2^2) [155]. Using [58], the following closed-form expression could be obtained for the probability of false alarm:

$$P_{FA} = \frac{\Gamma(\frac{5}{2}, \frac{\eta}{2})}{\Gamma(\frac{5}{2})}. \tag{5.43}$$

5.5 Comparison and analysis

The same measurement results are used than the ones obtained in the measurement campaign of chapter 2. An outdoor-to-indoor cognitive radio scenario is considered where the secondary network is deployed indoor and senses the signals received from an outdoor primary base station. For this purpose, the outdoor-to-indoor measurement campaign described in chapter 2 is used in order to obtain the path-loss models between the different polarized antennas at the transmitter and the receiver. These path-loss models are given in Table 4.1. The distribution parameters of the different sub-channels used further in the simulations are obtained from these path-loss models.

Monte-Carlo simulations are carried out using the path-loss models and the analytical expressions. For a given distance between the transmitter and the receiver, the Rayleigh distribution parameter of the channel (σ_{hi}) is obtained by using the value of the path-loss model at that distance. For a pre-specified probability of false alarm, the threshold η is obtained by simulation for the GLRT method and by numerically inversing the equations of probability of false alarm 5.39 and 5.43, for the SPD and Bartlett's test methods respectively. In the following analysis, only the vertical polarization is considered at the transmitter side. The conclusions hold for the horizontal transmit antenna.

5.5.1 Comparison of Multi-polarized blind spectrum sensing methods in dynamic and static channel scenarios

The probability of detection versus both the distance between the primary transmitter and the secondary terminal, and the corresponding SNR at the receive vertical antenna (Rx_V) is shown for the GLRT, the SPD and the Barlett's test spectrum sensing methods and for a dynamic channel scenario in figure 5.2.

These results are obtained using a pre-specified probability of false alarme $P_{FA} = 0.05$ and a fixed value of time-bandwidth product TW=50 (N=100). The transmit power was 19 dBm and the noise variance σ_n^2 was fixed in a way to have -5dB on the vertical receive antenna at 50 meters of distance. One should note that the SNR axis represents the SNR obtained on the receive antenna with the same orientation than the transmit antenna (TX_V RX_V). The same distance between the PTx and the STE will correspond to lower SNR value if the SNR at the horizontal receive antenna is considered.

In a dynamic channel scenario, similar spectrum sensing performances are obtained between the SPD and the GLRT methods. The best performances are obtained by the Barlett's test spectrum sensing method.

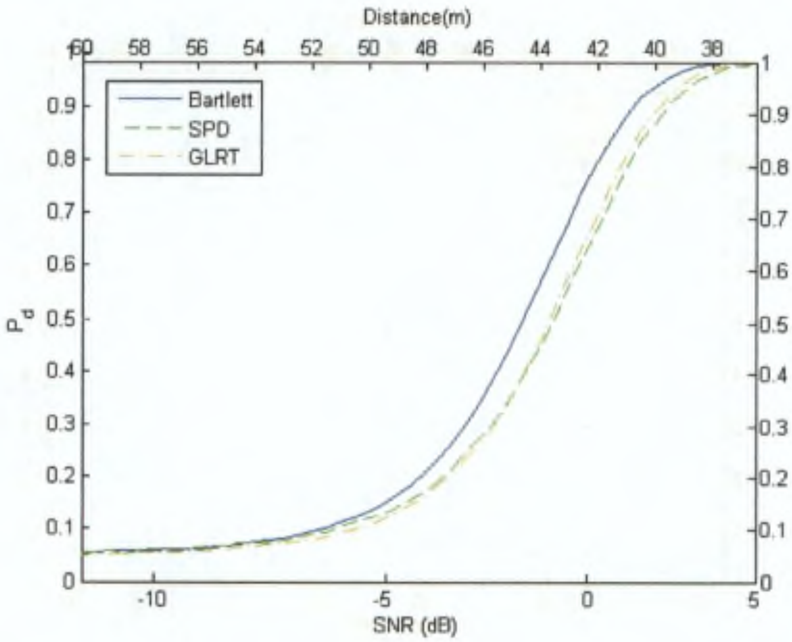

Figure 5.2: Comparison between blind spectrum sensing methods (Barlett's test, GLRT, SPD) in a dynamic channel scenario: $P_{FA} = 0.05$, $N = 100$, Vertical polarization used at transmitter side. SNR refers to as SNR obtained on vertical receive antenna.

The detection performances of the GLRT, the SPD and the Bartlett's test spectrum sensing methods and in a static channel scenario are presented in figure 5.3. The same simulation parameters were used than in the dynamic case. In a static channel scenario the best performances are obtained by the GLRT method. Better performances are obtained for the Bartlett's test method compared to the SPD method.

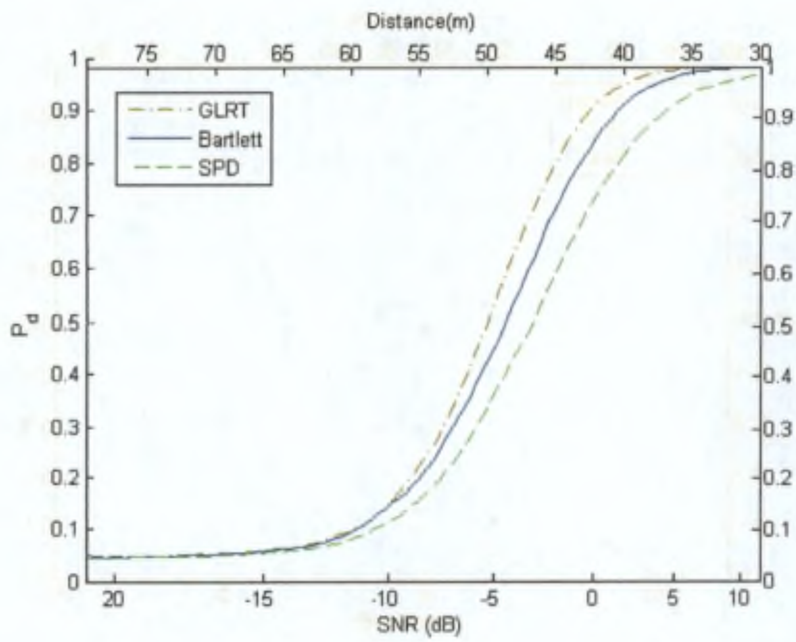

Figure 5.3: Comparison between blind spectrum sensing methods (Barlett's test, GLRT, SPD) in a static channel scenario: $P_{FA} = 0.05$, $N = 100$, Vertical polarization used at transmitter side. SNR refers to as SNR obtained on vertical receive antenna.

The two dynamic and static channel scenarios presented above are two extreme scenarios where for one of them the channel is completely dynamic during an observation time for sensing and for the other completely static. The channel can however have an intermediate behavior. In fact, during an observation time, the channel can stay static during some samples, while changing for the others. The application of cross-polarized antenna systems to the blind spectrum sensing through the proposed spectrum sensing methods, make the cognitive radio system able to detect both in a dynamic and a static scenario but also in intermediate dynamic schemes.

By fixing the value of acceptable probability of detection to 0.9, the probability that the probability of detection be above 0.9 is given in figure 5.4 for the Bartlett's test method and under dynamic channel scenario. Two cases of $N = 100$ and $N = 200$ are considered. We observe an abrupt decrease in this probability as the SNR is reduced. However the limite of SNR under which this probability becomes equal to zero could be decreased by increasing the number of samples used for sensing.

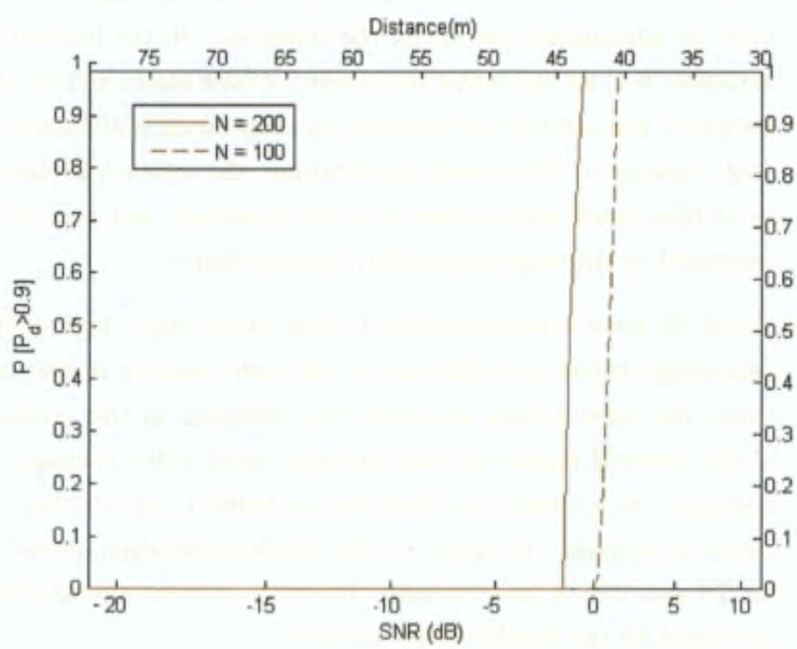

Figure 5.4: The probability that the probability of detection be above 0.9, Multi-polarized detection with Bartlett's test method for $N = 100$ and $N = 200$

All the blind spectrum sensing methods described above are based on the assumption that the same noise variance exists on all the three receive antennas. The difference in the noise variance of the antennas is indeed insignificant if we consider the use of front-ends composed of identical elements for the three receive antennas. Let us consider a situation where a difference occurs in the noise variance of antennas:

- Under H_0, the noise variances are not anymore identical at all three receive antennas which could result in additional false alarms. The threshold is obtained by fixing a target probability of false alarm and by assuming the same noise variance at all antennas. A difference in the noise variance at the receive antennas, results in an achieved probability of false-alarm higher than the target probability of false-alarm used to fix the threshold. In the interval of variation [0-1] for the target probability of false alarm and for the Bartlett's test method for instance, by considering a difference of noise variance of 5% between the antennas, the achieved probability of false alarm will increase by 2.5% on average and up to 8 % compared to the target probability of false alarm.

- Under H_1 for a fixed probability of false alarm and a fixed SNR, depending on how the difference in the noise variance is split between the three receive antennas, the difference in the variance of the received signals at each antenna could either increase or decrease. As a result, the detection probability could either increase or decrease. In figure 5.5, the limits of variation of the P_d for 5% and 10% of noise variance difference between antennas are presented for the Bartlett's test method.

  An increase in the probability of detection resulting from a difference in the noise variance of antennas does not mean that better detection performances are obtained as the probability of false alarm becomes higher.

5.5.2 Comparison with energy detection

As previously mentioned, energy detection has been widely used in the literature because of its simplicity and the good performances that are

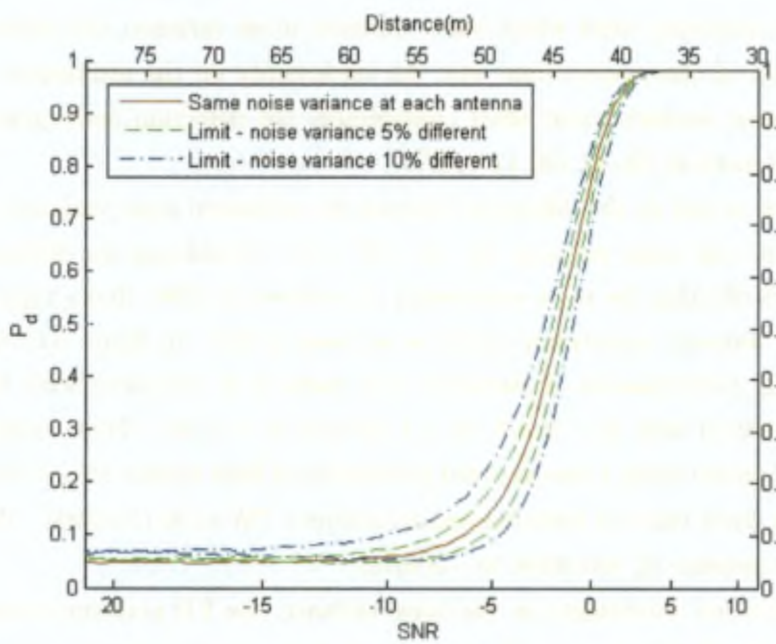

Figure 5.5: The limit of variation of the P_d for 5% and 10% of noise variance difference between antennas for Bartlett's method: TX_V, $P_{FA} = 0.05$ and $N = 100$.

achieved with this method [38, 39, 107]. If good sensing performances are obtained with the energy detection method it is mainly because it is assumed in this method that the variance of the noise is known. In fact, having the knowledge of the noise variance makes it possible to detect very weak signals by detecting any small increase in the power due to the sum of the noise and signal power [50, 108]. The background noise is an aggregation of difference sources such as the thermal noise, leakage of signals from other bands due to receiver nonlinearity, quantization error, etc [50, 156]. In practice the noise variance is not known exactly at the STE [50, 108]. Different factors could affect the noise uncertainty such as the thermal noise change or the amplifier gain change due to the temperature change, estimation of the noise variance on another frequency band which has a different noise variance, the limited amount of observation time, etc. An uncertainty on the estimation of the noise variance could affect considerably the detection performance of ED method [38, 50, 109, 110, 157].

Let us call Δ, the difference between the estimated noise variance $\tilde{\sigma}_n^2$ and the real noise variance σ_n^2: $\Delta = \tilde{\sigma}_n^2 - \sigma_n^2$. Combining the different factors effecting the noise uncertainty, it is shown in [108], that a typical noise variance uncertainty could be at least $0.7dB$. In figure 5.6, the sensing performances of Bartlett's test method is compared with the ED method with $\Delta = 0\ dB$, $\Delta = 1\ dB$ and $\Delta = 2\ dB$. These results are obtained using a pre-specified probability of false alarme $P_{FA} = 0.05$ and a fixed value of time-bandwidth product TW=150 (N=300). The noise variance σ_n^2 was fixed to $-50dBm$.

With no uncertainty on the noise variance, the ED performs better than the Bartlett's test. In presence of noise uncertainty the sensing performances of ED are degraded considerably. In presence of noise uncertainty, the blind spectrum sensing methods such as Bartlett's test method achieves much better performance than ED method since they do not depend on the knowledge of the noise variance.

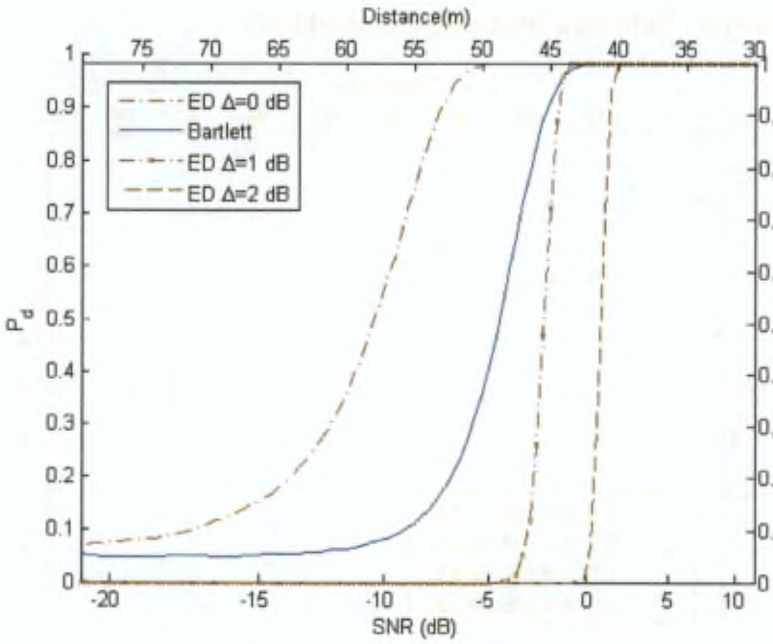

Figure 5.6: The effect of noise variance uncertainty (Δ) on sensing performance of ED technique and comparison with Bartlett's test technique: $P_{FA} = 0.05$, $N = 300$, Vertical polarization used at transmitter side. SNR refers to as SNR obtained on vertical receive antenna.

In the presence of noise variance uncertainty another phenomenon appears for the ED method which is referred to as the "SNR Wall" [50, 157]. While in the absence of noise variance uncertainty, the sensing performance of ED is improved by increasing the number of samples N, in the presence of noise variance uncertainty, even for very large number of samples N, there is a limit to the SNR under which the detector is unable to detect. This phenomenon is presented in figure 5.7 where the SNR wall is located around -3 dB.

Blind spectrum sensing methods such as Bartlett's test method, on the other hand, do not depend on the noise variance. As shown in figure 5.8, the sensing performance of the Bartlett's test method is constantly improved by increasing the number of samples N.

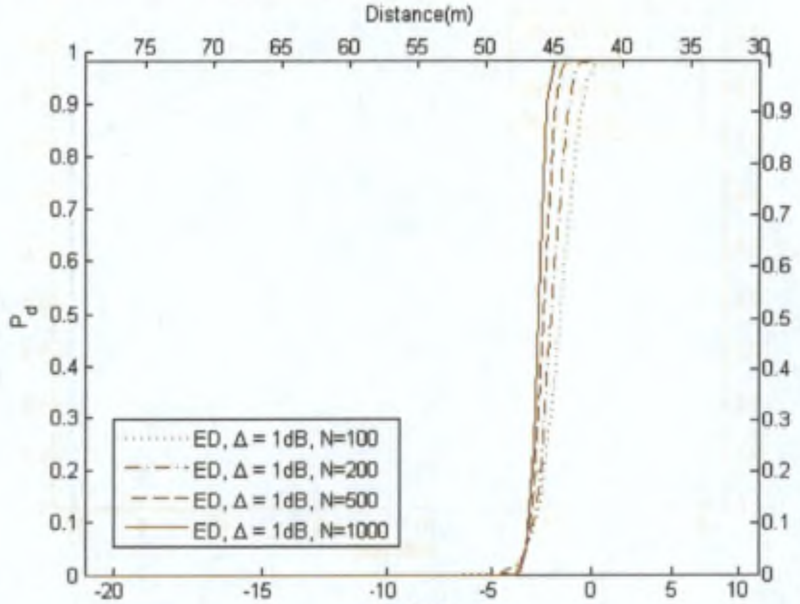

Figure 5.7: SNR wall in case of Noise Variance Uncertainty in Energy Detection method. P_{FA}=0.05. Vertical polarization used at transmitter side, SNR refers to as SNR obtained on vertical receive antenna.

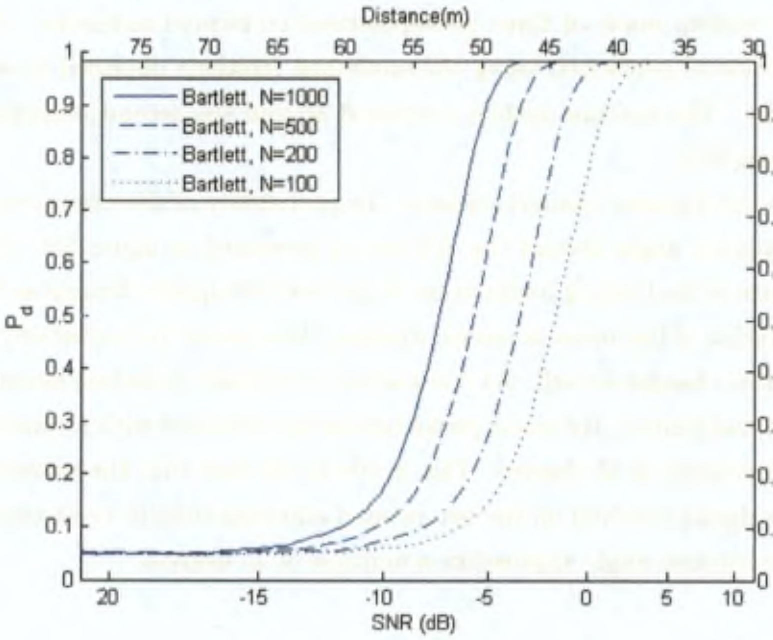

Figure 5.8: Improvement of performance of Bartlett's test method with the number of samples N, P_{FA}=0.05, Vertical polarization used at transmitter side, SNR refers to as SNR obtained on vertical receive antenna.

5.6 The effect of antenna orientation on the spectrum sensing performances

In this section, the effect of the orientation of the antenna system on the spectrum sensing performances of the Bartlett's test method is studied. For this purpose, the model of the elliptical polarization developed in chapter 3 is used. The receive elliptical polarization is projected onto a multi-polarized antenna system with different orientations.

The parameters of the elliptical polarization are generated in an NLOS Dynamic scenario and based on the mean values of μ and σ parameters of the Gaussian distributions given in the Table 3.2. The receive elliptical polarization is projected on each orientation of the antenna system made of three cross-polarized co-located antennas. The projection is performed using the analytical relations obtained in section 3.5. The antenna system is rotated around the second horizontal antenna($H2$).

In the dynamic channel scenario, the probability of detection versus the rotation angle around the $H2$ axis is presented in figure 5.9. The variance of the I and Q components of the received signals changes as the orientation of the antenna system changes. As a result the probability of detection changes as well. By considering a vertically polarized antenna at the transmitter, the worst performances are obtained with a rotation angle multiple of 45 degrees. This is due to the fact that the variances of the signals received on the two rotated antennas tend to be the same as the rotation angle approaches a multiple of 45 degrees.

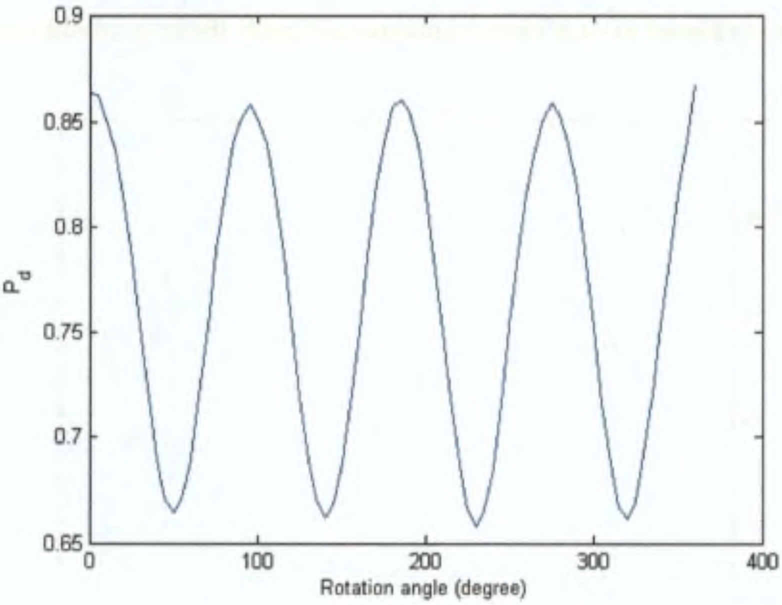

Figure 5.9: Bartlett's test, Dynamic channel: The probability of detection versus the rotation angle (in degree) around the $H2$ antenna for the dynamic channel scenario, Vertical polarization used at transmitter side, $N = 100$, $SNR = -2dB$, $P_{FA} = 0.05$.

In the static channel scenario, the probability of detection versus the rotation angle around the $H2$ axis is presented in figure 5.10. The variance of the received signals on the rotated antennas changes with the rotation around the $H2$ axis. The difference between the generated values of the channel is more likely to be higher if the difference in the variances is higher. As a result the worst performances are obtained for a rotation angle multiple of 45 degrees as the variances of the received signals on the two rotated antennas tend to be the same for a rotation angle multiple of 45 degrees.

Compared to the dynamic channel case, the detection performances are less degraded with the orientation of the antenna system in the static channel case. In fact even in the case of equal variances, the generated values of channel at each receive antenna are highly likely to be different.

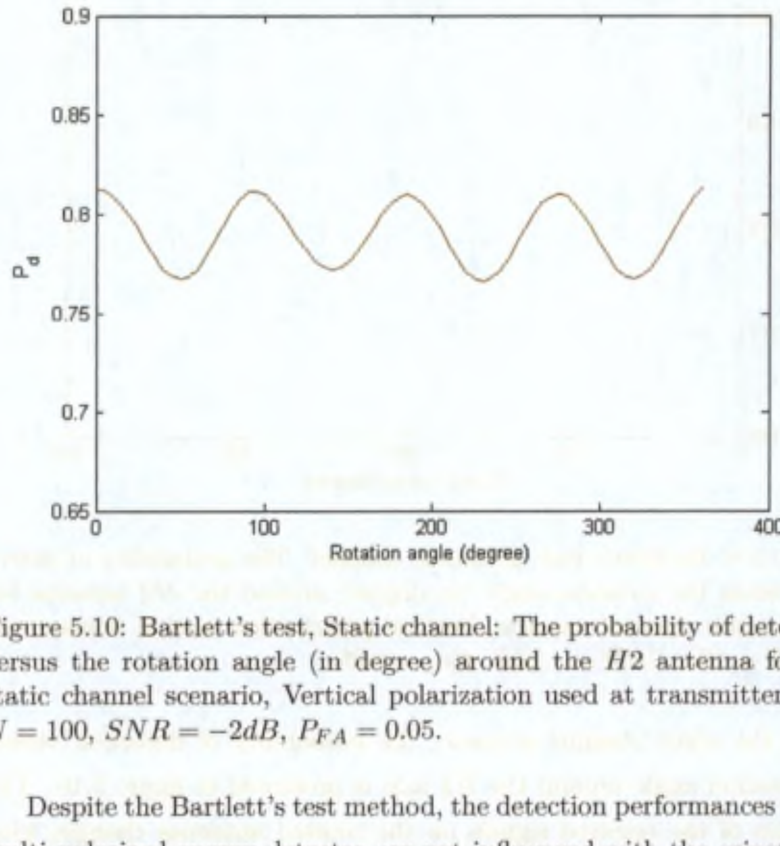

Figure 5.10: Bartlett's test, Static channel: The probability of detection versus the rotation angle (in degree) around the $H2$ antenna for the static channel scenario, Vertical polarization used at transmitter side, $N = 100$, $SNR = -2dB$, $P_{FA} = 0.05$.

Despite the Bartlett's test method, the detection performances of the multi-polarized energy detector are not influenced with the orientation of the antenna system. In fact, in a cross-polarized antenna system the output of the square-law combiner corresponds to the amplitude of the wave A which is independent of the orientation of the antenna system. However in a case where the orientation of the antenna system changes and in presence of noise variance uncertainty, while the performances of ED method are limited by the SNR wall, the performances of the Bartlett's test method are improved by increasing the number of samples N.

Let us now study in a particular scenario, the effect of the time-dynamics of the channel by including the correlation between temporal samples of the elliptical polarization parameters.

For this purpose, the mean values of the distribution parameters are used in order to obtain i.i.d. random samples of the elliptical polarization parameters. The autocorrelation models given in Table 3.5 are then introduced into the statistical distributions of each elliptical polarization parameter using the process explained in section 3.6. The resulting elliptical polarizations are then projected onto a multi-polarized antenna system with different orientations.

Two spectrum sensing cases are considered:

1. The first case which is analyzed is a scenario where the observation time for sensing (T) is higher than the coherence times of the channels given in Table 3.7. In this case, $N = 100$ samples are collected for sensing during an observation time $T = 1$ (s).

2. The second case which is analyzed is a scenario where the observation time for sensing is lower than the coherence times of the channels. In this case, $N = 100$ samples are collected for sensing during an observation time $T = 0.1$ (s).

The probability of detection as a function of the rotation angle around the $H2$ axis is presented for the first and the second time-variant scenarios in figures. 5.12 and 5.11 respectively.

In the first scenario where the observation time is higher than the coherence times of the channels, a similar trend is observed than in the dynamic channel case given in figure 5.9. This case which approaches a total dynamic channel case is characterized by its high range of variation of the probability of detection as a function of the rotation angle.

In the second scenario where the observation time for sensing is lower than the coherence times of the channels, a similar trend is observed than in the static channel case given in figure 5.10. This case which approaches a total static channel case is characterized by its lower range of variation of the probability of detection as a function of the rotation angle compared to the dynamic channel case.

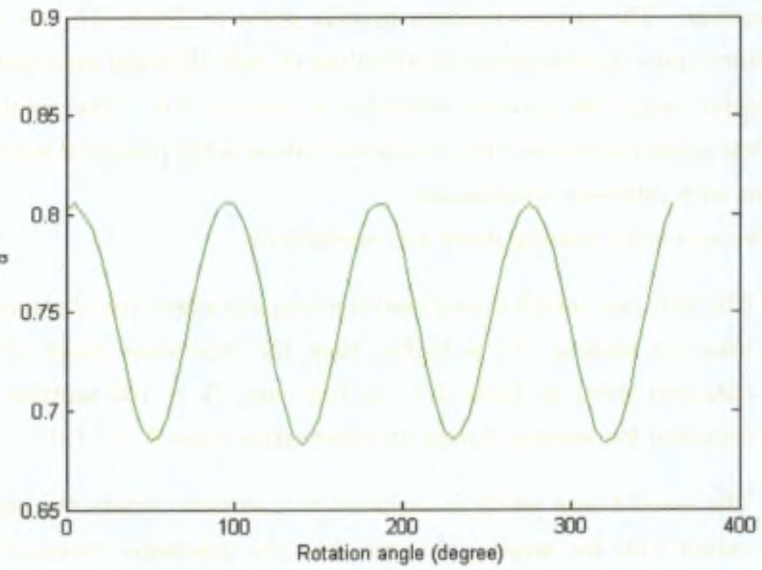

Figure 5.11: Bartlett's test, Time-variant scenario: $T = 1$ (s): The probability of detection versus the rotation angle (in degree) around the $H2$ antenna, Vertical polarization used at transmitter side, $N = 100$, $SNR = -2dB$, $P_{FA} = 0.05$.

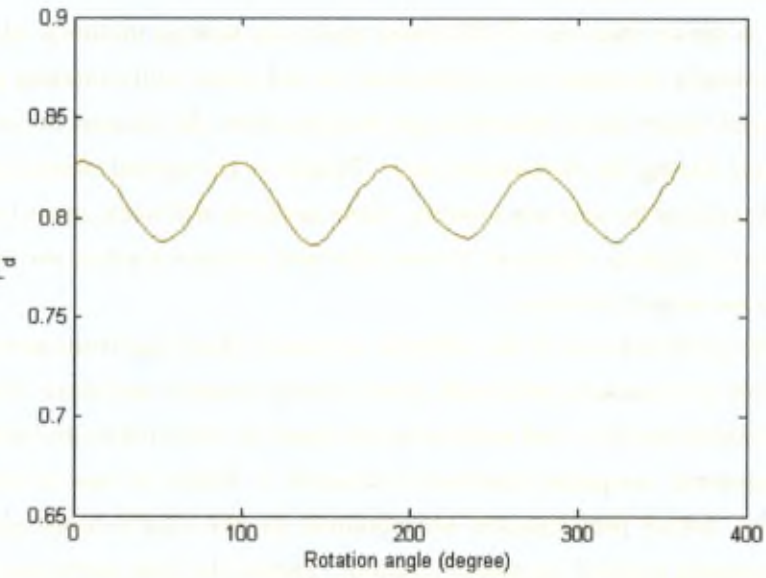

Figure 5.12: Bartlett's test, Time-variant scenario: $T = 0.1$ (s): The probability of detection versus the rotation angle (in degree) around the $H2$ antenna, Vertical polarization used at transmitter side, $N = 100$, $SNR = -2dB$, $P_{FA} = 0.05$.

5.7 Conclusion

In this chapter, the problem of blind spectrum sensing in multi-polarized cognitive radio systems is studied. The GLRT-based spectrum sensing methods are extended to the case of cross-polarized multi-antenna systems where a set of three co-located cross-polarized antennas are used at the secondary terminal. The two cases of dynamic and static channels during an observation time for sensing are considered. Two new multi-polarized blind spectrum sensing methods (Bartlett's test method and SPD method) are also proposed which do not require any a priori knowledge of the noise variance and are thus robust to the noise variance uncertainty. These methods are based on a particularity of multi-polarized systems.

It is shown than the GLRT-based spectrum sensing methods which were initially proposed in the literature for uni-polar multi-antenna systems and under static channel stops working when the channel becomes dynamic during the observation time. Thanks to the special characteristics of multi-polar antenna systems, these methods will work under both static and dynamic channels if cross-polarized antenna systems are used at the secondary terminal,

The performances of the different proposed blind spectrum sensing methods are compared with each other in both dynamic and static channel scenarios and in a real world scenario based on the outdoor-to-indoor measurement campaign described in chapter 2. While in case of static channel, better performances are obtained for the GLRT-based spectrum sensing method, in case of dynamic channel the best performances are obtained by the Bartlett's test method.

The performances of Bartlett's test method were compared with the classical ED method where the knowledge of the noise variance is required. In absence of any noise variance uncertainty, the ED method performs better than Bartlett's test method. In presence of noise variance uncertainty, the detection performance of the Bartlett's test method are considerably higher than the ED method as the Bartlett's test method does not require any a priori knowledge of the noise variance.

In presence of noise variance uncertainty, while the sensing performance of the ED method are limited by the "SNR wall" below which, even for very large number of samples, the detector is unable to detect, the sensing performance of the Bartlett's test method is constantly improved by increasing the number of samples. The use of co-located tri-polarized antennas, let the Secondary Terminal to be almost as compact as a single antenna system while having a significant better performance.

The effect of antenna orientation on the spectrum sensing performances of the Bartlett's test and ED methods was studied. This was done by projecting the elliptical polarization model developed in chapter 3 onto a multi-polarized antenna system with different orientations.

Appendix 1

Considering the definition of M'^{ai}_{bh}, two cases could be considered:

$$M'^{ai}_{bh} = \frac{min(V_{ai}, V_{bh})}{max(V_{ai}, V_{bh})} = \begin{cases} \frac{V_{ai}}{V_{bh}} & if \quad V_{ai} < V_{bh} \\ \frac{V_{bh}}{V_{ai}} & if \quad V_{ai} > V_{bh} \end{cases} \tag{5.44}$$

Taking into account that $V_{ai} \geq 0$ and $V_{bh} \geq 0$ it results that $0 \leq M'^{ai}_{bh} \leq 1$. The pdf of M'^{ai}_{bh}, $pdf_{M'^{ai}_{bh}}(x)$, could be defined by:

$$P[M1 \leq M'^{ai}_{bh} \leq M2] = \int_{M1}^{M2} pdf_{M'^{ai}_{bh}}(x)dx \qquad \forall \;\; 0 \leq M1, M2 \leq 1 \tag{5.45}$$

Considering the equation (5.44) and taking into account that $P[(V_{ai} < V_{bh}) \; and \; (V_{ai} > V_{bh})] = 0$, we have:

$$\begin{aligned} P[M1 \leq M'^{ai}_{bh} \leq M2] &= P[M1 \leq M'^{ai}_{bh} \leq M2 | V_{ai} < V_{bh}] \\ &\quad + P[M1 \leq M'^{ai}_{bh} \leq M2 | V_{ai} > V_{bh}] \qquad (5.46) \\ &= P[M1 \leq \frac{V_{ai}}{V_{bh}} \leq M2] + P[M1 \leq \frac{V_{bh}}{V_{ai}} \leq M2] \\ &= P[M1 \leq \frac{V_{ai}}{V_{bh}} \leq M2] + P[\frac{1}{M1} \geq \frac{V_{ai}}{V_{bh}} \geq \frac{1}{M2}] \\ &= \int_{M1}^{M2} pdf_{M''^{ai}_{bh}}(x)dx + \int_{\frac{1}{M2}}^{\frac{1}{M1}} pdf_{M''^{ai}_{bh}}(x)dx \\ &= \int_{M1}^{M2} pdf_{M''^{ai}_{bh}}(x)dx + \int_{M1}^{M2} \frac{pdf_{M''^{ai}_{bh}}(\frac{1}{x})}{x^2} dx \\ &= \int_{M1}^{M2} \left(pdf_{M''^{ai}_{bh}}(x) + \frac{pdf_{M''^{ai}_{bh}}(\frac{1}{x})}{x^2} \right) dx \qquad (5.47) \end{aligned}$$

It is finally deduced from equations (5.45) and (5.47) that:

$$pdf_{M'^{ai}_{bh}}(x) = pdf_{M''^{ai}_{bh}}(x) + \frac{pdf_{M''^{ai}_{bh}}(\frac{1}{x})}{x^2} \tag{5.48}$$

Chapter 6
Conclusion

Since their introduction in 1999, cognitive radio systems have been an important subject of research in the wireless communications. While the cognitive radio concept potentially opens a lot of interesting perspectives for the next generations of wireless communications systems, a lot of challenges remain in the conception, regulation and implementation of such systems. One of the main challenges is to limit the interference generated from the secondary network on the primary network. In order to achieve this goal the secondary users must be able to detect reliably and quickly the presence of a primary user in a frequency band. During this thesis, the polarization was used in order to enhance the spectrum sensing performances of cognitive radio systems.

The impact of polarization on cognitive radio systems has been addressed in very few works in the past. However, throughout this thesis we showed that this new dimension could have a significant impact on the sensing performance. This was achieved in two steps: First, an experimental part, where the principal aim was to characterize the polarization of electromagnetic waves and the wireless channel depolarization in real-world cognitive radio scenarios. And a second part where the impact of polarization on the sensing performance of cognitive radios was studied and new multi-polarized spectrum sensing methods were proposed.

- **Spatial statistics of the channel depolarization**

  In the first chapter of this thesis, the channel depolarization was characterized in two outdoor-to-indoor and indoor-to-indoor cognitive radio scenarios, based on an extensive measurement campaign. The XPD and the CPR which for the first one quantifies the amount of leakage from one polarization to another and for the second one compares the link quality of one polarization to the other one were separately characterized at three different scales: small-scale variations, large scale variations and distance variation.

The outdoor-to-indoor scenario corresponds to a typical cognitive radio scenario where the primary base station is deployed outside and the secondary network is deployed inside a building. The indoor-to-indoor scenario corresponds to a cognitive radio scenario where both the primary and the secondary networks are deployed inside a same building.

While a classical approach in the characterization of the polarization in wireless communications is to consider one vertically and only one of the two horizontally polarized antennas, a set of three cross-polarized antennas was used in this work. This approach has the advantage not to depend on the orientation of the antenna system and to take into account all depolarization possibilities.

It has been experimentally shown that for both scenarios, small-scale variations of XPD and CPR follow a doubly non-central F distribution. The distance variations and large scale variations of XPD and CPR have been analyzed independently from the small scale variations. For both scenarios, while the mean variation of XPD_V with distance is linearly decaying, the mean variation of XPD_H is constant with distance. The CPR mean variation was found to be ascending with distance. The overall transmission of the horizontal-to-horizontal link was found to be better than the vertical-to-vertical one. The vertical to vertical transmission is getting better with distance to the detriment of the horizontal to horizontal one. The large scale variations of all three parameters around their mean follow a zero-mean normal distribution.

The results obtained from the multi-polarized measurement campaign of this chapter was used in order to simulate the analytical expressions of multi-polarized spectrum sensing, developed in chapters 4 and 5.

- **Time-dynamics of wave polarization**

  In this chapter, a new approach was proposed for the characterization of wave polarization. In the context of system-based statistical channel modeling, the classical approach in modeling the multi-polarized MIMO channel is to consider the signals received on one vertical and two horizontal perpendicular antennas. The approach used in this chapter was to characterize the global polarization of the received fields from an electromagnetic point of view by characterizing the polarization ellipse.

  An analytical formulation was first proposed in order to obtain the parameters characterizing the polarization ellipse in the 3D space, based on the received signals at three cross-polarized antennas. The time dynamics of the different parameters describing the elliptical polarization in the 3D space was characterized based on a measurement campaign. The measurements were made in an indoor-to-indoor scenario. Different measurement positions were considered in a LOS and a NLOS scenario. Based on the proposed theoretical formulation and the measurement campaign, a time-varying statistical model of the polarization ellipse was developed. The statistical distributions of the different parameters describing the polarization ellipse were given. In order to study the time-variant dynamics of the channel, the autocorrelation functions of all the parameters were analyzed and models of autocorrelation were proposed.

An analytical formulation was also proposed in order to project the polarization ellipse onto an antenna system composed of three cross-polarized co-located antennas. Finally, the different steps needed in order to generate a time-varying multi-polarized channel series based on the proposed time-varying model of the polarization ellipse are given.

The receive antenna system is made of three perpendicular co-located antennas and, as the orientation of this antenna system changes, the channel changes as well. The approach used in this chapter for modeling the multi-polarized channel could be applied to any orientation of the receive antenna system, by projecting the receive elliptical polarization to the receive antenna system.

- **Multi-polarized Spectrum Sensing by Energy-Detection**

  In this chapter, the spectrum sensing performances of an energy detector applied to a multi-polarized antenna system were studied and compared to uni-polar single and multi-antenna cases. The main aim of this chapter was to study the effect of the polarization dimension on the spectrum sensing of cognitive radios. This analysis was first based on an analytical formulation of the energy detector in the context of multi-polarized antenna systems and second on the application of the theoretical formulation in a real-world multi-polarized cognitive radio scenario based on the measurement campaigns of chapter 2.

  A theoretical formulation was presented in order to analytically obtain the detection and false alarm probabilities of an energy detector applied to a multi-polarized antenna system for two combining methods and under correlated and uncorrelated Rayleigh fading channels. Based on this theoretical formulation and the results obtained from the measurement campaign of chapter 2, the sensing performance of an energy detector applied to a tri-polarized antenna where each antenna experiences different uncorrelated Rayleigh fading was studied and compared to the spatial diversity case where the secondary terminal is made of three co-polar spatially separated antennas.

It was shown that the poor sensing performance of a single antenna system could be significantly improved by the use of polarization and spatial diversity. It has been found that in a multi-path environment, the performance of spectrum sensing by spatial diversity could be significantly deteriorated depending on the matching between the orientation of the primary transmitter and the secondary terminal. In a practical case where the orientation of the secondary terminal is not the same all the time and the orientation of the Primary transmit antenna is not known by the secondary user, the spectrum sensing by polarization diversity scheme takes into account all the received polarizations and is thus a good compromise of performance. Moreover the space diversity scheme requires large spacing between antennas. By using co-located tri-polarized antennas, the STE could be almost as compact as a single antenna system while having significant better performance. The inter-antenna correlation was found to have a negative impact on the sensing performance. However, even with high inter-antenna correlation, the performance of tri-polarized sensing remains considerably better than the single antenna case.

- **Blind Spectrum Sensing in Cognitive Radios**

  An important limitation of energy detector is its dependence on the knowledge of the noise variance. An uncertainty on the estimation of the noise variance considerably affect the performance of energy detector. In this chapter, this limitation was resolved by proposing new spectrum sensing methods which do not require any knowledge neither on the primary signal nor on the noise variance. These methods, referred to as "Blind spectrum sensing methods", are based on the use of three cross-polarized antennas at the secondary terminal.

The performances of the proposed methods are compared with each other in two dynamic and static channel scenarios. This analysis is based on an analytical formulation applied to the outdoor-to-indoor measurement campaign of chapter 2. The performances of the proposed methods are also compared with the energy detection method with an without noise variance uncertainty.

In absence of any noise variance uncertainty, the ED method performs better than the proposed methods. In presence of noise variance uncertainty, the detection performance of the proposed methods are considerably higher than the energy detection method as the proposed methods does not require any a priori knowledge of the noise variance.

In presence of noise variance uncertainty, while the sensing performance of the energy detection method are limited by the "SNR wall" below which even for very large number of samples, the detector is unable to detect, the sensing performance of the proposed methods is constantly improved by increasing the number of samples.

The effect of antenna orientation on the spectrum sensing performances of the proposed blind spectrum sensing methods and the energy detection method was studied. This was done by projecting the elliptical polarization model developed in chapter 3 onto a multi-polarized antenna system with different orientations.

6.1 Outlooks

Spectrum sensing is an important functionality of a cognitive radio system. Throughout this thesis we laid stress on the great contribution that the polarization dimension, so far neglected in cognitive radio systems, could bring to such systems. This thesis opens new research perspectives in the cognitive radio systems. In the following some of these outlooks are listed:

- Throughout this thesis, cross-polarized antenna systems were considered. In fact, the multi-polarized antenna systems exhibit low inter-antenna correlation and enable the use of diversity in wireless systems. In the case where the antennas are not perpendicularly oriented but oriented with an angles lower than 90°, the received signals at the different antennas will not be uncorrelated anymore. This correlation between the received signals at the different multi-oriented antennas could be used in order to sens the spectrum for the presence of primary signals. In fact, while under H_1 the received signals are correlated with each-other, under H_0 the background noise at each antenna is uncorrelated with the other antennas. As a result the inter-antenna correlation could be used in order to define new "Blind" spectrum sensing metrics. The spectrum sensing based on the inter-antenna correlation has been addressed in a previous work in the context of uni-polar multi-antenna systems where a spectrum sensing method is proposed which is based on the inter-antenna correlation [148]. This method could be applied to the case of multi-oriented antennas. For this purpose, a wireless channel model between the primary base station and each of the oriented antennas of the secondary terminal is required. This could be obtained using the theoretical framework given in section 3.5 in order to project the elliptical polarization onto each of the oriented antennas.

- The polarization orthogonality could also be used in order to improve the communication functionalities of cognitive radio systems. In fact, in absence of any depolarization, two networks could coexist in the same frequency ressource if each of them transmits on the orthogonal polarization of the other one. A secondary user will create much less interference if its transmitted waves at the primary user are in an orthogonal polarization than the one used at the primary user. Several works have treated the implementation of multiple networks on the same frequency resources by using orthogonal polarization in each network [111, 114, 117, 118]. Because of the depolarization phenomena, a perfect orthogonality between networks using orthogonal polarizations is not feasible. The depolarization model developed in chapter 2 has been used in [111] for the study of the performances of two networks using orthogonal polarizations.

- By receiving all the incident polarizations and by their low inter-antenna correlation, the multi-polarized antenna systems reduce the channel depolarization and small-scale fading effects and thus improve the spectrum sensing performances. However, spectrum sensing is also subject to the channel large-scale fading effects. The channel large-scale fading effects could be reduced by the cooperation of multiple cognitive radio users at different spatial positions sharing their informations with each-other. The combination of cooperative cognitive radio users using multi-polarized antenna systems could considerably improve the spectrum sensing performances of the system.

Bibliography

[1] *spectrum policy task force report*, Federal Communications Commission, Tech. Rep. 02-155, Nov 2002, retrived from www.sharedspectrum.com/measurements on 27/10/2009.

[2] I. Akyildiz, B. Lo, and R. Balakrishnan, "Cooperative spectrum sensing in cognitive radio networks: A survey," *Physical Communication*, 2010.

[3] *ITU Radio Regulations*, International Telecommunications Union, Geneva, 2008.

[4] *Et Docket No 03-222 Notice of proposed rule making and order*, FCC, december 2003.

[5] *Spectrum Occupancy Measurements*, Shared Spectrum Company, 2005, retrived from www.sharedspectrum.com/measurements on 27/10/2009.

[6] K. Steadman, A. Rose, and T. Nguyen, "Dynamic spectrum sharing detectors," in *New Frontiers in Dynamic Spectrum Access Networks, 2007. DySPAN 2007. 2nd IEEE International Symposium on*, april 2007, pp. 276 -282.

[7] M. Wellens and P. Mahonen, "Lessons learned from an extensive spectrum occupancy measurement campaign and a stochastic duty cycle model," in *Testbeds and Research Infrastructures for the Development of Networks Communities and Workshops, 2009. TridentCom 2009. 5th International Conference on*, april 2009, pp. 1 -9.

[8] M. Lopez-Benitez and F. Casadevall, "On the spectrum occupancy perception of cognitive radio terminals in realistic scenarios," in *Cognitive Information Processing (CIP), 2010 2nd International Workshop on*, june 2010, pp. 99 –104.

[9] V. Valenta, R. Marsalek, G. Baudoin, M. Villegas, M. Suarez, and F. Robert, "Survey on spectrum utilization in europe: Measurements, analyses and observations," in *Cognitive Radio Oriented Wireless Networks Communications (CROWNCOM), 2010 Proceedings of the Fifth International Conference on*, june 2010, pp. 1 –5.

[10] I. Mitola, J. and J. Maguire, G.Q., "Cognitive radio: making software radios more personal," *Personal Communications, IEEE*, vol. 6, no. 4, pp. 13 –18, aug 1999.

[11] S. Haykin, "Cognitive radio: brain-empowered wireless communications," *Selected Areas in Communications, IEEE Journal on*, vol. 23, no. 2, pp. 201–220, 2005.

[12] J. Mitola *et al.*, "Cognitive radio: An integrated agent architecture for software defined radio," *Doctor of Technology, Royal Inst. Technol.(KTH), Stockholm, Sweden*, pp. 271–350, 2000.

[13] R. Thomas, L. DaSilva, and A. MacKenzie, "Cognitive networks," in *New Frontiers in Dynamic Spectrum Access Networks, 2005. DySPAN 2005. 2005 First IEEE International Symposium on*. Ieee, 2005, pp. 352–360.

[14] F. K. Jondral, "Software-defined radio-basic and evolution to cognitive radio," *EURASIP Journal on Wireless Communication and Networking*, 2005.

[15] A. Sahai, N. Hoven, and R. Tandra, "Some fundamental limits on cognitive radio," in *Allerton Conference on Communication, Control, and Computing*, 2004, pp. 1662–1671.

[16] D. Cabric, S. Mishra, and R. Brodersen, "Implementation issues in spectrum sensing for cognitive radios," in *Signals, Systems and Computers, 2004. Conference Record of the Thirty-Eighth Asilomar Conference on*, vol. 1. Ieee, 2004, pp. 772–776.

[17] A. Fehske, J. Gaeddert, and J. Reed, "A new approach to signal classification using spectral correlation and neural networks," in *New Frontiers in Dynamic Spectrum Access Networks, 2005. DySPAN 2005. 2005 First IEEE International Symposium on.* Ieee, 2005, pp. 144–150.

[18] H. Tang, "Some physical layer issues of wide-band cognitive radio systems," in *New Frontiers in Dynamic Spectrum Access Networks, 2005. DySPAN 2005. 2005 First IEEE International Symposium on.* IEEE, 2005, pp. 151–159.

[19] I. Akyildiz and Y. Li, "Ocra: Ofdm-based cognitive radio networks," *Broadband and Wireless Networking Laboratory Technical Report*, 2006.

[20] C. Peng, H. Zheng, and B. Zhao, "Utilization and fairness in spectrum assignment for opportunistic spectrum access," *Mobile Networks and Applications*, vol. 11, no. 4, pp. 555–576, 2006.

[21] H. Zheng and C. Peng, "Collaboration and fairness in opportunistic spectrum access," in *Communications, 2005. ICC 2005. 2005 IEEE International Conference on*, vol. 5. IEEE, 2005, pp. 3132–3136.

[22] V. Brik, E. Rozner, S. Banerjee, and P. Bahl, "Dsap: a protocol for coordinated spectrum access," in *New Frontiers in Dynamic*

Spectrum Access Networks, 2005. DySPAN 2005. 2005 First IEEE International Symposium on. IEEE, 2005, pp. 611–614.

[23] L. Cao and H. Zheng, "Distributed spectrum allocation via local bargaining," in *Proc. IEEE SECON*, vol. 5, 2005, pp. 119–127.

[24] L. Ma, X. Han, and C. Shen, "Dynamic open spectrum sharing mac protocol for wireless ad hoc networks," in *New Frontiers in Dynamic Spectrum Access Networks, 2005. DySPAN 2005. 2005 First IEEE International Symposium on.* Ieee, 2005, pp. 203–213.

[25] J. Huang, R. Berry, and M. Honig, "Spectrum sharing with distributed interference compensation," in *New Frontiers in Dynamic Spectrum Access Networks, 2005. DySPAN 2005. 2005 First IEEE International Symposium on.* Ieee, 2005, pp. 88–93.

[26] S. Sankaranarayanan, P. Papadimitratos, A. Mishra, and S. Hershey, "A bandwidth sharing approach to improve licensed spectrum utilization," in *New Frontiers in Dynamic Spectrum Access Networks, 2005. DySPAN 2005. 2005 First IEEE International Symposium on.* IEEE, 2005, pp. 279–288.

[27] J. Stine, "Spectrum management: the killer application of ad hoc and mesh networking," in *New Frontiers in Dynamic Spectrum Access Networks, 2005. DySPAN 2005. 2005 First IEEE International Symposium on.* IEEE, 2005, pp. 184–193.

[28] I. Akyildiz, X. Wang, and W. Wang, "Wireless mesh networks: a survey," *Computer networks*, vol. 47, no. 4, pp. 445–487, 2005.

[29] P. Kyasanur, X. Yang, and N. Vaidya, "Mesh networking protocols to exploit physical layer capabilities," in *Proc. First IEEE Workshop on Wireless Mesh Networks (WiMesh).* Citeseer, 2005.

[30] L. Berlemann, S. Mangold, and B. Walke, "Policy-based reasoning for spectrum sharing in radio networks," in *New Frontiers in Dynamic Spectrum Access Networks, 2005. DySPAN 2005. 2005 First IEEE International Symposium on.* IEEE, 2005, pp. 1–10.

[31] D. Maldonado, B. Le, A. Hugine, T. Rondeau, and C. Bostian, "Cognitive radio applications to dynamic spectrum allocation: a discussion and an illustrative example," in *New Frontiers in Dynamic Spectrum Access Networks, 2005. DySPAN 2005. 2005 First IEEE International Symposium on.* Ieee, 2005, pp. 597–600.

[32] C. Cordeiro, K. Challapali, D. Birru, and N. Sai Shankar, "Ieee 802.22: the first worldwide wireless standard based on cognitive radios," in *New Frontiers in Dynamic Spectrum Access Networks, 2005. DySPAN 2005. 2005 First IEEE International Symposium on.* Ieee, 2005, pp. 328–337.

[33] "IEEE 802.22 working group on wireless regional area networks, available from: <http://www.ieee802.org/22/>."

[34] I. S. Association, "Ieee 802.22$^{\text{TM}}$-2011 standard for wireless regional area networks in tv whitespaces completed."

[35] T. Weiss and F. Jondral, "Spectrum pooling: an innovative strategy for the enhancement of spectrum efficiency," *Communications Magazine, IEEE*, vol. 42, no. 3, pp. S8–14, 2004.

[36] J. Proakis, *Digital communications.* McGraw-hill, 1987, vol. 1221.

[37] S. Kay, "Fundamentals of statistical signal processing, volume ii: Detection theory," *Upper Saddle River (New Jersey)*, vol. 7, 1998.

[38] D. Cabric, A. Tkachenko, and R. Brodersen, "Experimental study of spectrum sensing based on energy detection and network co-

operation," in *Proceedings of the first international workshop on Technology and policy for accessing spectrum.* ACM, 2006, p. 12.

[39] K. Haghighi, A. Svensson, and E. Agrell, "Wideband sequential spectrum sensing with varying thresholds," in *GLOBECOM 2010, 2010 IEEE Global Telecommunications Conference.* IEEE, 2010, pp. 1–5.

[40] A. Tkachenko, "Testbed design for cognitive radio spectrum sensing experiments," Ph.D. dissertation, Department of Electrical Engineering and Computer Sciences, University of California, 2007.

[41] R. Tandra and A. Sahai, "Fundamental limits on detection in low snr under noise uncertainty," in *Wireless Networks, Communications and Mobile Computing, 2005 International Conference on*, vol. 1. IEEE, 2005, pp. 464–469.

[42] D. Donoho, "Compressed sensing," *Information Theory, IEEE Transactions on*, vol. 52, no. 4, pp. 1289–1306, 2006.

[43] B. Wang, K. Liu, and T. Clancy, "Evolutionary cooperative spectrum sensing game: how to collaborate?" *Communications, IEEE Transactions on*, vol. 58, no. 3, pp. 890–900, 2010.

[44] Z. Tian and G. Giannakis, "Compressed sensing for wideband cognitive radios," in *Acoustics, Speech and Signal Processing, 2007. ICASSP 2007. IEEE International Conference on*, vol. 4. Ieee, 2007, pp. IV–1357.

[45] A. Goldsmith, *Wireless communications.* Cambridge Univ Pr, 2005.

[46] R. Vaughan, "Polarization diversity in mobile communications," *Vehicular Technology, IEEE Transactions on*, vol. 39, no. 3, pp. 177–186, 1990.

[47] I. Akyildiz, W. Lee, M. Vuran, and S. Mohanty, "Next generation/dynamic spectrum access/cognitive radio wireless networks: a survey," *Computer Networks*, vol. 50, no. 13, pp. 2127–2159, 2006.

[48] A. Ghasemi and E. Sousa, "Collaborative spectrum sensing for opportunistic access in fading environments," in *New Frontiers in Dynamic Spectrum Access Networks, 2005. DySPAN 2005. 2005 First IEEE International Symposium on.* Ieee, 2005, pp. 131–136.

[49] S. Mishra, A. Sahai, and R. Brodersen, "Cooperative sensing among cognitive radios," in *Communications, 2006. ICC'06. IEEE International Conference on*, vol. 4. Ieee, 2006, pp. 1658–1663.

[50] R. Tandra and A. Sahai, "Snr walls for signal detection," *Selected Topics in Signal Processing, IEEE Journal of*, vol. 2, no. 1, pp. 4–17, 2008.

[51] G. Ganesan and Y. Li, "Cooperative spectrum sensing in cognitive radio networks," in *New Frontiers in Dynamic Spectrum Access Networks, 2005. DySPAN 2005. 2005 First IEEE International Symposium on.* IEEE, 2005, pp. 137–143.

[52] J. Zhao, H. Zheng, and G. Yang, "Distributed coordination in dynamic spectrum allocation networks," in *New Frontiers in Dynamic Spectrum Access Networks, 2005. DySPAN 2005. 2005 First IEEE International Symposium on.* IEEE, 2005, pp. 259–268.

[53] A. Al-Abbasi and T. Fujii, "A novel spectrum sensing method using multi-antennas without channel state information," in *Wireless Communication Systems, 2009. ISWCS 2009. 6th International Symposium on*, 7-10 2009, pp. 373 –377.

[54] V. Kuppusamy and R. Mahapatra, "Primary user detection in ofdm based mimo cognitive radio," in *Cognitive Radio Oriented*

Wireless Networks and Communications, 2008. CrownCom 2008. 3rd International Conference on, 15-17 2008, pp. 1 –5.

[55] S. Kim, J. Lee, H. Wang, and D. Hong, "Sensing performance of energy detector with correlated multiple antennas," *Signal Processing Letters, IEEE*, vol. 16, no. 8, pp. 671 –674, aug. 2009.

[56] R. Mahapatra, "Wideband spectrum sensing in multiantenna based cognitive radio," in *India Conference (INDICON), 2009 Annual IEEE*, 18-20 2009, pp. 1 –3.

[57] W. Ma, M. Q. Wu, D. Liu, and M. L. Wang, "User sensing based on mimo cognitive radio sensor networks," in *Computer Science and Information Technology, 2009. ICCSIT 2009. 2nd IEEE International Conference on*, 8-11 2009, pp. 205 –208.

[58] F. F. Digham, M.-S. Alouini, and M. K. Simon, "On the energy detection of unknown signals over fading channels," *Communications, IEEE Transactions on*, vol. 55, no. 1, pp. 21 –24, jan. 2007.

[59] A. Pandharipande and J.-P. Linnartz, "Performance analysis of primary user detection in a multiple antenna cognitive radio," in *Communications, 2007. ICC '07. IEEE International Conference on*, 24-28 2007, pp. 6482 –6486.

[60] B. Lindmark and M. Nilsson, "On the available diversity gain from different dual-polarized antennas," *Selected Areas in Communications, IEEE Journal on*, vol. 19, no. 2, pp. 287 –294, feb 2001.

[61] P. Kyritsi, D. Cox, R. Valenzuela, and P. Wolniansky, "Effect of antenna polarization on the capacity of a multiple element system in an indoor environment," *Selected Areas in Communications, IEEE Journal on*, vol. 20, no. 6, pp. 1227 - 1239, aug 2002.

[62] M. Andrews, P. Mitra, and R. deCarvalho, "Tripling the capacity of wireless communications using electromagnetic polarization," *Letters to Nature*, vol. 409, pp. 316–318, 2001.

[63] L. Lukama, K. Konstantinou, and D. Edwards, "Performance of a three-branch orthogonal polarization diversity scheme," in *Vehicular Technology Conference, 2001. VTC 2001 Fall. IEEE VTS 54th*, vol. 4, 2001, pp. 2033 –2037 vol.4.

[64] V. Erceg, P. Soma, D. Baum, and S. Catreux, "Multiple-input multiple-output fixed wireless radio channel measurements and modeling using dual-polarized antennas at 2.5 ghz," *Wireless Communications, IEEE Transactions on*, vol. 3, no. 6, pp. 2288 – 2298, nov. 2004.

[65] L.Jiang, L.Thiele, and V.Jungnickel, "On the modelling of polarized mimo channel," in *13th European Wireless Conference*, 2007.

[66] V. Anreddy and M. Ingram, "Capacity of measured ricean and rayleigh indoor mimo channels at 2.4 ghz with polarization and spatial diversity," in *Wireless Communications and Networking Conference, 2006. WCNC 2006. IEEE*, vol. 2, 3-6 2006, pp. 946 –951.

[67] M. Coldrey, "Modeling and capacity of polarized mimo channels," in *Vehicular Technology Conference, 2008. VTC Spring 2008. IEEE*, 11-14 2008, pp. 440 –444.

[68] C. Oestges, V. Erceg, and A. Paulraj, "Propagation modeling of mimo multipolarized fixed wireless channels," *Vehicular Technology, IEEE Transactions on*, vol. 53, no. 3, pp. 644 – 654, may 2004.

[69] S. Ramo, J. Whinnery, and T. Van Duzer, *Fields and waves in communication electronics.* Wiley-India, 2007.

[70] E. Kennaugh, "Polarization dependence of rcs– a geometrical interpretation," *IEEE TRANS. ANTENNAS AND PROPAG.*, vol. 29, no. 2, pp. 412–413, 1981.

[71] A. Molisch, *Wireless communications.* Wiley, 2011.

[72] S. Seidel and T. Rappaport, "Site-specific propagation prediction for wireless in-building personal communication system design," *Vehicular Technology, IEEE Transactions on*, vol. 43, no. 4, pp. 879–891, 1994.

[73] M. Cátedra and J. Pérez, *Cell planning for wireless communications.* Artech House, Inc., 1999.

[74] M. Iskander and Z. Yun, "Propagation prediction models for wireless communication systems," *Microwave Theory and Techniques, IEEE Transactions on*, vol. 50, no. 3, pp. 662–673, 2002.

[75] V. Degli-Esposti, D. Guiducci, A. de'Marsi, P. Azzi, and F. Fuschini, "An advanced field prediction model including diffuse scattering," *Antennas and Propagation, IEEE Transactions on*, vol. 52, no. 7, pp. 1717–1728, 2004.

[76] L. Correia, *Mobile broadband multimedia networks: techniques, models and tools for 4G.* Academic Press, 2006.

[77] H. Sampath and A. Paulraj, "Linear precoding for space-time coded systems with known fading correlations," *Communications Letters, IEEE*, vol. 6, no. 6, pp. 239–241, 2002.

[78] F. Quitin, F. Horlin, C. Oestges, and P. De Doncker, "A new precoding scheme for compact cross-polarized multi-antenna systems," in *29th Symposium on Information Theory in the Benelux*, 2008.

[79] C. Oestges, B. Clerckx, M. Guillaud, and M. Debbah, "Dual-polarized wireless communications: from propagation models to system performance evaluation," *Wireless Communications, IEEE Transactions on*, vol. 7, no. 10, pp. 4019 -4031, october 2008.

[80] P. Soma, D. Baum, V. Erceg, R. Krishnamoorthy, and A. Paulraj, "Analysis and modeling of multiple-input multiple-output (mimo) radio channel based on outdoor measurements conducted at 2.5 ghz for fixed bwa applications," in *Communications, 2002. ICC 2002. IEEE International Conference on*, vol. 1, 2002, pp. 272 -276.

[81] X. Zhao, S. Geng, L. Vuokko, J. Kivinen, and P. Vainikainen, "Polarization behaviours at 2, 5 and 60 ghz for indoor mobile communications," *Wireless Personal Communications*, vol. 27, no. 2, pp. 99–115, 2003.

[82] T. Rappaport and D. Hawbaker, "Wide-band microwave propagation parameters using circular and linear polarized antennas for indoor wireless channels," *Communications, IEEE Transactions on*, vol. 40, no. 2, pp. 240–245, 1992.

[83] J. Toftgard and P. Eggers, "Experimental characterization of the polarization state dynamics of personal communication radio channels," in *Vehicular Technology Conference, 1993 IEEE 43rd*. IEEE, 1993, pp. 65–69.

[84] T. Neubauer and P. Eggers, "Simultaneous characterization of polarization matrix components in pico cells," in *Vehicular Technology Conference, 1999. VTC 1999-Fall. IEEE VTS 50th*, vol. 3. IEEE, 1999, pp. 1361–1365.

[85] W. Kotterman, G. Sommerkorn, and R. Thoma, "Cross-correlation values for dual-polarised indoor mimo links and re-

alistic antenna elements," in *Wireless Communication Systems, 2006. ISWCS'06. 3rd International Symposium on.* IEEE, 2006, pp. 505–509.

[86] W. Kotterman, M. Landmann, G. Sommerkorn, and R. Thomä, "Power ratios and distributions in indoor nlos channels for dual-polarized 2 x 2 mimo systems," in *Proc. NEWCOM-ACoRN Joint Workshop*, 2006.

[87] H. Asplund, J. Berg, F. Harrysson, J. Medbo, and M. Riback, "Propagation characteristics of polarized radio waves in cellular communications," in *Vehicular Technology Conference, 2007. VTC-2007 Fall. 2007 IEEE 66th.* IEEE, 2007, pp. 839–843.

[88] S. Kozono, T. Tsuruhara, and M. Sakamoto, "Base station polarization diversity reception for mobile radio," *Vehicular Technology, IEEE Transactions on*, vol. 33, no. 4, pp. 301–306, 1984.

[89] J. Lempiainen and J. Laiho-Steffens, "The performance of polarization diversity schemes at a base station in small/micro cells at 1800 mhz," *Vehicular Technology, IEEE Transactions on*, vol. 47, no. 3, pp. 1087–1092, 1998.

[90] F. Lotse, J. Berg, U. Forssen, and P. Idahl, "Base station polarization diversity reception in macrocellular systems at 1800 mhz," in *Vehicular Technology Conference, 1996.'Mobile Technology for the Human Race'., IEEE 46th*, vol. 3. IEEE, 1996, pp. 1643–1646.

[91] T. Sorensen, A. Nielsen, P. Mogensen, M. Tolstrup, and K. Steffensen, "Performance of two-branch polarisation antenna diversity in an operational gsm network," in *Vehicular Technology Conference, 1998. VTC 98. 48th IEEE*, vol. 2. IEEE, 1998, pp. 741–746.

[92] A. Kainulainen, L. Vuokko, and P. Vainikainen, "Polarization behavior in different urban radio environments at 5.3 ghz," *COST273 TD (05)*, vol. 18, pp. 19–21, 2005.

[93] D. Chizhik, J. Ling, D. Samardzija, and R. Valenzuela, "Spatial and polarization characterization of mimo channels in rural environment," in *Vehicular Technology Conference, 2005. VTC 2005-Spring. 2005 IEEE 61st*, vol. 1. IEEE, 2005, pp. 161–164.

[94] P. Kyritsi, D. Cox, R. Valenzuela, and P. Wolniansky, "Correlation analysis based on mimo channel measurements in an indoor environment," *Selected Areas in Communications, IEEE Journal on*, vol. 21, no. 5, pp. 713–720, 2003.

[95] J. Wallace and M. Jensen, "Modeling the indoor mimo wireless channel," *Antennas and Propagation, IEEE Transactions on*, vol. 50, no. 5, pp. 591–599, 2002.

[96] C. Oestges, "A comprehensive model of dual-polarized channels: from experimental observations to an analytical formulation," in *Communications and Networking in China, 2008. ChinaCom 2008. Third International Conference on*. IEEE, 2008, pp. 1071–1075.

[97] G. Calcev, D. Chizhik, B. Goransson, S. Howard, H. Huang, A. Kogiantis, A. Molisch, A. Moustakas, D. Reed, and H. Xu, "A wideband spatial channel model for system-wide simulations," *Vehicular Technology, IEEE Transactions on*, vol. 56, no. 2, pp. 389–403, 2007.

[98] A. Jagannatham and V. Erceg, "Mimo indoor wlan channel measurements and parameter modeling at 5.25 ghz," in *Vehicular Technology Conference, 2004. VTC2004-Fall. 2004 IEEE 60th*, vol. 1, sept. 2004, pp. 106 – 110 Vol. 1.

[99] F. Quitin, C. Oestges, F. Horlin, and P. De Doncker, "Small-scale variations of cross-polar discrimination in ricean fading channels," *Electronics letters*, vol. 45, no. 4, pp. 213–214, 2009.

[100] S.-C. Kwon and G. Stu¨ andber, "3-d geometry-based statistical modeling of cross-polarization discrimination in wireless communication channels," in *Vehicular Technology Conference (VTC 2010-Spring), 2010 IEEE 71st*, may 2010, pp. 1 –5.

[101] S.-C. Kwon and G. Stuber, "Cross-polarization discrimination in vehicle-to-vehicle channels: Geometry-based statistical modeling," in *Global Telecommunications Conference (GLOBECOM 2010), 2010 IEEE*, dec. 2010, pp. 1 –5.

[102] ——, "Geometrical theory of channel depolarization," *Vehicular Technology, IEEE Transactions on*, vol. 60, no. 8, pp. 3542 –3556, oct. 2011.

[103] M. Shafi, M. Zhang, A. Moustakas, P. Smith, A. Molisch, F. Tufvesson, and S. Simon, "Polarized mimo channels in 3-d: models, measurements and mutual information," *Selected Areas in Communications, IEEE Journal on*, vol. 24, no. 3, pp. 514–527, 2006.

[104] F. Quitin, F. Bellens, A. Panahandeh, J. Dricot, F. Dossin, F. Horlin, C. Oestges, and P. De Doncker, "A time-variant statistical channel model for tri-polarized antenna systems," in *Personal Indoor and Mobile Radio Communications (PIMRC), 2010 IEEE 21st International Symposium on.* IEEE, 2010, pp. 64–69.

[105] A. Panahandeh, F. Quitin, J. Dricot, F. Horlin, C. Oestges, and P. De Doncker, "Multi-polarized channel statistics for outdoor-to-indoor and indoor-to-indoor channels," in *71st Vehicular Technology Conference (VTC2010 – Spring)*, 15-19 May 2010.

[106] K. Jeon, B. Hui, K. Chang, H. Park, and Y. Park, "Siso polarized flat fading channel modeling for dual-polarized antenna systems," in *Information Networking (ICOIN), 2012 International Conference on*, feb. 2012, pp. 368 –373.

[107] H. Urkowitz, "Energy detection of unknown deterministic signals," *Proceedings of the IEEE*, vol. 55, no. 4, pp. 523 – 531, april 1967.

[108] S. Shellhammer and G. Chouinard, "Spectrum sensing requirements summary," June. 2006.

[109] G. JI and H. ZHU, "On the noise power uncertainty of the low snr energy detection in cognitive radio," *Journal of Computational Information Systems*, vol. 6, no. 8, pp. 2457–2463, 2010.

[110] W. Jouini, "Energy detection limits under log-normal approximated noise uncertainty," *Signal Processing Letters, IEEE*, no. 99, pp. 1–1, 2010.

[111] J.-M. Dricot, G. Ferrari, A. Panahandeh, F. Horlin, and P. D. Doncker, "Probabilistic coexistence and throughput of cognitive dual-polarized networks." *EURASIP J. Wireless Comm. and Networking*, vol. 2010, 2010.

[112] L. Berlemann, S. Mangold, and I. ebrary, *Cognitive radio and dynamic spectrum access.* Wiley Online Library, 2009.

[113] E. Baccarelli, M. Biagi, C. Pelizzoni, and N. Cordeschi, "Multi-antenna cognitive radio for broadband access in 4g-wlans," in *Proceedings of the 5th ACM international workshop on Mobility management and wireless access.* ACM, 2007, pp. 66–73.

[114] J.-M. Dricot, F. Horlin, and P. De Doncker, "On the co-existence of dual-polarized cdma networks," in *Cognitive Radio Oriented Wire-*

less Networks and Communications, 2009. CROWNCOM '09. 4th International Conference on, june 2009, pp. 1 –6.

[115] J. Bazerque and G. Giannakis, "Distributed scheduling and resource allocation for cognitive ofdma radios," *Mobile Networks and Applications*, vol. 13, no. 5, pp. 452–462, 2008.

[116] X. Wang and W. Xiang, "An ofdm-tdma/sa mac protocol with qos constraints for broadband wireless lans," *Wireless Networks*, vol. 12, no. 2, pp. 159–170, 2006.

[117] J. M. Dricot, F. Horlin, and P. . Doncker, "Interference and throughput analyses in Dual-Polarized wireless networks subject to rayleigh fading," in *IWCMC 2009 General Symposium*, Leipzig, Germany, June 2009.

[118] J. Dricot, G. Ferrari, F. Quitin, A. Panahandeh, F. Horlin, and P. De Doncker, "Polarization orthogonality for the co-existence of wideband fading cognitive networks," in *Cognitive Radio Oriented Wireless Networks Communications (CROWNCOM), 2010 Proceedings of the Fifth International Conference on*, june 2010, pp. 1 –5.

[119] C. Chuah, D. Tse, J. Kahn, and R. Valenzuela, "Capacity scaling in mimo wireless systems under correlated fading," *Information Theory, IEEE Transactions on*, vol. 48, no. 3, pp. 637–650, 2002.

[120] D. Shiu, G. Foschini, M. Gans, and J. Kahn, "Fading correlation and its effect on the capacity of multielement antenna systems," *Communications, IEEE Transactions on*, vol. 48, no. 3, pp. 502–513, 2000.

[121] J. Kermoal, L. Schumacher, K. Pedersen, P. Mogensen, and F. Frederiksen, "A stochastic mimo radio channel model with ex-

perimental validation," *Selected Areas in Communications, IEEE Journal on*, vol. 20, no. 6, pp. 1211–1226, 2002.

[122] D. Bicout and C. Brosseau, "Multiply scattered waves through a spatially random medium: entropy production and depolarization," *Journal de Physique I*, vol. 2, no. 11, pp. 2047–2063, 1992.

[123] C. Dietrich Jr, K. Dietze, J. Nealy, and W. Stutzman, "Spatial, polarization, and pattern diversity for wireless handheld terminals," *Antennas and Propagation, IEEE Transactions on*, vol. 49, no. 9, pp. 1271–1281, 2001.

[124] W. Malik, "Polarimetric characterization of ultrawideband propagation channels," *Antennas and Propagation, IEEE Transactions on*, vol. 56, no. 2, pp. 532–539, 2008.

[125] C. Balanis, *Antenna theory: analysis and design/Constantine A. Balanis*. J. Wiley, New York, 1982.

[126] F. Gallee, "Development of an isotropic sensor 2ghz–6ghz," in *Microwave Conference, 2007. European*. IEEE, 2007, pp. 91–93.

[127] L. Schmetterer, "Introduction to mathematical statistics," *Die Grundlehren der Mathematischen Wissenschaften in Einzeldarstellungen, Berlin: Springer, 1974*, vol. 1, 1974.

[128] N. I. of Standards, T. (US), C. Croarkin, P. Tobias, C. Zey, and I. SEMATECH., *Engineering statistics handbook*. The Institute, 2001.

[129] V. Erceg, P. Soma, D. Baum, and S. Catreux, "Multiple-input multiple-output fixed wireless radio channel measurements and modeling using dual-polarized antennas at 2.5 ghz," in *IEEE Trans. wireless Commun*, vol. 3, Nov 2004, pp. 2288 – 2298.

[130] C. Oestges and B. Clerckx, *MIMO wireless communications: from real-world propagation to space-time code design*, ser. Electronics & Electrical. Academic Press, 2007.

[131] G. Smith, *An introduction to classical electromagnetic radiation*. Cambridge University Press, 1997.

[132] T. Carozzi, R. Karlsson, and J. Bergman, "Parameters characterizing electromagnetic wave polarization," *Physical Review E*, vol. 61, pp. 2024–2028, 2000.

[133] P. Moon and D. Spencer, *Field theory handbook: including coordinate systems, differential equations, and their solutions*. Springer-Verlag, 1961.

[134] N. Das, T. Inoue, T. Taniguchi, and Y. Karasawa, "An experiment on mimo system having three orthogonal polarization diversity branches in multipath-rich environment," in *60st Vehicular Technology Conference (VTC2004 - Fall)*, vol. 2, 26-29 Sep 2004, pp. 1528 - 1532.

[135] S. Coles, *An introduction to statistical modeling of extreme values*. Springer Verlag, 2001.

[136] B. Sutradhar, "On the characteristic function of multivariate student t-distribution," *Canadian Journal of Statistics*, vol. 14, no. 4, pp. 329–337, 1986.

[137] F. Pérez-Fontán and P. Espiñeira, *Modeling the wireless propagation channel: a simulation approach with MATLAB*, ser. Wiley series on wireless communications and mobile computing. Wiley, 2008.

[138] J. Harris and H. Stöcker, *Handbook of mathematics and computational science*. Springer Verlag, 1998.

[139] A. Böttcher and B. Silbermann, *Analysis of Toeplitz operators.* Springer Verlag, 2006.

[140] F. Liu, C. Feng, C. Guo, Y. Wang, and D. Wei, "Polarization spectrum sensing scheme for cognitive radios," in *Wireless Communications, Networking and Mobile Computing, 2009. WiCom '09. 5th International Conference on*, sept. 2009, pp. 1 –4.

[141] ——, "Virtual polarization detection: A vector signal sensing method for cognitive radios," in *Vehicular Technology Conference (VTC 2010-Spring), 2010 IEEE 71st*, may 2010, pp. 1 –5.

[142] J. Ma and Y. Li, "Soft combination and detection for cooperative spectrum sensing in cognitive radio networks," in *Global Telecommunications Conference, 2007. GLOBECOM '07. IEEE*, nov. 2007, pp. 3139 –3143.

[143] I. R. I.S. Gradshteyn, *Table of Integrals, Series and products, 6th ed.* San Diego, CA Academic, 2000.

[144] J. Marcum, "A statistical theory of target detection by pulsed radar," *Information Theory, IRE Transactions on*, no. 2, pp. 59–267.

[145] A. Nuttall, "Some integrals involving the Q_M function," *IEEE Transactions on Information Theory*, 1975.

[146] J. Pierce and S. Stein, "Multiple diversity with nonindependent fading," *Proceedings of the IRE*, vol. 48, no. 1, pp. 89 –104, jan. 1960.

[147] W. Gardner and C. Spooner, "Signal interception: performance advantages of cyclic-feature detectors," *Communications, IEEE Transactions on*, vol. 40, no. 1, pp. 149 –159, jan 1992.

[148] M. Orooji, R. Soosahabi, and M. Naraghi-Pour, "Blind spectrum sensing using antenna arrays and path correlation," *Vehicular Technology, IEEE Transactions on*, no. 99, pp. 1–1, 2011.

[149] T. J. Lim, R. Zhang, Y. C. Liang, and Y. Zeng, "Glrt-based spectrum sensing for cognitive radio," in *Global Telecommunications Conference, 2008. IEEE GLOBECOM 2008. IEEE*, 30 2008-dec. 4 2008, pp. 1 –5.

[150] R. Zhang, T. Lim, Y. Liang, and Y. Zeng, "Multi-antenna based spectrum sensing for cognitive radios: A glrt approach," *Communications, IEEE Transactions on*, vol. 58, no. 1, pp. 84–88, 2010.

[151] Y. Zeng and Y. Liang, "Maximum-minimum eigenvalue detection for cognitive radio," in *Personal, Indoor and Mobile Radio Communications, 2007. PIMRC 2007. IEEE 18th International Symposium on*. IEEE, 2007, pp. 1–5.

[152] A. Taherpour, M. Nasiri-Kenari, and S. Gazor, "Multiple antenna spectrum sensing in cognitive radios," *Wireless Communications, IEEE Transactions on*, vol. 9, no. 2, pp. 814–823, 2010.

[153] M. Abramowitz and I. Stegun, *Handbook of mathematical functions with formulas, graphs, and mathematical tables*, ser. Applied mathematics series. U.S. Govt. Print. Off., 1964, no. v. 55, no. 1972.

[154] M. Bartlett, "Properties of sufficiency and statistical tests," *Proceedings of the Royal Society of London. Series A-Mathematical and Physical Sciences*, vol. 160, no. 901, pp. 268–282, 1937.

[155] W. Dixon and F. Massey Jr, "Introduction to statistical analysis ." 1957.

[156] J. Connelly, *Low-Noise Electronic System Design.* John Wiley & Sons, Inc., 1993.

[157] A. Sonnenschein and P. Fishman, "Radiometric detection of spread-spectrum signals in noise of uncertain power," *Aerospace and Electronic Systems, IEEE Transactions on*, vol. 28, no. 3, pp. 654–660, 1992.

List of publications

Journal Publications

- Ali Panahandeh, Claude Oestges, Jean-Michel Dricot, François Horlin and Philippe De Doncker, *Tri-polarized Spectrum Sensing Based on an Experimental Outdoor-to-Indoor Cogntive-Radio Scenario*, Physical Communication Journal special issue on Polarization in wireless communications, 2012
- Ali Panahandeh, François Horlin, Jean-Michel Dricot, Claude Oestges and Philippe De Doncker, *Spectrum Sensing Based on the Difference of the Variance of Received Signals in Multi-polarized Antenna Systems*, submitted to Physical Communication Journal special issue on Cognitive Radios, 2012
- J.-M. Dricot, G. Ferrari, A. Panahandeh, F. Horlin, and P. De Doncker, *Probabilistic co- existence and throughput of cognitive dual-polarized networks*, EURASIP Journal on Wireless Communications and Networking, 2010
- François Quitin, Claude Oestges, Ali Panahandeh, François Horlin and Philippe De Doncker, *Tri-polarized MIMO systems in real-world channels: channel investigation and performance analysis*, Physical Communications Journal special issue on Polarization in wireless communications, 2012
- Ali Panahandeh, Claude Oestges, Jean-Michel Dricot, François Horlin and Philippe De Doncker, *Time-dynamics modeling of Multi-polarized indoor communication channel from an electro-*

magnetic approach and based on measurements, to be submitted to Progress In Electromagnetics Research (PIER) journal

Conference Publications

- Ali Panahandeh, François Quitin, Jean-Michel Dricot, François Horlin, Claude Oestges and Philippe De Doncker, *Cross-Polar Discrimination Statistics for Outdoor-to-Indoor and Indoor-to-Indoor Channels*, COST 2100 TD(09) 815, Valencia, Spain, May, 18th-19th 2009
- Ali Panahandeh, François Quitin, Jean-Michel Dricot, François Horlin, Claude Oestges and Philippe De Doncker, *Orientation-Free XPD and CPR Model in Outdoor-to-Indoor and Indoor-to-Indoor Channels*, 4th European Conference on Antennas and Propagation (Eucap2010), Barcelona, Spain, 12th-16th April 2010
- Ali Panahandeh, François Quitin, Jean-Michel Dricot, François Horlin, Claude Oestges and Philippe De Doncker, *Multi-Polarized Channel Statistics for Outdoor-to-Indoor and Indoor-to-Indoor Channels*, 71st Vehicular Technology Conference (VTC2010 – Spring), Taipei, Taiwan, 16th – 19th May 2010
- J.M. Dricot, G. Ferrari, A. Panahandeh, F. Horlin and Ph. De Doncker, *Polarization Orthogonality for the Co-Existence of Wideband Fading Cognitive Networks*, 5th International Conference on Cognitive Radio Oriented Wireless Networks and Communications (CROWNCOM 2010), Cannes, France, June 2010
- F. Qutin, F. Bellens, A. Panahandeh, C. Oestges, F. Horlin and Ph. De Doncker, *A Time-Variant Statistical Channel Model for Tri-polarized Antenna Systems*, IEEE International Symposium on Personal, Indoor and Mobile Radio Communications (PIMRC 2010), Istanbul, Turkey, September 2010

- Ali Panahandeh, François Quitin, Jean-Michel Dricot, François Horlin, Claude Oestges and Philippe De Doncker, *A Time-Variant Statistical Model for the Polarization of Received Electromagnetic Waves in Indoor Communication Channels*, International Conference on Computing, Networking and Communications (ICNC 2012), Maui, USA, February 2012

- Ali Panahandeh, François Quitin, Jean-Michel Dricot, François Horlin, Claude Oestges and Philippe De Doncker, *Characterization of the Polarization of Received Electromagnetic Waves in Indoor Communication Channels*, Progress In Electromagnetics Research Symposium (PIERS 2012), Kuala Lumpur, Malaysia, March 2012

- Ali Panahandeh, Claude Oestges, Jean-Michel Dricot, François Horlin, and Philippe De Doncker, *Study of the Temporal Dynamics of the Polarization of Received Electromagnetic Waves Based on an Indoor-to-Indoor Measurement Campaign*, IEEE International Symposium on Personal, Indoor and Mobile Radio Communications (PIMRC 2012), Sydney, Australia, September 2012